

On the Theory of Ductile-Brittle Transition (Cold Brittleness)

Ya. S. Semenov

Presented by Academician G.F. Krymskiĭ October 16, 2000

Received March 16, 2001

The ductile-brittle transition (DBT) is known [1–4] to depend on temperature, chemical composition, stressed state, and loading rate. Moreover, as was established in studies [4, 5], there exists a unified DBT mechanism consisting in the disordering of the electron structure responsible for chemical bonds. This mechanism involves either the recovery (or rupture) of the directed component of chemical bonds at the critical temperatures T_{cr} of a DBT or the so-called “crystallization” of valence electrons. The Wigner crystallization in the presence of a uniform compensating field of the lattice is the simplest example of such a mechanism [6, 7].

As was noted in [5], a decrease in thermal vibrations or a change in the doping element leads to the initiation of directed chemical bonds, i.e., crystallization of the electron structure at the temperature T_{cr} of the DBT. In this case, we can use the theory of the second-order phase transition, as was done, for example, in studies [6–8].

We consider an electron system with the following Hamiltonian in the x -representation:

$$H = \int dx \hat{a}^{s*}(x) \left\{ \frac{\hat{p}^2}{2m} + U(x) - \mu \right\} \hat{a}^s(x) + \frac{1}{2} \int dx dy v(x-y) \hat{a}^{s*}(x) \hat{a}^{s'*}(y) \hat{a}^{s'}(y) \hat{a}^s(x). \quad (1)$$

Here, $\hat{a}^{s*}(x)$ and $\hat{a}^s(x)$ are the production and annihilation operators, respectively, for particles with the spin $s = \pm \frac{1}{2}$; $v(x, y)$ is a two-body interaction potential independent of s ; $U(x) = U(x + R)$ is the periodic field of the crystal lattice $\{R\}$; $\frac{\hat{p}^2}{2m}$ is the kinetic energy operator ($\hbar = 1$); and μ is the chemical potential. The integration is carried out over the whole volume of the system. Cyclic boundary conditions are imposed. The summa-

tion is performed over the repeating superscripts s' and s .

The operators $\hat{a}^{s*}(x)$ and $\hat{a}^s(x)$ can be expressed in terms of the second quantization operator in the basis of the Wannier electron functions $W_n(x - R)$:

$$\hat{a}^{s*}(x) = \sum_{R, n} \hat{a}_n^{s*}(R) W_n^*(x - R), \quad (2)$$

$$\hat{a}^s(x) = \sum_{R, n} \hat{a}_n^s(R) W_n(x - R).$$

The Wannier functions $W_n(x - R)$ are defined by Bloch functions:

$$W_n(x - R) = \frac{1}{\sqrt{N}} \sum_k u_{k, n}(x) e^{ik \cdot R}, \quad (2a)$$

where the summation is extended over k within the first Brillouin zone of the lattice $\{R\}$ and N is the number of lattice sites in the cyclic volume V . The Bloch functions $u_{k, n}(x)$ relating to the n th zone are solutions to the Schrödinger equation:

$$\left[\frac{\hat{p}^2}{2m} + U(x) \right] u_{k, n}(x) = L_n^0(k) u_{k, n}(x), \quad (3)$$

with the eigenvalues $L_n^0(k)$.

We now take into account the valence angle and a certain broadening of the energy gaps between the bands due to thermal vibrations and which causes the gaps to be more broad than the corresponding characteristic interaction energies. In the new representation, the Hamiltonian can be written out as

$$H = \sum_{n, R_1, R_2} L_n(R_1 - R_2) \hat{a}_n^{s*}(R_1) \hat{a}_n^s(R_2) + \frac{1}{2} \sum_{n; R_1, R_2, R_3, R_4} v_n(R_1 R_2 R_3 R_4) \times \hat{a}_n^{s*}(R_1) \hat{a}_n^{s'*}(R_2) \hat{a}_n^{s'}(R_3) \hat{a}_n^s(R_4), \quad (4)$$

$$L_n(R_1 - R_2) = \sum_k (L_n^0(k) - \mu) e^{ik(R_1 - R_2)},$$

where

$$v(R_1 R_2 R_3 R_4) = \int dx dy v(x - y) W_n^*(x - R_1) \times W_n^*(y - R_2) W_n(y - R_3) W_n(x - R_4). \tag{5}$$

We introduce the Green function

$$G_n(RR'; t - t') = -2\pi i \theta(t - t') \langle [a_n^s(R, t), \bar{a}_n^s(R', t')]_{\pm} \rangle. \tag{6}$$

Here, $\hat{a}_n^s(R, t)$ and $\bar{a}_n^s(R', t')$ are the operators in the Heisenberg representation; $\theta(t - t')$ is the Heaviside step function; $[\cdot, \cdot]_{\pm}$ is the anticommutator; $\langle \cdot \rangle$ is the averaging over a grand canonical ensemble defined by Hamiltonian (4) and the parameter $\beta = \frac{1}{T}$, where T is the absolute temperature in energy units; and the summation is performed over the superscript s . It is obvious that this Green function obeys the equation

$$\sum_{R_1} \{ G_n^{(0)-1}(R - R_1; E) - \hat{M}(R, R_1; E) \} \times G_n(R_1, R'; E) = 2, \tag{7}$$

where $G_n^{(0)-1}$ is the inverse nonperturbed Green function, $G_n^{(0)-1}(R - R_1; E) = E\delta_{RR_1} - L_n(R - R_1)$, and \hat{M} is the mass operator $\{E$ is the parameter of the Fourier transform with respect to time $(t - t')$ \}.

Analysis of the solutions leads to the first density matrix (see [8–10]),

$$\rho(R, R') \equiv \hat{a}^{s*}(R) \hat{a}^s(R') = \frac{i}{2\pi} \int_{-\infty}^{+\infty} \frac{G(R, R'; E + i\varepsilon) - G(R, R'; E - i\varepsilon)}{e^{\beta E} + 1} dE. \tag{8}$$

Furthermore, by means of (2a), it is possible to determine the density $n(x)$ of actual particles. In a certain limit, the mass operator $M(R, R'; E)$ can be written out as a functional of the expression $\rho(R, R'; E)$. After performing certain transformations in accordance with [8–10], we obtain the nonlinear equation

$$G^{(0)-1}(p)G_0(p) + G_1(p) \sum_{\{k_s\}} \alpha(k_s) G^{(0)-1}\left(p + \frac{k_s}{2}\right) e^{ik_s X} - M_0(p)G_0(p) - \sum_{\{k_s\}} M_1(p, k_s) G_0\left(p - \frac{k_s}{2}\right) \alpha(k_s) e^{ik_s X} - \sum_{\{k_s\}} \sum_{\{k'_s\}} M_1\left(p - \frac{k_s}{2}, k_s\right) G_1\left(p + \frac{k'_s}{2}\right) \tag{9}$$

$$\times \alpha(k'_s) \alpha(k'_s) e^{i(k_s + k'_s) X} = 2,$$

which is reduced to a set of finite difference equations determining $G_0(p)$ and $G_1(p)$. Using (8), we then pass from $G_0(p)$ and $G_1(p)$ to $\eta_0^{(1)}(p)$ and $\eta_1^{(1)}(p)$, which obey the set of equations

$$\eta_0^{(1)}(p) = \hat{\Psi}_1\{\eta_0^{(1)}(p), \eta_1^{(1)}(p)\}, \tag{10}$$

$$\eta_1^{(1)}(p) = \hat{\Psi}_2\{\eta_0^{(1)}(p), \eta_1^{(1)}(p)\},$$

where Ψ_1 and Ψ_2 are nonlinear integral operators.

From physical considerations, the solution to Eq. (7) is spatially uniform as $T \rightarrow \infty$; i.e.,

$$\rho(R, R') = \rho^0(R, R') = \eta_0^{(1)}(R - R'). \tag{11}$$

For the set of Eqs. (7) with $T > T_{cr}$, we obtain that $\eta_1^{(1)} \equiv 0$ and $\eta_0^{(1)} \equiv \eta_0^{(0)}(R - R')$. In this case, the temperature T_{cr} is the point of a phase transition, i.e., loss of stability for the spatially uniform solution.

However, T_{cr} can be determined using the branching method, as was done in paper [9]. This method is based on the fact that, for $T < T_{cr}$, $T \rightarrow T_{cr}$, the functions

$$\delta\eta_0(p) = \eta_0^{(1)}(p) - \eta_0^{(0)}(p), \quad \delta\eta_1(p) = \eta_1^{(1)}(p) \tag{12}$$

tend to zero, remaining infinitesimal. Varying Eq. (10) with regard to (12), we obtain

$$\delta\eta_0(p) = \hat{A}_1\{\delta\eta_0(p), \delta\eta_1(p)\}, \tag{13}$$

$$\delta\eta_1(p) = \hat{A}_2\{\delta\eta_0(p), \delta\eta_1(p)\}.$$

Here, \hat{A}_1 and \hat{A}_2 are linear integral operators dependent on $\beta = \frac{1}{T}$ and μ .

The least positive eigenvalue β_{cr} of set (13) defines the highest phase transition temperature T_{cr} , depending on the particle density through μ . If a band is filled, then the particle density corresponding to it is $n(R) \equiv 2$ and the redistribution of the quantum state population is impossible; therefore, electronic crystallization does not occur.

Thus, the crystallization of the electron structure responsible for chemical bonds is possible only for atoms with unfilled electron shells. The theory proposed describes the DBT mechanism quite correctly. In the case of binary alloys of iron, this crystallization occurs provided the impurities have unfilled np -, nd -, and nf -electron shells [4, 5]. In order to reduce T_{cr} of the DBT for an alloy of iron, it is necessary to alloy the iron matrix using elements having filled np -, nd -, and nf -electron shells with large valence angles and long chemical bonds.

REFERENCES

1. A. A. Presnyakov, *Cold Brittleness* (Nauka, Alma-Ata, 1972).
2. V. I. Trefilov, Yu. V. Mil'man, and S. A. Firstov, *Physical Foundations of Refractory Metal Strength* (Naukova Dumka, Kiev, 1975).
3. *Mechanics. Novel in Foreign Science*, Vol. 40: *Atomic Theory of Fracture: Collection of Articles*, Ed. by V. V. Gol'dshtein (Mir, Moscow, 1987).
4. V. P. Larionov and Ya. S. Semenov, *Physical Foundations of Ductile-Brittle Transition of Low-Alloyed Steels of Iron Alloys* (Nauka, Novosibirsk, 1992).
5. V. P. Larionov and Ya. S. Semenov, Dokl. Akad. Nauk **335**, 54 (1994) [Phys. Dokl. **39**, 179 (1994)].
6. E. P. Wigner, Trans. Faraday Soc. **34**, 678 (1938).
7. G. L. Krasko, Fiz. Tverd. Tela (Leningrad) **7**, 1324 (1965) [Sov. Phys. Solid State **7**, 1070 (1965)].
8. A. G. Khachaturyan, *The Theory of Phase Transformations and the Structure of Solid Solutions* (Nauka, Moscow, 1974).
9. A. G. Khachaturyan, Fiz. Tverd. Tela (Leningrad) **5**, 26 (1963) [Sov. Phys. Solid State **5**, 16 (1963)].
10. S. V. Tyablikov, *Methods in the Quantum Theory of Magnetism* (Nauka, Moscow, 1965; Plenum, New York, 1967).

Translated by V. Bukhanov

The Avalanche-Development Rate for Runaway Relativistic Electrons under Normal Atmospheric Conditions

L. P. Babich, E. N. Donskoy, Corresponding Member of the RAS R. I. Il'kaev,
A. Yu. Kudryavtsev, I. M. Kutsyk, and B. N. Shamraev

Received March 19, 2001

INTRODUCTION

In [1], the authors proposed a mechanism governing giant ascending atmospheric discharges. This mechanism involves the development of an avalanche of relativistic runaway electrons. The avalanche is characterized by its exponential development with temporal and spatial scales t_e and $l_e = c \times t_e$ (where e is the avalanche-development rate). The quantity $\frac{1}{l_e}$ is the relativistic analog of the Townsend ionization coefficient α_T .

Three approaches were employed in the calculations: the numerical solution of the kinetic equation [2–4, 6, 7], the Monte Carlo simulation [5, 6], and the coarse-particle method [8]. In [6], the values of t_e calculated with the help of the kinetic equation and Monte Carlo simulation were compared. These values differ by a factor of 3 to 4 within the electric-field intensity range under consideration. Such a strong discrepancy leads to principle differences in the modeling of natural phenomena. The urgent necessity of thorough analysis of this discrepancy stimulated new calculations of t_e . These calculations are based on methods of the kinetic equation and Monte Carlo simulation with allowance (in the former case) for the exact correlation between the directions of motion of two electrons participating in an ionization event. The results of this analysis are presented below.

THE KINETIC EQUATION

We solve the following kinetic equation similar to that given in [2–4]:

$$\begin{aligned} & \frac{\partial f}{\partial t} + \frac{1}{p^2} \frac{\partial}{\partial p} [p^2 f (\mu e E - F(\epsilon))] \\ & + \frac{\partial}{\partial \mu} \left[e E \frac{1 - \mu^2}{p} f \right] - \frac{(Z/2 + 1) F(\epsilon)}{4 \gamma p} \frac{\partial}{\partial \mu} \left[(1 - \mu^2) \frac{\partial f}{\partial \mu} \right] \quad (1) \\ & = N \beta c \int_{2\epsilon + \epsilon_i}^{\infty} d\epsilon' \left(\frac{\gamma'^2 - 1}{\gamma^2 - 1} \right) \sigma_d(\epsilon, \epsilon') \frac{1}{\pi} \int_0^\pi d\alpha f(t, \epsilon', \mu'). \end{aligned}$$

Here, $f(t, p, \mu)$ is the electron distribution function for momenta and cosines of angles between the directions of p and the electric force eE , $F(\epsilon)$ is the Bethe friction force [9], ϵ_i is the energy of ionization, and N is the molecule concentration. The Möller formula [2, 3] is used for calculating the ionization differential cross section. In contrast to [2–4, 6], where the integral over α is replaced by the trapezoid formula, here the angles between the directions of the force eE and the momenta of primary ($\mu' = \cos \vartheta'$) and secondary ($\mu = \cos \theta$) electrons are linked by an exact relation [10]:

$$\begin{aligned} \mu' &= \mu \mu_0 + \sqrt{1 - \mu_0^2} \sin \theta \cos \alpha, \\ \mu_0 &= \frac{\sqrt{\epsilon(\epsilon' + 2mc^2)}}{\sqrt{\epsilon'(\epsilon + 2mc^2)}}. \end{aligned}$$

Since inelastic loss on the order of dozens of electronvolts dominates, it is assumed in (1) that the energy and angular distributions of primary electrons do not change in the ionization process [2–4]. This implies violation of the conservation laws, which are fulfilled only on the average: the actual energy loss in individual collisions is described by the averaged energy loss with the help of the continuous friction force $F(\epsilon)$. The average variation of the primary-electron momentum turns out to be zero because the friction force is always directed opposite to the momentum. These kinetic equations do not make it possible to allow for either energy-loss fluctuations or angular fluctuations; this is automatically taken into account by the Monte Carlo method.

Russian Federal Nuclear Center,
All-Russia Research Institute of Experimental Physics,
Sarov, Nizhni Novgorod oblast, 607180 Russia

We solved kinetic equation (1) using the finite difference method with splitting over the p and μ variables. Implicit conservative finite-difference schemes of first-order accuracy were employed. In calculating the diffusion part of the kinetic equation, we used the flow-sweep method. The integral over α was calculated according to the Simpson formula with the maximum number of points $n = 11$. Since the ionization time is much longer than the characteristic times of the electron transfer and scattering, the contribution of the ionization integral was recalculated after a given number of time steps and remained constant at intermediate steps. It was sufficient to calculate the ionization-integral contribution only for energies $\varepsilon > \varepsilon_{\text{th}}$ where the runaway threshold ε_{th} corresponds to the mean root of the equation $F(\varepsilon_{\text{th}}) = eE$ [11]. In the region $\varepsilon \leq \varepsilon_{\text{th}}$ under the description in terms of the averaged friction force, the electrons certainly cannot become runaway electrons.

MONTE CARLO SIMULATION

The Monte Carlo simulation is based on the codes used in [5, 6], namely, the basic ELIZA code and the simplified Monte Carlo (SMC) code. The ELIZA code [12] is intended for solving problems of the combined transfer of photons, electrons, and positrons. In the case of photons, Compton scattering (with allowance for the bound state of atomic electrons), Rayleigh scattering, photoabsorption (with due regard to the emission of fluorescent photons and Auger electrons), and electron-positron pair production are taken into consideration. For electrons and positrons, we took into account the elastic scattering on nuclei and free electrons, atomic K -shell ionization, bremsstrahlung, and two-photon annihilation. The description is based on the EPDL92 (photons), EEDL92 (electrons), and EADL92 (atomic-shell relaxation) cross-section data-banks. Here, a number of modifications improving the calculation accuracy were introduced compared to the code version used in [5, 6]. In the case of the SMC code, the motion of electrons between subsequent collisions is described by the electric force eE and the friction force $F(\varepsilon)$. Only elastic scattering and ionization collisions accompanied by the production of electrons with energies on the order of several kiloelectronvolts are statistically simulated. The Rutherford cross section for the screened Coulomb potential is used to describe the elastic scattering of electrons on atomic nuclei. For the ionization differential cross section σ_d , the Möller formula is used. The SMC code makes it possible to efficiently perform necessary calculations in the framework of the physical model corresponding to the kinetic equation. A provision for eliminating variations in the energy and momentum of the primary electron in an ionizing collision is made that corresponds to violation of the conservation laws in kinetic equation (1).

DISCUSSION OF THE RESULTS

The calculations were performed in air ($\varepsilon_r = 15$ eV) under atmospheric pressure ($P = 1$ atm, $N = 2.7 \times 10^{19}$ cm $^{-3}$). It was assumed that two-MeV electrons had been injected at the initial time moment into a homogeneous electric field along the direction of the electric-force action. The number $N_{\text{run}}(t)$ of runaway electrons as a function of time was calculated. In the kinetic equation, the number N_{run} is defined as the number of electrons with energies $\varepsilon \geq \varepsilon_{\text{th}}$. In the case of the Monte Carlo method, N_{run} corresponds to the number of electrons whose trajectories are traced to the energies $\varepsilon = 1$ keV. Since the fraction of electrons in the region $\varepsilon \leq \varepsilon_{\text{th}}$ is on the order of several percent, both definitions are close to each other to within good accuracy. To reduce the role of the initial stage of developing the relativistic-electron avalanche, the quantity t_e is defined as

$\left(\frac{\partial \ln N_{\text{run}}}{\partial t}\right)^{-1}$, where the derivative is taken in that time moment when the dependence $\ln N_{\text{run}}(t)$ becomes linear. In the Monte Carlo calculations, smoothing of $\ln N_{\text{run}}(t)$ was performed. Analytical estimates similar to those performed in [5] were carried out. The values of t_e were calculated for three overvoltages $\delta = \frac{eE}{F_{\text{min}}P}$ with

respect to the relativistic minimum of the Bethe force $F_{\text{min}} = 2.18$ keV/(cm atm) (see Table 1).

Results without allowance for elastic scattering.

In this case, the analytical estimates agree with the results based on the SMC code. The results that take into account the conservation laws in the ionization process turned out to be intermediate between the results for the SMC code, which admit the violation of the conservation laws, and the results for the ELIZA code. The discrepancy between the calculations according to the SMC code with and without violation of the conservation laws taken into account are explained by fluctuations in the energy loss. The divergence of 25 to 30% for the results obtained in accordance with the ELIZA and SMC codes under the condition that the conservation laws are valid is caused by the difference in the ionization cross sections and different descriptions of the inelastic processes.

By virtue of the same physical models, the values of t_e obtained from the solution to kinetic equation (1) must be close to the SMC-code calculations without exact fulfillment of the conservation laws in the ionization process. However, the results of the solution to kinetic equation (1) for $n = 11$ are considerably higher than in the case of the calculations according to the SMC code with the violated conservation laws and are close to the results of the ELIZA code. This fact, apparently, is a consequence of the rough angular-coordinate net and the numerical diffusion in solving the kinetic equation.

Characteristic time t_e , ns of the avalanche development in air, $P = 1$ atm

| Method | Electron scattering is ignored | | | Electron scattering is taken into account | | |
|------------------------------------|--------------------------------|--------------|--------------|---|--------------|--------------|
| | $\delta = 2$ | $\delta = 5$ | $\delta = 8$ | $\delta = 2$ | $\delta = 5$ | $\delta = 8$ |
| Analytical estimates [5] | 48–59 | 11–18 | 6–10 | 145 | 31.4 | 16.7 |
| Coarse-particle method [8] | | | | ? | 26 | 12.5 |
| Kinetic equation | | | | | | |
| reduction of [4] to 1 atm, $n = 2$ | 19.5 | 4.3 | 2.17 | 96 | 13 | 6 |
| this work, $n = 2$ | 19.9 | 5.05 | 2.24 | 95 | 13 | 5.6 |
| this work, $n = 11$ | 98 | 31 | 16.3 | 197 | 39.9 | 21.2 |
| Monte Carlo Method | | | | 174.4 | 33.2 | 17.3 |
| paper [7] SMC code: | | | | | | |
| conservation laws are violated | 46.1 | 14.8 | 8.6 | 182 | 34.1 | 17.9 |
| conservation laws are fulfilled | 77.6 | 20.8 | 11.2 | 200 | 35.6 | 18.6 |
| ELIZA code | 107 | 28 | 15.8 | 440 | 54 | 27.5 |

Note: $\delta = \frac{E}{2.18 \text{ kV cm}^{-1}}$.

The results of calculating t_e according to the kinetic equation with $n = 2$ (i.e., with using the trapezoid formula as was done in [4]) are close to the results of [4]. For $n = 11$, the values for t_e differ by several times from those obtained according to the SMC and ELIZA codes.

Results with allowance for elastic scattering. All conclusions made for calculations without elastic scattering taken into account remain valid. However, there also exist certain differences: (i) The analytical estimates being dependent (the SMC-code results are used for the fraction of electrons passing to the runaway mode) satisfactorily agrees with the calculations by the SMC code without exact fulfillment of the conservation laws. (ii) Another difference consists in the fact that the calculation results for the kinetic equation ($n = 11$) and for the SMC code are close to one another. It is probable that with the elastic scattering taken into account, the numerical diffusion weakly affects the results obtained. (iii) The SMC code yields very close values of t_e for both the validity and violation of the conservation laws. This implies that the effect of scattering is stronger than the fluctuation effect. (iv) In contrast, the allowance for scattering enhances the divergence up to 35 to 100% between the values of t_e obtained according to the ELIZA and SMC codes with the conservation laws fulfilled. This fact is most likely associated with the difference in the values used for the scattering cross sections. As a whole, the allowance for elastic collisions increases the energy threshold ε_{th} . The calculation results differ by a factor of 1.5 to 3.5 for different variants under consideration.

As is seen from the table, the simplified methods, namely, the kinetic equation, the use of the SMC code, the calculations of Lehtinen *et al.* [7], and the coarse-

grain method [8], yield surprisingly close results. Inadequacy of the coarse-grain method to the stochastic nature of runaway electrons provides, most likely, the lowest value of t_e [8]. The ELIZA code involving the most complete and accurate set of cross sections for elementary interactions is the most exact. Being free of simplifications (explicitly or implicitly) intrinsic to other approaches, the ELIZA code realizes a direct numerical experiment whose results, in essence, can be reasonably used for calibration of less precise methods.

CONCLUSION

There exists a main reason for the divergence of the development rate for an avalanche of relativistic runaway electrons, which was obtained in [2–4, 6] by the Monte Carlo method and from the solution to the kinetic equation. This reason is the inadequacy of the accepted approximation for the ionization-collision-integral used in solving the kinetic equation to the strongly anisotropic runaway process.

Solving the kinetic equation using the finite-difference method with a rough approximation of the ionization integral ($n = 2$), which is similar to that employed in [2–4, 6], yields results that coincide with those of [2–4, 6].

For sufficiently high overvoltages ($\delta = 5$ and 8), the calculated results for t_e , which are based on the kinetic equation with improved approximation of the ionization integral ($n = 11$), and the simulation results obtained by the Monte Carlo method (SMC code, the calculations of Lehtinen *et al.* [7]) are close to each other. They agree with analytical estimates and considerably approach the calculation results obtained according to the ELIZA code.

With decreasing δ , the divergence from the ELIZA-code results is enhanced. This fact is, most likely, associated with the differences in interaction cross sections, as well as in the method of description of the elementary interactions.

ACKNOWLEDGMENTS

The authors express their gratitude to Mrs. S. Voss and Dr. S. Gitomer for their invaluable work in organizing the collaboration between the Los Alamos National Laboratory and the All-Russia Scientific Research Institute of Experimental Physics. The authors are also grateful to Corresponding Member of the RAS A.V. Gurevich, Dr. R. Roussel-Dupre, and Dr. E. Symbalisty for their fruitful cooperation in the framework of the International Scientific-Technological Center, project no. 490.

REFERENCES

1. A. V. Gurevich, G. M. Milikh, and R. A. Roussel-Dupre, *Phys. Lett. A* **165**, 463 (1992).
2. R. A. Roussel-Dupre, A. V. Gurevich, T. Tunnell, and G. M. Milikh, *Kinetic Theory of Runaway Air Breakdown and Implications for the Lightning Initiation*, Report LA-12601-MS (LANL, Los Alamos, 1993), pp. 1–51.
3. R. A. Roussel-Dupre, A. V. Gurevich, T. Tunnell, and G. M. Milikh, *Phys. Rev. E* **49**, 2257 (1994).
4. E. M. D. Symbalisty, R. A. Roussel-Dupre, and V. Yukhimuk, *IEEE Trans. Plasma Sci.* **26**, 1575 (1998).
5. L. P. Babich, I. M. Kutsyk, E. N. Donskoy, and A. Yu. Kudryavtsev, *Phys. Lett. A* **245**, 460 (1998).
6. E. M. D. Symbalisty, R. A. Roussel-Dupre, L. P. Babich, *et al.*, *EOS Trans. Am. Geophys. Union* **78**, 4760 (1997).
7. N. G. Lehtinen, T. F. Bell, and U. S. Inan, *J. Geophys. Res.* **104**, 24699 (1999).
8. A. A. Solovyev, V. A. Terekhin, V. T. Tikhonchuk, and L. L. Altgilbers, *Phys. Rev. E* **60**, 7360 (1999).
9. H. A. Bethe and J. Ashkin, in *Experimental Nuclear Physics* (Wiley, New York, 1953), Vol. 1, p. 277.
10. T. Holstein, *Phys. Rev.* **70**, 367 (1946).
11. L. P. Babich, *Teplofiz. Vys. Temp.* **33**, 659 (1995).
12. E. N. Donskoy, *Vopr. At. Nauki Tekh., Ser. Mat. Model. Fiz. Protsessov* **1**, 3 (1993).

Translated by G. Merzon

Phenomenological Molecular Theory of the Translational Absorption Band and of the Isotopic Effect for Liquid Water near 200 cm^{-1} [¶]

V. I. Gaiduk*, B. M. Tseitlin*, and Ch. M. Briskina**

Presented by Academician N.D. Devyatkov November 16, 2000

Received December 27, 2000

The icelike structure and diffusion of molecules of liquid water exhibit both a two-humped far-infrared (far-IR) absorption spectrum and a low-frequency Debye relaxation spectrum [3–5]. An absorption translational band with wave number $\nu_T = 200\text{ cm}^{-1}$ appears due to the vibration of neighboring oxygen H-bonded atoms [6–8]. This wave number $\nu = \frac{\omega}{2\pi c}$ (furthermore called frequency) is approximately the same for ordinary and heavy water (isotopic effect). (Here, ω is the angular frequency and c is the speed of light.) In the libration band that is due to the reorientation of polar molecules, the frequency ν_L of the absorption peak, by approximately a factor of $\sqrt{2}$, is lower for D_2O compared to H_2O , namely, $\nu_L \approx 670\text{ cm}^{-1}$ for H_2O , while it is $\approx 500\text{ cm}^{-1}$ for D_2O . This difference corresponds to that of the moments of inertia I for these molecules. In the libration band, the absorption spectrum $\alpha(\nu)$ and complex-permittivity spectra $\epsilon^*(\nu) = \epsilon' + i\epsilon''$ (* is the complex-conjugation symbol) can be described [9] on the basis of phenomenological molecular theory. An adequate description has not thus far been given for the frequency dependences $\alpha(\nu)$ and $\epsilon^*(\nu)$ of a translational band.

In this paper, a theory of the translational bands and of the isotopic effect, which is based on the simplified model of a nonrigid dipole, is proposed. The model is illustrated in Fig. 1. The dipole moment of a molecule is assumed to comprise a superposition of time-inde-

pendent and time-dependent components $\bar{\mu}$ and $\tilde{\mu}(t) = \mu_T \sin(\omega_T t + \gamma)$, where $\omega_T = 2\pi c\nu_T$. This idea is implied by the fact that the average dipole moment μ of a molecule in a liquid differs from the moment μ_0 of an isolated molecule. The time-dependent component $\tilde{\mu}(t)$ is considered to be stipulated by the vibration of H-bonded oxygen atoms. In Fig. 1, the latter are denoted by white circles. These vibrations are directed along the H-bond. The hydrogen atoms (denoted by symbols B) penetrate into the negatively charged cloud formed by a nonshared electron pair of the oxygen atom (denoted by the symbol A) and thereby change the charge distribution in the cloud. Thus, the resulting dipole moment of a water molecule varies with time. We suppose it to be directed along a line connecting the centers of masses of the oxygen atom A and the pair B,B of the hydrogen atoms of a neighboring water molecule.

In the theory developed in [9, 10], a dipole spectral function $L(z)$ is introduced, where z is the complex frequency (which is defined below). Then, with allowance for the time-dependent component of the dipole-moment $\tilde{\mu}$, the modified spectral function [henceforth

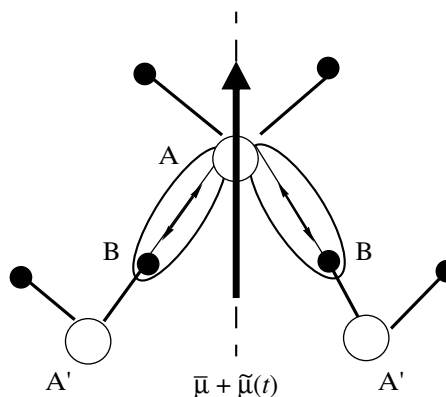


Fig. 1. Explanation of the appearance of the time-dependent dipole moment in a water molecule (the resulting moment is marked by the thick vertical arrow).

[¶] This paper is based on reports [1, 2]. The article was submitted by the authors in English.

* Institute of Radio Engineering and Electronics
(Fryazino Branch), Russian Academy of Sciences,
pr. Vvedenskogo 1, Fryazino,
Moscow oblast, 141120 Russia

** Institute of Radio Engineering and Electronics,
Russian Academy of Sciences,
Mokhovaya ul. 18, Moscow, 103907 Russia

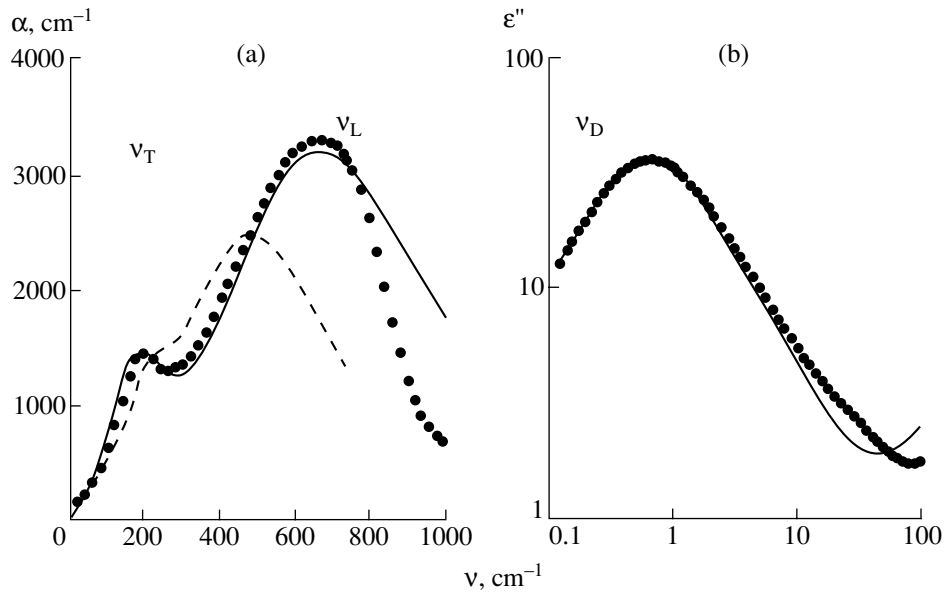


Fig. 2. Frequency dependences for (a) the absorption coefficient and (b) permittivity imaginary part of liquid water at 27°C. Solid and dashed lines correspond to calculations for ordinary and heavy water on the basis of the hybrid model. Dots in Fig. 2a are experimental data for the absorption coefficient [3, 4, 12]. Dots in Fig. 2b correspond to the results of dielectric-loss calculations based on the empirical formula [4]. ν_T , ν_L , and ν_D are experimental values of the absorption-peak frequencies in the translational band, in the libration band, and in the dielectric-loss frequency maximum, respectively.

denoted by $S(z)$] can be written out in terms of $L(z)$ in the form

$$S(z) \approx L(z) + \frac{\sigma^2}{4} \left[\frac{p}{p-z} + \frac{p}{p+z} + z \left\{ \frac{L(z+p)}{p+z} - \frac{L(z-p)}{p-z} \right\} \right]. \quad (1)$$

Here, $p = \omega_T \eta$ is the normalized frequency of the translational-band peak; $\eta \equiv \sqrt{\frac{I}{2k_B T}}$, k_B is the Boltzmann constant; T is temperature; $z = x + iy$; $x = \eta\omega$; $y = \frac{\eta}{\tau}$; and τ is the mean lifetime of a dipole libration in a potential well of a given shape. The model parameter $\sigma^2 = \left\langle \frac{\tilde{\mu}^2(0)}{\bar{\mu}^2} \right\rangle$ is fitted by comparing experimental and theoretical data. The value of this parameter is used for estimating the time-independent component $\bar{\mu}$ and the amplitude μ_T of the time-dependent component. They are related to the average dipole moment of a molecule in the liquid by the relations

$$\bar{\mu} = \frac{\mu}{\sqrt{1 + \sigma^2}}, \quad \mu_T = \frac{\mu \bar{\sigma}}{\sqrt{1 + \sigma^2}} \sqrt{1 - f(X)},$$

where

$$X = \frac{\sigma_0}{\bar{\sigma}}, \quad f(X) = \frac{\exp(-X^2)}{\sqrt{\pi} \operatorname{erf}(X)},$$

and σ is found as the solution to the transcendental equation

$$\sigma^2 = \frac{\sigma_0^2}{2X^2} [1 - 2f(X)],$$

while $\sigma_0 = 1 - \frac{\mu_0}{\mu}$ is determined by known values of μ_0 and μ of the dipole moment. In addition, the ratio $X = \frac{\sigma_0}{\bar{\sigma}}$ must satisfy the inequality $\frac{1}{X^2} [1 - f(X)] \leq 1$.

The main contribution to the translational band is given by the Lorentzian $\frac{p}{p-z} + \frac{p}{p+z}$. However, the translational band calculated from Eq. (1) is too narrow. This drawback to the theory can be excluded by introducing the lifetime τ_T of the dipole moment $\tilde{\mu}(t)$, which differs from τ . In other words, we decrease the duration of an individual period in the regular variation of $\tilde{\mu}(t)$. In this case, we replace z and y in the Lorentzian and in the terms $\frac{z}{z \pm p}$ by $Z = x + iY$ and $Y \equiv \frac{\eta}{\tau_T}$, respectively.

Further calculations were carried out for a rectangular intermolecular potential well having a finite depth U_0 , which was considered in the framework of the hybrid model developed in [9, 11]. The orientational susceptibility χ^* is connected (see [9, p. 191; 10, 11]) to the resulting spectral function S through the rational relation

$$\chi^*(x) = \frac{gGzS}{gx + iy(1 + gxz)S},$$

$$g = \frac{\epsilon_s - n_\infty^2}{4\pi G} \frac{2\epsilon_s + n_\infty^2}{3\epsilon_s},$$

$$G = \frac{\bar{\mu}^2 N}{3k_B T}, \quad N = \frac{N_A \rho}{M}, \quad \mu = \frac{\mu_0 k_\mu (n_\infty^2 + 2)}{3}.$$

Here, g is the Kirkwood correlation factor; ϵ_s is the static permittivity; n_∞ is the optic refractive index; ρ is the density of the liquid; M is the molecular mass; N_A is the Avogadro's number; and k_μ is the correcting factor for the dipole moment of a molecule in the liquid. The formulas given above can be used for calculating the frequency dependences $\epsilon^*(\nu)$ and $\alpha(\nu)$.

The following parameters are used in the hybrid-model version under consideration: β , which is the libration amplitude entering into the spectral function, and L , τ , τ_T , σ^2 , and k_μ . The frequency dependence $\alpha(\nu)$ of the absorption coefficient for ordinary and heavy water is shown in Fig. 2a. The theoretical and experimental spectra of the dielectric loss $\epsilon''(\nu)$ are compared in Fig. 2b. The fitted and estimated model parameters for ordinary and heavy water at 27°C are presented here.

| Molecular constants | ϵ_s | τ_D , ps | n_∞^2 | $I \times 10^{40}$, g cm ² | ν_L , cm ⁻¹ | ν_T , cm ⁻¹ | M |
|-------------------------|--------------|---------------|---------------|---|----------------------------|----------------------------|-------------|
| H ₂ O | 76.6 | 7.85 | 1.7 | 1.483 | 670 | 200 | 18 |
| D ₂ O | 79.2 | 8.5 | 1.7 | 2.765 | 505 | 200 | 20 |
| Hybrid-model parameters | | τ , ps | τ_T , ps | k_μ | β | $\langle \sigma^2 \rangle$ | p |
| H ₂ O | | 0.38 | 0.054 | 1.080 | 19.9° | 0.010 | 1.7 |
| D ₂ O | | 0.33 | 0.089 | 1.116 | 19.9° | 0.014 | 2.2 |
| Estimated parameters | | y | Y | σ_0 | $\bar{\sigma}$ | $\bar{\mu}/\mu$ | μ_T/μ |
| H ₂ O | | 0.11 | 0.78 | 0.25 | 0.150 | 0.995 | 0.146 |
| D ₂ O | | 0.17 | 0.65 | 0.27 | 0.340 | 0.99 | 0.255 |

Our model makes it possible to explain the far-IR isotopic effect (cf. solid and dashed lines in Fig. 2a near the absorption-peak frequency ν_T) and the low-frequency dependence $\epsilon''(\nu)$ of the dielectric loss. The ratio of the lifetime τ to the mean libration period $\langle T_L \rangle$ is approximately half an order of magnitude. Therefore, dipoles execute several cycles of libration motion during their lifetime. The translational oscillations are more damped: the lifetime τ_T is shorter than the period $\frac{2\pi}{\omega_T}$. This result is in agreement with the conclusion of [13] on the rapid energy dissipation via the H-bond network in water. The time-independent component $\bar{\mu}$ is close to its mean value μ , while the amplitude μ_T of the time-dependent component comprises a noticeable fraction of μ : it is 15% for H₂O and 25% for D₂O. As distinct from ordinary water, heavy water is characterized by a deeper potential well.

We emphasize the fact that, previously, in [9, 14], only the formal description of the spectra $\alpha(\omega)$ and $\epsilon^*(\omega)$ in ordinary and heavy water and of the isotopic effect was given by introducing an additional potential well. In this study, the consideration is restricted to only one (rectangular) well.

ACKNOWLEDGMENTS

The authors are grateful to A.K. Lyashchenko for fruitful discussion of the results of this work.

REFERENCES

1. V. I. Gaïduk and V. F. Zolin, in *Millimeter Waves in Medicine and Biology* (Inst. Radiotekh. Élektron., Ross. Akad. Nauk, Moscow, 2000), pp. 141–143.
2. T. A. Babushkina, Ch. M. Briskina, V. I. Gaïduk, and T. P. Klimova, in *Millimeter Waves in Medicine and Bio-*

- logy (Inst. Radiotekh. Élektron., Ross. Akad. Nauk, Moscow, 2000), pp. 136–138.
3. H. D. Downing and D. Williams, *J. Geophys. Res.* **80**, 1656 (1975).
 4. H. J. Liebe, G. A. Hufford, and T. Manabe, *Int. J. Infrared Millim. Waves* **12**, 659 (1991).
 5. C. Rønne, P.-O. Astrand, and S. R. Keiding, *Phys. Rev. Lett.* **82**, 2888 (1999).
 6. C. H. Cartwright, *Phys. Rev.* **49**, 470 (1936).
 7. G. E. Walrafen, in *Water, a Comprehensive Treatise* (Plenum, New York, 1972), Vol. 1, pp. 151–214.
 8. N. Agmon, *J. Chem. Phys.* **100**, 1072 (1996).
 9. V. I. Gaiduk, *Dielectric Relaxation and Dynamics of Polar Molecules* (World Scientific, Singapore, 1999).
 10. V. I. Gaiduk and B. M. Tseitlin, *Adv. Chem. Phys.* **87**, 125 (1994).
 11. V. I. Gaïduk and V. V. Gaïduk, *Zh. Fiz. Khim.* **71**, 1818 (1997).
 12. P. P. Sethna, K. F. Palmer, and D. Williams, *J. Opt. Soc. Am.* **68**, 815 (1978).
 13. S. Woutersen and H. J. Bakker, *Nature* **402**, 507 (1999).
 14. V. I. Gaïduk, O. F. Nielsen, and T. A. Perova, *J. Mol. Liquids* (2001) (in press).

PHYSICS

The Rouse Model for Oligomer Chains

V. I. Irzhak

Presented by Academician G.M. Eliashberg February 7, 2001

Received March 5, 2001

The Rouse model [1], which represents a system of Maxwell elements—dampers (balls) and springs connected-in-series—is widely used to describe the relaxation properties of polymer chains. To calculate this model, it is important to assume that the number of such elements is sufficiently large. In this case, a discrete set of differential-difference equations describing the motion of balls can be represented in a continuous form [1–3] as a single second-order equation in partial derivatives. It is evident that, for sufficiently short chains, one should solve the problem using a relatively small number of equations. The objective of the present work is to find such a solution.

Let a force F be applied through a spring to the first element of the system. The initial deformation of the spring connected with the first element decreases as a result of the displacement of this element, and the rate of strain change is assumed to be equal to the rate of change of element displacement. Thus,

$$\frac{dL}{dt} = \frac{1}{E} \frac{dF}{dt} = \frac{dx_1}{dt} = \frac{1}{\eta} F - \frac{E}{\eta} (x_1 - x_2). \quad (1)$$

Here, L is the spring length, η is the viscosity of the medium (viscous interaction between the ball and the medium), and x_i is the coordinate of the i th ball.

The rate of displacement of all the n balls is determined by the elastic action of the springs connected to the given ball. Therefore, the relaxation of the system comprising n balls is accounted for by the set of $n + 1$ equations

$$\begin{aligned} \tau \dot{F} &= -F + E(x_1 - x_2), \\ \tau \dot{x}_1 &= \frac{F}{E} - x_1 + x_2, \\ \tau \dot{x}_2 &= x_1 - 2x_2 + x_3, \\ &\dots \end{aligned} \quad (2)$$

$$\tau \dot{x}_i = x_{i-1} - 2x_i + x_{i+1},$$

...

$$\tau \dot{x}_n = x_{n-1} - x_n,$$

where $\tau = \frac{\eta}{E}$ is the time of relaxation of a Maxwell element.

Note that the Rouse model [1] considers system (2) without the first, second, and last equations, because the role of these equations for a system consisting of a large number of elements is assumed to be inessential. However, for short chains, we cannot ignore these equations.

To solve set (2) as a combination of exponential terms, it is necessary to find their indices, which are determined as the roots of the polynomial [4]:

$$D_n = \begin{vmatrix} z-1 & E & -E & 0 & 0 \dots 0 & 0 & 0 \\ \frac{1}{E} & z-1 & 1 & 0 & 0 \dots 0 & 0 & 0 \\ 0 & 1 & z-2 & 1 & 0 \dots 0 & 0 & 0 \\ \dots & & & & & & \\ 0 & 0 & 0 & 0 & 0 \dots 1 & z-2 & 0 \\ 0 & 0 & 0 & 0 & 0 \dots 0 & 1 & z-1 \end{vmatrix} = 0. \quad (3)$$

The transformation of the determinant D_n results in the determinant B_n :

$$D_n = z \begin{vmatrix} z-2 & 1 & 0 & 0 \dots 0 & 0 & 0 \\ 1 & z-2 & 1 & 0 \dots 0 & 0 & 0 \\ 0 & 1 & z-2 & 1 \dots 0 & 0 & 0 \\ \dots & & & & & \\ 0 & 0 & 0 & 0 \dots 1 & z-2 & 1 \\ 0 & 0 & 0 & 0 \dots 0 & 1 & z-1 \end{vmatrix} = z B_n. \quad (4)$$

Equality (4) means that nonzero roots of the polynomial D_n are determined by the equality $B_n = 0$.

Institute of Chemical Physics Problems,
Russian Academy of Sciences, Chernogolovka,
Moscow oblast, 142432 Russia

It can be readily shown that the quantity B_n obeys the recurrence relationship

$$B_n = (z - 2)B_{n-1} - B_{n-2}, \quad (5)$$

which, on account of the obvious equalities

$$B_1 = z - 1, \quad B_2 = (z - 2)(z - 1) - 1,$$

enables one to find numerical solutions to polynomials of arbitrarily high degree.

Table 1 lists the roots of Eq. (4) for some values of n . As can be seen, the minimum relaxation time τ_{\min} is close to $\frac{\tau}{4}$. Only one third of all the values of τ_i turns out to be higher than τ .

Figure 1 shows the dependence of τ_i (in the coordinates of the Rouse equation) on the mode number (the highest value of τ_i corresponds to the minimum mode number). According to [1],

$$\tau_i^{-1} = 4 \sin^2\left(\frac{\pi i}{2n+1}\right). \quad (6)$$

It is seen that this dependence tends asymptotically

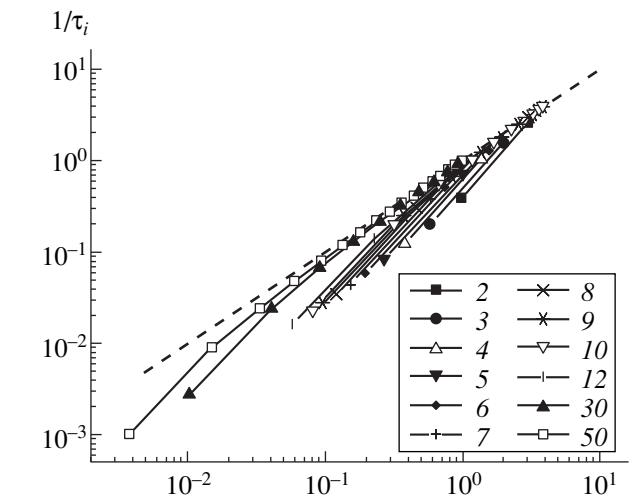


Fig. 1. Dependence of relaxation time on the mode number in the coordinates of the Rouse equation. The number of the mode is shown in the figure. The straight line corresponds to the dependence based on the Rouse model.

to the value defined by formula (6) as the time of relaxation decreases and the number n increases; however, for high values, the deviations (toward higher τ_i values) are quite significant.

Table 1. Parameters of Eq. (7) for various chain lengths n

| i | 1 | 2 | 3 | 4 | 5 | 6 | 7 | 8 | 9 | 10 |
|-----------|-------|--------|--------|-------|-------|-------|-------|-------|-------|-------|
| p_{1i} | 1 | | | | | | | | | |
| a_{1i} | 1 | | | | | | | | | |
| p_{2i} | 0.382 | 2.618 | | | | | | | | |
| a_{2i} | 0.724 | 0.276 | | | | | | | | |
| p_{3i} | 0.198 | 1.555 | 3.247 | | | | | | | |
| a_{3i} | 0.605 | 0.237 | 0.157 | | | | | | | |
| p_{4i} | 0.121 | 1.000 | 2.347 | 3.532 | | | | | | |
| a_{4i} | 0.431 | 0.333 | 0.184 | 0.052 | | | | | | |
| p_{5i} | 0.081 | 0.690 | 1.715 | 2.831 | 3.682 | | | | | |
| a_{5i} | 0.356 | 0.301 | 0.208 | 0.106 | 0.029 | | | | | |
| p_{6i} | 0.058 | 0.503 | 1.291 | 2.241 | 3.136 | 3.771 | | | | |
| a_{6i} | 0.303 | 0.269 | 0.2083 | 0.135 | 0.066 | 0.018 | | | | |
| p_{7i} | 0.044 | 0.382 | 1.000 | 1.791 | 2.618 | 3.338 | 3.827 | | | |
| a_{7i} | 0.264 | 0.241 | 0.200 | 0.147 | 0.092 | 0.044 | 0.011 | | | |
| p_{8i} | 0.034 | 0.300 | 0.795 | 1.453 | 2.184 | 2.891 | 3.478 | 3.865 | | |
| a_{8i} | 0.233 | 0.218 | 0.188 | 0.150 | 0.107 | 0.065 | 0.031 | 0.008 | | |
| p_{9i} | 0.027 | 0.241 | 0.645 | 1.197 | 1.835 | 2.491 | 3.094 | 3.578 | 3.892 | |
| a_{9i} | 0.209 | 0.1969 | 0.179 | 1.444 | 0.118 | 0.074 | 0.055 | 0.020 | 0.003 | |
| p_{10i} | 0.022 | 0.198 | 0.534 | 1.000 | 1.555 | 2.149 | 2.731 | 3.247 | 3.652 | 3.911 |
| a_{10i} | 0.188 | 0.182 | 0.164 | 0.143 | 0.116 | 0.088 | 0.060 | 0.036 | 0.017 | 0.004 |

Table 2. Coefficients of the initial values of the k th derivatives of $F^{(k)}(0)$

| k | $\frac{F^{(k)}(0)}{F(0)}$ |
|-----|---------------------------|
| 1 | $-\frac{1}{\tau}$ |
| 2 | $\frac{2}{\tau^2}$ |
| 3 | $-\frac{5}{\tau^3}$ |
| 4 | $\frac{14}{\tau^4}$ |
| 5 | $-\frac{42}{\tau^5}$ |
| 6 | $\frac{132}{\tau^6}$ |
| 7 | $-\frac{429}{\tau^7}$ |
| 8 | $\frac{1430}{\tau^8}$ |
| 9 | $-\frac{4862}{\tau^9}$ |
| 10 | $\frac{16896}{\tau^{10}}$ |

Once the roots of Eq. (4), i.e., the indices of exponential terms, are found, it is possible to calculate the pre-exponential terms a_i in the equation

$$F(t) = \sum_{i=1}^n a_i \exp\{-p_i t\}. \quad (7)$$

To do so, we should set up n algebraic equations relating the coefficients a_i to the initial conditions.

The consecutive differentiation of the set of equations (2) gives rise to the following set of algebraic equations, in which superscript (k) denotes the initial value of the k th derivative of the corresponding quantity:

$$\begin{aligned} \tau F^{(1)}(0) &= -F(0), \\ \tau F^{(2)}(0) &= -F^{(1)}(0) + E x_1^{(1)}(0), \\ \tau F^{(3)}(0) &= -F^{(2)}(0) + E(x_1^{(2)}(0) - x_2^{(2)}(0)), \dots, \\ \tau F^{(k)}(0) &= -F^{(k-1)}(0) + E(x_1^{(k-1)}(0) - x_2^{(k-1)}(0)), \dots, \end{aligned}$$

$$\tau x_1^{(1)}(0) = \frac{1}{E} F(0),$$

$$\tau x_1^{(2)}(0) = \frac{1}{E} F^{(1)}(0) - x_1^{(1)}(0) + x_2^{(1)}(0),$$

$$\tau x_1^{(3)}(0) = \frac{1}{E} F^{(2)}(0) - x_1^{(2)}(0) + x_2^{(2)}(0), \dots,$$

$$\tau x_1^{(k)}(0) = \frac{1}{E} F^{(k-1)}(0) - x_1^{(k-1)}(0) + x_2^{(k-1)}(0), \dots, \quad (8)$$

$$\tau x_2^{(1)}(0) = 0,$$

$$\tau x_2^{(2)}(0) = x_1^{(1)}(0),$$

$$\tau x_2^{(3)}(0) = x_1^{(2)}(0) - 2x_2^{(2)}(0),$$

$$\tau x_2^{(4)}(0) = x_1^{(3)}(0) - 2x_2^{(3)}(0) + x_3^{(3)}(0), \dots,$$

$$\tau x_3^{(1)}(0) = \tau x_3^{(2)}(0) = 0,$$

$$\tau x_3^{(3)}(0) = x_2^{(2)}(0),$$

$$\tau x_3^{(4)}(0) = x_2^{(3)}(0) - 2x_3^{(3)}(0),$$

$$\tau x_3^{(5)}(0) = x_2^{(4)}(0) - 2x_3^{(4)}(0) + x_4^{(4)}(0), \dots$$

The results of calculations are given in Table 2. The consecutive differentiation of Eq. (7) yields

$$F^{(k)}(0) = (-1)^k \sum_{i=1}^n p_i^k a_i. \quad (9)$$

Using n such equations with coefficients $F^{(k)}(0)$ listed in Table 2 enables us to determine all a_i values, which are given in Table 1.

Using the obtained values of the relaxation times τ_i (in units of τ) and their spectrum (a_i), we can calculate the mean values

$$\langle \tau \rangle_n = \sum_{i=1}^n a_i \tau_i \quad \text{and} \quad \langle \tau \rangle_w = \frac{\sum_{i=1}^n a_i \tau_i^2}{\sum_{i=1}^n a_i \tau_i}. \quad (10)$$

These values are given in Table 3, and their dependence on n is shown in Fig. 2.

As with the Rouse model, the quantity $\langle \tau \rangle_n$ turns out to be proportional to the length of the chain, whereas the dependence of $\langle \tau \rangle_w$ and τ_{\max} on the length of the chain is stronger. In the latter case, the relationship

Table 3. The mean values of the relaxation time

| n | $\langle \tau \rangle_n$ | $\langle \tau \rangle_w$ | $\gamma = \frac{\langle \tau \rangle_w}{\langle \tau \rangle_n}$ | τ_{\max} | $\langle \tau \rangle_n^*$ | $\langle \tau \rangle_w^*$ | $\langle \tau \rangle_w^{**}$ |
|-----|--------------------------|--------------------------|--|---------------|----------------------------|----------------------------|-------------------------------|
| 2 | 2.00 | 2.50 | 1.25 | 2.62 | 1.91 | 2.62 | 2.62 |
| 3 | 3.02 | 4.77 | 1.46 | 5.05 | 3.06 | 5.05 | 5.05 |
| 4 | 3.99 | 7.47 | 1.87 | 8.29 | 3.90 | 7.64 | 7.48 |
| 5 | 5.00 | 11.00 | 2.20 | 12.34 | 4.83 | 11.36 | 11.20 |
| 6 | 6.01 | 15.20 | 2.53 | 17.21 | 5.76 | 15.82 | 15.66 |
| 7 | 6.97 | 19.83 | 2.85 | 22.88 | 6.83 | 20.24 | 21.81 |
| 8 | 8.01 | 25.55 | 3.19 | 29.32 | 7.82 | 26.14 | 25.81 |
| 9 | 9.08 | 32.03 | 3.53 | 36.63 | 8.84 | 32.88 | 32.56 |
| 10 | 10.10 | 39.13 | 3.87 | 44.84 | 9.95 | 39.73 | 40.00 |

$\tau_{\max} \sim n^2$, which is inherent in the Rouse model, is virtually satisfied.

It is worth noting that the coefficients a_i increase with the relaxation time. As a result, small relaxation times play an insignificant role in determining the mean values. Indeed, the mean values calculated with allowance for the values of $\tau_i > \tau$ (denoted by the asterisk in Table 3) are close to the exactly calculated values. Comparison of a_i and τ_i likewise shows that, for high n

values, the a_i values are leveled for large τ_i values. This enables us to estimate the mean values (at least, $\langle \tau \rangle_w$) while completely ignoring the relaxation time spec-

trum, i.e., using the approximate formula $\langle \tau \rangle_w \approx \frac{\sum_i \tau_i^2}{\sum_i \tau_i}$

and taking into account only the series terms that are higher than τ . The validity of such an approach is confirmed by the data given in Table 3.

Thus, our analysis shows both a certain similarity and essential differences in the Rouse model between long and short chains.

REFERENCES

1. P. E. Rouse, *J. Chem. Phys.* **21**, 1272 (1953).
2. A. Yu. Grossberg and A. R. Khokhlov, *Statistical Physics of Macromolecules* (Nauka, Moscow, 1989).
3. M. Doi and S.F. Edwards, *The Theory of Polymer Dynamics* (Clarendon, Oxford, 1986; Mir, Moscow, 1998).
4. E. Kamke, *Differentialgleichungen. Lösungsmethoden und Lösungen, Bd. 1: Gewöhnliche Differentialgleichungen* (Leipzig, 1959; Fizmatgiz, Moscow, 1961).

Translated by A. Kozlenkov

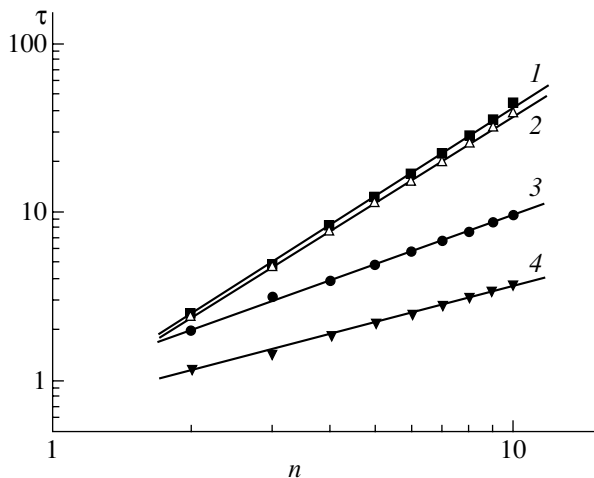


Fig. 2. Relaxation time versus the chain length: (1) maximum relaxation time τ_{\max} ; (2) weighted-mean time $\langle \tau \rangle_w$; (3) average time $\langle \tau \rangle_n$; (4) the ratio of these quantities defining the spectrum distribution width.

Growth of $\text{Ge}_{1-x}\text{Sn}_x$ Solid Solutions from the Liquid Phase

A. Sh. Razzakov

Presented by Academician V.V. Osiko March 15, 2001

Received October 30, 2000

The rapid development of modern semiconductor electronics is accompanied by a growing demand for novel semiconductor materials and structures possessing specific properties. Therefore, search for novel solid solutions and structures based on them are of urgent necessity in semiconductor technology.

In this paper, some results of studying the growth of $\text{Ge}_{1-x}\text{Sn}_x$ solid-solution layers from a tin solution-melt are presented. The growth method employed forced cooling within the temperature range 740–450°C in a hydrogen ambient. The growth process occurred from the volume of the solution-melt placed between two horizontal substrates and was stopped by removing the solution-melt from the gap between the substrates with the help of a centrifuge. Germanium wafers oriented along the [111] crystallographic direction with a resistivity of 40 Ω cm and *p*-type conductivity served as the substrates. The diameter and thickness of the substrates reached 50 and 350–400 mm, respectively. The content of the Sn + Ge, Sn + Ge + Zn, and Sn + Ge + Zn + Se solution-melts and the corresponding temperature-growth range were determined from literature data and preliminary experiments [1].

The content of the $\text{Ge}_{1-x}\text{Sn}_x$ solid solution and the distribution of components in the epitaxial layers grown were studied using a JEOL microanalyzer. It was shown that the value of *x* and the homogeneity of the component distribution (both across the thickness of the epitaxial layer and along the directions parallel to the crystallization front) depend on the temperatures of both the solution-melt and crystallization-onset. With increasing the content of zinc, especially of zinc and selenium in the solution-melt, the tin content in the solid solution drastically increases. This fact is likely associated with the influence of the third component on the effective value of the distribution coefficient. It is established that under similar conditions and contents of the solution-melt, the Sn content in a $\text{Ge}_{1-x}\text{Sn}_x$ solid solution increases with the temperature of the crystallization onset.

We have grown homogeneous mirror-smooth epitaxial layers of a $\text{Ge}_{1-x}\text{Sn}_x$ solid solution from a Ge + Sn + ZnSe solution-melt in the case of crystallization-onset temperatures $T_{\text{co}} = 740^\circ\text{C}$ for $x = 0.1$ and $T_{\text{co}} = 540^\circ\text{C}$ for $x = 0.03$. The X-ray fluorescence spectral analysis was performed prior to and after subsequent removal of the surface layers. The analysis revealed high-intensity peaks corresponding to Ge ($\lambda = 1244$ mÅ) and Sn ($\lambda = 925$ mÅ) and showed that the Ge and Sn content in the solid solution is the same across the film thickness and along the directions of layer growth. The thickness of epitaxial layers grown on Ge varied within the range 5–35 μm depending on both the gap thickness *d* between the substrates and the growth regime.

The quality of $\text{Ge}_{1-x}\text{Sn}_x$ epitaxial layers grown onto Ge substrates depended also on the rate of the forced cooling, which varied in the range 0.5–7.5°C/min. The optimum cooling rate for producing mirror-smooth layers of $\text{Ge}_{1-x}\text{Sn}_x$ solid solution turned out to be 0.5–1.5°C/min; this corresponds to an actual layer-crystallization rate of 0.13–0.2 $\mu\text{m}/\text{min}$. The structural perfection of the layers grown with all other conditions being equal depended also on the gap size δ between horizontally placed substrates. The gap could be varied within the range 0.25–2.5 mm with the help of special graphite supports. For the gaps $\delta < 0.25$ mm, the growth of epitaxial films was not observed at all, probably, due to the absence of the substrate wettability by the solution-melt. The most structurally perfect layers of solid solutions on both upper and lower substrates were grown at the gap value δ ranging between 0.65 and 1 mm. For $\delta > 0.85$ mm, the quality of layers grown on the upper and lower substrates strongly differed. The quality of epitaxial layers grown on the lower substrates always turned out to be higher than that for the upper substrates. This fact also affected the surface dislocation density for the layers grown. The difference increased with a rise in δ . In our opinion, this is associated with the predominance of the convection stream to the crystallization front in the mass transfer mechanism in comparison with the molecular diffusion in the case of gap increase, which we established previously [2].

The qualitative estimate for the distribution of the solution-forming components across the thickness of

Physicotechnical Institute, NPO "Fizika–Solntse,"
Academy of Sciences of the Republic of Uzbekistan,
Tashkent

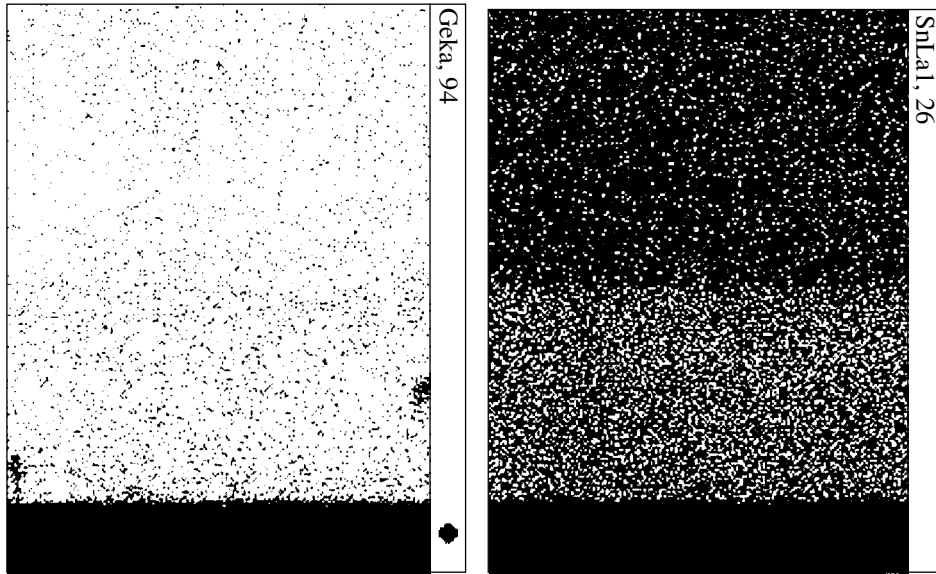


Fig. 1. Raster images of cleavages for $\text{Ge-Ge}_{1-x}\text{Sn}_x$ structures, $x = 0.03$.

the epitaxial layer can also be made by examining raster images for cleavages of the $\text{Ge-Ge}_{1-x}\text{Sn}_x$ structures obtained. These images are evidence of the almost homogeneous distribution of the components across the thickness of the epitaxial layer (Fig. 1).

Analysis of raster images and morphological studies have shown that defects appear at the substrate–film interface depending on the value of x . The difference between the lattice parameters of the first crystalline layer and of the substrate appears due to the fact that the first grown layer consists of $\text{Ge}_{1-x}\text{Sn}_x$ with $x > 0$ and the substrate consists of pure germanium. With the growth of subsequent epitaxial layers, this difference reduces due to the fact that these layers differ insignificantly with respect to the $\text{Ge}_{1-x}\text{Sn}_x$ content. As a result of elastic deformation of the layer produced that plays the role of the substrate, the total energy of the system decreases. Through crystallization of the next layer without a change in the lattice parameter, this energy turns out to be lower than that at the initial stage of the process. Varying conditions for the growth regime, we can govern the action of heteroboundaries. It was found that with an Sn-content increase in the $\text{Ge}_{1-x}\text{Sn}_x$ solid solution, the structural perfection of layers sharply deteriorates beginning from $x > 0.1$ and, moreover, precipitations of the second phase appear.

The crystalline perfection and the lattice parameters of the solid solutions were studied using the X-ray diffraction method with a DRON-UM1 setup. Specially grown samples with a layer thickness $d = 3\text{--}5\ \mu\text{m}$ were selected for this analysis. The diffraction spectra were obtained using continuous recording for the Cu-anode lines ($\lambda_\alpha = 1.5418\ \text{\AA}$, $\lambda_\beta = 1.3922\ \text{\AA}$). The anode voltage and current were 30 kV and 10 mA,

respectively. The exposure time was varied within the range 1–3 h. As is seen from the X-ray diffraction pattern (Fig. 2), the peak positions for substrates and films differ insignificantly. This implies the closeness of lattice parameters for these structures ($a_{\text{Ge}} = 5.656\ \text{\AA}$, $a_{\text{Ge}_{1-x}\text{Sn}_x} = 5.681\ \text{\AA}$). At the same time, the absence of other peaks on the diffraction pattern yields additional information on the single-crystallinity of the epitaxial layers obtained [3].

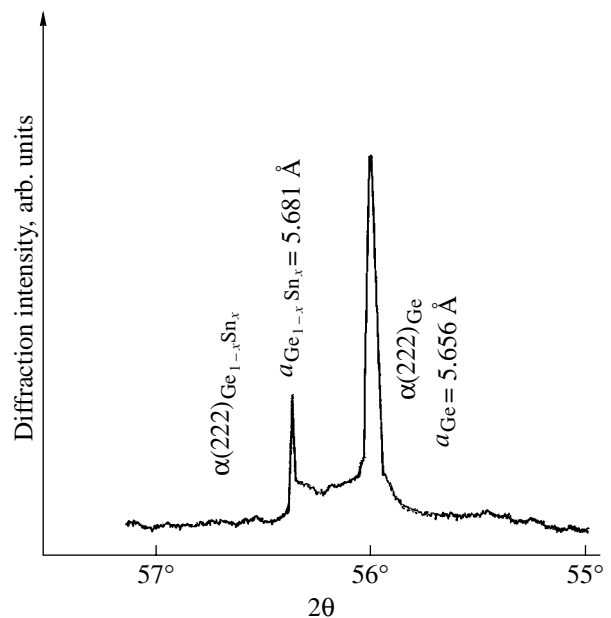


Fig. 2. Diffraction pattern for $\text{Ge-Ge}_{1-x}\text{Sn}_x$ heterostructures, $x = 0.03$.

Certain electrical parameters of the epitaxial layers produced were determined using the van der Pauw method. These layers turned out to have p -type conductivity with a carrier concentration of 10^{17} – 10^{18} cm^{-2} and mobility of 15–20 V s cm^{-2} at 300 K.

In conclusion, it is worth noting that by selecting the conditions of liquid-phase epitaxy, we can obtain structurally perfect epitaxial layers of $\text{Ge}_{1-x}\text{Sn}_x$ solid solutions on Ge substrates; this could be of interest in modern microelectronics.

REFERENCES

1. V. M. Andreev, L. M. Dolginov, and D. N. Tret'yakov, *Liquid Epitaxy in Technology of Semiconductor Devices* (Sov. Radio, Moscow, 1975), p. 328.
2. A. S. Saidov, É. A. Koshchanov, A. Sh. Razzakov, and D. V. Saparov, *Uzb. Fiz. Zh.*, No. 1, 16 (1997).
3. A. S. Saidov, É. A. Koshchanov, and A. Sh. Razzakov, *Pis'ma Zh. Tekh. Fiz.* **24** (2), 12 (1998) [*Tech. Phys. Lett.* **24**, 47 (1998)].

Translated by T. Galkina

Bending of a Piezoelectric-Ceramic Layer Weakened by Through Holes in the Case of Sliding Fixation of Its Ends

Corresponding Member of the RAS É. I. Grigolyuk*, L. A. Fil'shtinskiĭ**, and Yu. D. Kovalev**

Received July 24, 2000

Bending of an isotropic layer (or semilayer) weakened by a through noncircular hole was considered in [1]. A similar problem for an isotropic layer with a circular hole was solved in [2, 3] using different methods. Study of a stressed isotropic layer weakened by through holes in the case of sliding fixation of its ends (the so-called symmetric case) was undertaken in [4]. In all the papers mentioned above, the solutions to the boundary value problems were based on the Vorovich semi-inverse method. A number of electroelasticity problems for a layer under various boundary conditions imposed at its ends was considered in [5]. A method, distinct from that developed in [4], for solving mixed boundary value problems in the theories of elasticity and electroelasticity for a layer weakened by through inhomogeneities was described in [6].

We consider a piezoelectric-ceramic layer ($-h \leq x_3 \leq h$, $-\infty < x_1, x_2 < \infty$) weakened by a tunnel (i.e., directed along the $0x_3$ -axis) through holes (cavities) whose cross sections are smooth closed contours L_j , $j = 1, 2, \dots, k$. We assume that the side surfaces of the cavities are force-free and the bending–torsional stress at infinity is given by the uniform field σ_{ij}^∞ ($i, j = 1, 2, 3$).

The problem set above is described by the following complete system of equations (volume forces and charges are assumed to be absent):

the equilibrium equations (the summation over the repeating subscripts is implied)

$$\partial_j \sigma_{ij} = 0, \quad \partial_i = \frac{\partial}{\partial x_i}, \quad i, j = 1, 2, 3; \quad (1)$$

the electrostatics equations

$$\partial_m D_m = 0, \quad E_m = -\partial_m \varphi; \quad (2)$$

the Cauchy relations

$$\varepsilon_{ij} = \frac{1}{2}(\partial_i u_j + \partial_j u_i); \quad (3)$$

the equations of state for the piezoelectric ceramics preliminary polarized in the direction of the $0x_3$ -axis

$$\begin{aligned} \sigma_x &= c_{11}\varepsilon_x + c_{12}\varepsilon_y + c_{13}\varepsilon_z - e_{31}E_z, \\ \tau_{yz} &= 2c_{44}\varepsilon_{yz} - e_{15}E_y, \\ \sigma_y &= c_{12}\varepsilon_x + c_{11}\varepsilon_y + c_{13}\varepsilon_z - e_{31}E_z, \\ \tau_{xz} &= 2c_{44}\varepsilon_{xz} - e_{15}E_x, \\ \sigma_z &= c_{13}(\varepsilon_x + \varepsilon_y) + c_{33}\varepsilon_z - e_{33}E_z, \\ \tau_{xy} &= (c_{11} - c_{12})\varepsilon_{xy}, \end{aligned} \quad (4)$$

$$\begin{aligned} D_x &= \varepsilon_{11}E_x + 2e_{15}\varepsilon_{xz}, \quad D_y = \varepsilon_{11}E_y + 2e_{15}\varepsilon_{yz}, \\ D_z &= \varepsilon_{33}E_z + e_{31}(\varepsilon_x + \varepsilon_y) + e_{33}\varepsilon_z; \end{aligned}$$

the boundary conditions at $x_3 = \pm h$

$$u_3 = 0, \quad \sigma_{13} = 0, \quad \sigma_{23} = 0, \quad \varphi = 0; \quad (5)$$

and, finally, the boundary conditions on the cavity surface

$$\begin{aligned} \sigma_{kj}n_j &= 0, \quad k, j = 1, 2, 3, \\ D_n &= 0. \end{aligned} \quad (6)$$

Furthermore, it is reasonable to use the set of equilibrium equations in displacements obtained from (1)–(4) as an initial system. These equations are

$$\begin{aligned} V\nabla^2 u + c_{44}\partial_3^2 u + \partial_1 \theta &= 0, \\ V\nabla^2 v + c_{44}\partial_3^2 v + \partial_2 \theta &= 0, \quad \nabla^2 = \partial_1^2 + \partial_2^2, \\ c_{44}\nabla^2 w + c_{33}\partial_3^2 w \\ + \partial_3 \{c(\partial_1 u + \partial_2 v) + e_{15}\nabla^2 \varphi + e_{33}\partial_3^2 \varphi\} &= 0, \end{aligned}$$

* Moscow State Technical University—
Moscow Automotive Institute, Moscow,
ul. Bol'shaya Semenovskaya 38, 105830 Russia

** Sumy State University,
ul. Rymkogo-Korsakova 2, Sumy, 400007 Ukraine

$$\begin{aligned} &\varepsilon_{11}\nabla^2\varphi + \varepsilon_{33}\partial_3^2\varphi - e_{15}\nabla^2w \\ &- e_{33}\partial_3^2w - \partial_3\{e(\partial_1u + \partial_2v)\} = 0, \\ U &= \frac{1}{2}(c_{11} + c_{12}), \quad V = \frac{1}{2}(c_{11} - c_{12}), \\ c &= c_{13} + c_{44}, \quad e = e_{15} + e_{31}, \\ \theta &= U(\partial_1u + \partial_2v) + c\partial_3w + e\partial_3\varphi. \end{aligned} \tag{7}$$

We will seek the solution to set (7), which is skew-symmetric with respect to the median plane $x_3 = 0$ of the layer. We assume that

$$\begin{aligned} \{u, v\} &= \sum_{k=0}^{\infty} \{u_k, v_k\} \sin\gamma_k x_3, \quad \gamma_k = \frac{2k+1}{2h}\pi, \\ \{w, \varphi\} &= \sum_{k=0}^{\infty} \{w_k, \varphi_k\} \cos\gamma_k x_3. \end{aligned} \tag{8}$$

With regard to these relationships and Eqs. (7), we have

$$\begin{aligned} V\kappa_k u_k + \partial_1\theta_k &= 0, \quad V\kappa_k v_k + \partial_2\theta_k = 0, \\ L_{13}w_k + L_{14}\varphi_k + \frac{c}{U}\gamma_k\theta_k &= 0, \\ L_{23}w_k + L_{24}\varphi_k + \frac{e}{U}\gamma_k\theta_k &= 0, \\ \kappa_k &= \nabla^2 - \gamma_k^2\mu_0^2, \quad L_{13} = c_{44}\nabla^2 - \gamma_k^2\delta_1, \end{aligned} \tag{9}$$

$$\begin{aligned} L_{14} = L_{23} &= e_{15}\nabla^2 - \gamma_k^2\delta_2, \quad L_{24} = \gamma_k^2\delta_3 - \varepsilon_{11}\nabla^2, \\ \theta_k &= U(\partial_1u_k + \partial_2v_k) + \gamma_k c w_k + \gamma_k e \varphi_k, \\ \delta_1 &= c_{33} - \frac{c^2}{U}, \quad \delta_2 = e_{33} - \frac{ce}{U}, \quad \delta_3 = \varepsilon_{33} + \frac{e^2}{U}. \end{aligned}$$

Solving this system of equations, we arrive at

$$\begin{aligned} u_k - i v_k &= 2\gamma_k \frac{U}{V} \sum_{m=1}^3 \frac{p_4^*(\mu_m)}{\mu_m^2 - \mu_0^2} \frac{\partial}{\partial z} \Omega_k^{(m)} + 2i \frac{\partial}{\partial z} \Omega_k, \\ w_k &= \gamma_k^2 \sum_{m=1}^3 (d_2\mu_m^2 - \delta_k) \Omega_k^{(m)}, \quad k = 0, 1, \dots, \tag{10} \\ \varphi_k &= \gamma_k^2 \sum_{m=1}^3 (\delta_4 - d_1\mu_m^2) \Omega_k^{(m)}. \end{aligned}$$

Here, the function $\Omega_k^{(m)}$ is an arbitrary solution to the Helmholtz wave equation $(\nabla^2 - \gamma_k^2\mu_m^2)\Omega_k^{(m)} = 0$, Ω_k

is an arbitrary solution to the equation $(\nabla^2 - \gamma_k^2\mu_0^2)\Omega_k = 0$, and μ_m are the roots of a bicubic equation [6].

The desired metaharmonic functions entering into (10) are sought in the form

$$\begin{aligned} \Omega_k &= \int_L p_k(\zeta) K_0(\gamma_k \mu_0 r) ds, \\ r &= |\zeta - z|, \quad z = x_1 + ix_2, \\ \Omega_k^{(m)} &= \int_L p_k^{(m)}(\zeta) K_0(\gamma_k \mu_m r) ds, \end{aligned} \tag{11}$$

$$\zeta = \xi_1 + i\xi_2 \in L, \quad m = 1, 2, 3,$$

where $K_n(z)$ is the n th-order MacDonald function and $p_k(\zeta)$ and $p_k^{(m)}(\zeta)$ are desired densities, with $p_k^{(3)} = \bar{p}_k^{(2)}$.

In what follows, we assume that, on the cavity surface, the stress vector components and the normal component of the electric induction satisfy the expansions

$$\begin{aligned} N &= \sum_{k=0}^{\infty} N_k \sin\gamma_k x_3, \quad T = \sum_{k=0}^{\infty} T_k \sin\gamma_k x_3, \\ Z &= \sum_{k=0}^{\infty} Z_k \cos\gamma_k x_3, \quad D_n = \sum_{k=0}^{\infty} D_n^{(k)} \cos\gamma_k x_3. \end{aligned} \tag{12}$$

It is reasonable to represent the boundary condition on the cavity surface as

$$\begin{aligned} \sigma_{11} + \sigma_{22} - e^{2i\psi}(\sigma_{22} - \sigma_{11} + 2i\sigma_{12}) &= 2(N - iT), \\ \text{Re}\{e^{i\psi}(\sigma_{13} - i\sigma_{23})\} &= Z, \\ D_n &= 0. \end{aligned} \tag{13}$$

Here, ψ is the angle between the positive normal to the contour L and the Ox_1 -axis and N and T are, respectively, the normal and tangential vector components of the stress applied to the body surface from outside.

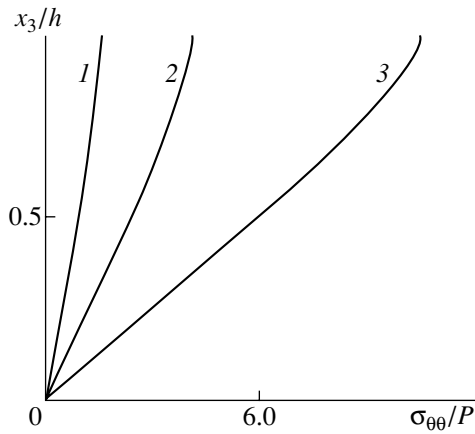
With the help of representations (11) and expansions (8) and (12), the boundary value problem (13) can be reduced to a set of integro-differential singular equations, which cannot be written out here due to its awkwardness.

As an example, we here consider a layer weakened by a cavity whose cross section is a square with rounded angles,

$$\xi_1 = a(\cos\varphi + c\cos 3\varphi),$$

$$\xi_2 = a(\sin\varphi - c\sin 3\varphi): 0 \leq \varphi \leq 2\pi, \quad c = 0.14036$$

with a bending load $\sigma_{11}^\infty = Px_3$ applied at infinity.



The distribution of the relative circumferential stress $\sigma_{\theta\theta}/P$ along the thickness coordinate.

The distribution of the relative circumferential stress $\sigma_{\theta\theta}/P$ at the point $\varphi = \frac{\pi}{2}$ (where this stress is maximal) along the thickness coordinate is shown in the figure. Curves 1, 2, and 3 correspond to $\frac{h}{a} = 0.5, 1, \text{ and } 2,$

respectively. The numerical results were obtained for piezoelectric ceramics PZT-4.

REFERENCES

1. É. I. Grigolyuk, Yu. D. Kovalev, and L. A. Fil'shtinskiĭ, Dokl. Akad. Nauk **345**, 54 (1995) [Phys. Dokl. **40**, 592 (1995)].
2. A. S. Kosmodamianskiĭ and V. A. Shal'dyrvan, *Thick Multiconnected Plates* (Naukova Dumka, Kiev, 1978).
3. A. F. Ulitko, *Method of Vector Eigen-Functions in Three-Dimensional Problems of Elasticity Theory* (Naukova Dumka, Kiev, 1979).
4. G. S. Bulanov and V. A. Shal'dyrvan, in *Theoretical and Applied Mechanics* (Osnova, Kharkov, 1984), Vol. 15, pp. 5–9.
5. V. T. Grinchenko, A. F. Ulitko, and N. A. Shul'ga, *Electroelasticity*, in *Mechanics of Coupled Fields in Structure Components* (Naukova Dumka, Kiev, 1989), Vol. 5.
6. L. A. Fil'shtinskiĭ, in *Theoretical and Applied Mechanics* (Osnova, Kharkov, 1990), Vol. 21, pp. 13–20.

Translated by V. Chechin

Electric Field Discontinuities above Stratus Thunderstorm Clouds

P. V. Mironychev

Presented by Academician V.V. Osiko April 13, 2001

Received March 22, 2001

To date, descriptions of numerous observations of unusual optical glows proceeding at low or middle latitudes and at altitudes of 15 to 100 km in the evening or night Earth atmosphere have been published. The mechanisms of initiation of these glows termed red sprites, blue jets, elves, and blue starters are unclear today [1–3]. However, its correlation with the underlying thunderstorm activity is without doubt. It has been noted that red sprites correlate with positive lightnings and are observed above regions of stratified clouds that produce a convective-line trace in large thunderstorm complexes. A structure consisting of 4 to 6 layers and a high frequency of positive lightnings that transfer negative charge upward are intrinsic to these clouds [4–8].

Various explanations of the origin of these glows were proposed. However, in all cases, an initiator is assumed to be close to lightning. This lightning causes an initially short ($\sim 100 \mu\text{s}$) electromagnetic pulse in the atmosphere and, furthermore, a long-time ($\sim 100 \text{ms}$) rise of the electric field (a consequence of the charge transfer by the quasi-continuous lightning current) [9]. At present, a number of versions are being discussed in the literature. According to them, the glow of red sprites is caused by either a usual breakdown of the atmosphere [2] or a relativistic runaway-electron discharge [10–12]. In the latter case, a weaker (by an order of magnitude) field is required.

Recently, a series of measurements of the electric field above a region of stratus clouds in large thunderstorm complexes were carried out [4–8]. The authors of [4] also performed calculations of electric-field discontinuities above a stratiform cloud caused by positive lightning. In the cloud model [4], the electric field is formed by one charged layer and its image. An instantaneous neutralization of the lightning charges is suggested, all values of the physical parameters being taken from experiments. As a result of these simplifications, the multilayer cloud structure and polarization of the atmosphere are not taken into account. Thus, the

possibility of both imitating the intracloud charge transfer and calculating the electrostatic cloud energy and dynamics of the intracloud electric field is absent.

In this paper, a three-layer model of a thundercloud is described. Calculation results for the cloud structure, parameters, and jumps of the quasistatic electric field caused by positive lightning with allowance for atmosphere polarization are presented. A possible correlation of the electric-field jumps with the initiation of atmospheric optical phenomena is discussed.

MODEL OF A STRATIFIED THUNDERCLOUD

Let cloud layers be represented by three coaxial charged disks with radius R and thickness d , which are parallel to the Earth's surface and placed at the altitudes Gh_i . The corresponding uniform charge volume densities are $\rho_1 < 0$, $\rho_2 > 0$, and $\rho_3 < 0$ (the enumeration occurs from top to bottom). The charge surface densities are $\sigma_i = d\rho_i$; the disk charges are $Q_i = \pi R^2 \sigma_i$. We assume the cloud, as a whole, to be electrically neutral: $\sigma_1 + \sigma_2 + \sigma_3 = 0$. In calculating the electric field, we additionally introduce nine image disks. The first three are symmetric to the cloud layers with respect to the Earth's surface. The other six are obtained as a result of the reflection of the cloud layers and three first images from the boundary of the conducting atmosphere, which is located at an altitude H_e . The allowance for the electrosphere is important since near its boundary, the fields of the lower and upper charges have the same magnitude and are equally directed, which doubles the field. The images are charged and located in such a manner that the following 18 relations can be written out in the accepted notation:

$$\begin{aligned} h_4 &= -h_3, & h_5 &= -h_2, & h_6 &= -h_1, \\ h_7 &= 2H_e + h_1, & h_8 &= 2H_e + h_2, & h_9 &= 2H_e + h_3, \\ h_{10} &= 2H_e - h_3, & h_{11} &= 2H_e - h_2, & h_{12} &= 2H_e - h_1, \\ \sigma_4 &= -\sigma_3, & \sigma_5 &= -\sigma_2, & \sigma_6 &= -\sigma_1, \\ \sigma_7 &= \sigma_1, & \sigma_8 &= \sigma_2, & \sigma_9 &= \sigma_3, \\ \sigma_{10} &= -\sigma_3, & \sigma_{11} &= -\sigma_2, & \sigma_{12} &= -\sigma_1. \end{aligned} \quad (1)$$

Russian Federal Nuclear Center,
All-Russia Research Institute of Experimental Physics,
Sarov, Nizhni Novgorod oblast, 607188 Russia

On the axis of the disk system at an altitude z , the electric field is represented by the formula

$$E(z) = \sum_{i=1}^{12} \sigma_i \varphi(z, h_i, R), \quad (2)$$

where

$$\varphi(z, h_i, R) = \frac{1}{2\epsilon_0} \left[\frac{z - h_i}{|z - h_i|} - \frac{z - h_i}{\sqrt{R^2 + (z - h_i)^2}} \right]$$

and ϵ_0 is the dielectric constant.

Multiple probing of stratified thunderclouds showed that the strength of the intracloud quasisteady electric field usually do not exceed a certain critical value $E_{be}(z)$ (z is the altitude) [4–6]. The quantity $eE_{be}(z)$ corresponds to the minimum friction force of a relativistic electron in air. This quantity is interesting in the fact that when it is exceeded, the development of a specific electric discharge, namely, a relativistic runaway-electron discharge, can arise [10–12]. The friction force is proportional to the gas density:

$$eE_{be}(z) = eE_0 f(z), \quad (3)$$

where $E_0 = 0.204$ MV/m is the electric-field strength corresponding to the minimum friction force at normal air density and an electron kinetic energy of 1.2 MeV [10–12] and $f(z)$ is the relative atmospheric density. The threshold for the air breakdown by thermal electrons is considerably higher, namely, $E_{bd}(z) \approx 3f(z)$ MV/m. We now define the overvoltage $\delta(z)$ as a local ratio of the field strength to its threshold value (3):

$$\delta(z) \equiv \frac{E(z)}{E_{be}(z)}. \quad (4)$$

Based on measurement results for the electric field in stratified clouds and above them [4–6], we set the field magnitudes, i.e., the overvoltages at four points of the cloud axis, at altitudes of $z_1 = 16$ km, $z_2 = h_1$, $z_3 = h_2$, and $z_4 = 1$ km:

$$\begin{aligned} E(z_1) &= -1 \text{ kV/m} \quad \text{or} \quad \delta_1 = \delta(z_1) = -0.0363, \\ \delta_2 &= \delta(z_2) = +1, \quad \delta_3 = \delta(z_3) = -1, \\ E(z_4) &= +10 \text{ kV/m} \quad \text{or} \quad \delta_4 = \delta(z_4) = +0.05. \end{aligned} \quad (5)$$

The choice of the points z_2 and z_3 immediately below the upper and the middle disks is not accidental. Since the distance between the neighboring disks is much smaller than their diameters, the field between the disks is almost uniform. As far as the quantity $E_{be}(z)$, like the

atmosphere density, exponentially decreases with altitude, the maximum value $|\delta|$ between neighboring disks is attained below the upper disk, as follows from (4). Measurements of the intracloud electric field do not exhibit values $|\delta| > 1$ [4–8]. Therefore, we can consider that in the limiting cases (that we analyze) and immediately before a lightning strike, the value $|\delta| = 1$ is attained at two axis points in a cloud. The values of δ_2 and δ_3 were chosen in (5) in accordance with this consideration. Combining the neutrality condition with formula (2) and condition (5), we write out a system of algebraic equations for determining the unknown cloud parameters:

$$\begin{aligned} \sum_{i=1}^{12} \sigma_i \varphi(z_j, h_i, R) &= \delta_j E_{be}(z_j), \quad j = 1, 2, 3, 4, \\ \sigma_1 + \sigma_2 + \sigma_3 &= 0. \end{aligned} \quad (6)$$

By setting free parameters h_3 and R and solving the system of equations with allowance for relations (1), we can find the parameters $h_1, h_2, \sigma_1, \sigma_2$, and σ_3 . The value of the field jump is

$$\Delta E(z) = \sum_{i=1}^{12} (\sigma_{ik} - \sigma_i) \varphi(z, h_i, R), \quad (7)$$

where σ_{ik} are the final charge densities (after the lightning has occurred), which are here, in a certain extent, free parameters since they depend on the method of layer neutralization.

To determine the electric field above a cloud at altitudes exceeding 30 km after a lightning strike, it is more reasonable to calculate the field jump (7) than the field in itself (2). This is substantiated by the fact that, prior to this event, the field intensity at altitudes of 30 km and higher was much lower than 1 kV/m. Thus, we assume that the cloud layers were screened by additional charged regions located at altitudes between 16 and 30 km, which were not taken into account in our calculations. Actually, in calculating the field inside a cloud or that at a small height above it, we should use formula (2) with the values of σ_i taken before or after the lightning strike.

The assumption on the instantaneous charge transfer by a lightning has two consequences. First, the field jump penetrates upward without attenuation because the atmosphere has no time for polarization. On the other hand, the longer the duration of the lightning, the lower the electrosphere boundary in which the field-relaxation time is shorter than the lightning duration. In subsequent calculations, we assumed that the charge transfer by a lightning occurs in accordance with the

exponential law with a characteristic time $\tau = 10$ ms:

$$\sigma_2(t) = \sigma_{2k} + [\sigma_2(0) - \sigma_{2k}] \exp\left\{-\frac{t}{\tau}\right\}.$$

This value of τ corresponds to the night altitude of the electrosphere boundary $H_e \approx 60$ km [12]. A multiplier

$$\lambda(t) = \frac{1}{1 - 4\pi\tau\xi(z)} \left[\exp(-4\pi t\xi(z)) - \exp\left(-\frac{t}{\tau}\right) \right]$$

was used to take into consideration the vertical polarization of the atmosphere and the weakening of the electric field. Here, t is time and $\xi(z)$ is the conductivity of the night atmosphere [12]. The electric-field jump above a cloud (but with allowance for the atmosphere relaxation) is $-\Delta E(z, t) = \Delta E(z)\lambda(t)$.

ELECTRIC-FIELD DISCONTINUITIES ABOVE STRATIFIED THUNDER CLOUDS INITIATED BY A POSITIVE LIGHTNING

To calculate cloud parameters prior to a lightning strike, we assumed that the altitude of the lower layer, the thickness of the layers, and the cloud radius were 2 to 5 km, 500 m, and 5 to 10 km, respectively. It was found that the upper and middle cloud layers can be located correspondingly at altitudes of 6.2 to 12.4 and 3.7 to 8.0 km. The calculated charge densities in the upper and lower disks vary within -2.5 to -0.86 nC/m³, while in the middle disk they vary within $+2.5$ to $+4.55$ nC/m³. All these values are close to those observed previously [4–6]. The values of charges for the positive layer turned out to be within the range 115–626 C. These values correspond to charges trans-

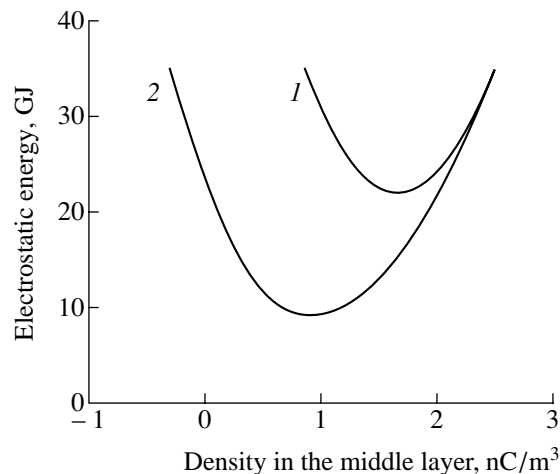


Fig. 1. Electrostatic energy of a cloud in the process of layer discharge for $h_3 = 5$ km and $R = 10$ km.

ferred by a positive lightning [9]. However, as is shown below, complete neutralization of the entire positive charge by a lightning is unlikely. According to the charge values and disk altitudes obtained, the electrostatic energy of the plane-capacitor system is calculated with corrections for edge effects taken into account. Figure 1 exhibits the energy of a system consisting of 12 layers as a function of the current charge density of the middle and lower cloud layers. The right-hand branch of curve 1 corresponds to a situation when the lower and upper cloud layers preserve their charge and only the middle layer is neutralized by the charge coming from the Earth until the minimum energy has been attained (this is the first variant of neutralization). The energy minimum (in variant 1) is attained as a result of discharging the middle layer from 2.5 to 1.67 nC/m³. To this time moment, the charge of -130 C is transferred from the Earth, whereas the energy dissipation is close to 13 GJ. Furthermore, we assume that the lightning channel has a sufficient induction and a small resistance, so that the charge transfer from the Earth can be continued until the cloud energy comes back to the initial energy (this is the second variant of neutralization). The left-hand edge of curve 1 in Fig. 1 corresponds to the end of the lightning in the latter variant. The residual charge density in the middle layer is now equal to 0.863 nC/m³, i.e., to 30% of the initial layer charge. The charge transferred from the Earth is -257 C. Thus, it turns out that the complete discharge of one positive layer by a lightning, as it was assumed for certain cases in [4], is most likely impossible. Whence it follows that the field-jump values are overestimated in [4].

The third variant of neutralization (the right-hand part of curve 2 in Fig. 1) consists in the transfer by the intracloud lightning of the entire charge of -136 C from the lower layer to the middle layer. The energy minimum is attained for $\rho_{2k} \approx +0.86$ nC/m³ $\approx -\rho_1$ and $\rho_{3k} \approx 0$, while the energy release is ~ 25.7 GJ. The fourth discharge variant (the left-hand branch of curve 2 in Fig. 1) consists in the continuation of the negative-charge transfer onto the middle layer. However, the process occurs from the Earth until a state is formed with an energy equal to the initial state. This condition determines the final values of both $\rho_{2k} \approx -0.29$ nC/m³ and the charge of -182 C transferred from the Earth.

Figure 2 demonstrates the results of one of the calculations for the distribution of the vertical electric field on the cloud axis at time moments prior to and after a lightning in the case of the fourth neutralization variant when the field undergoes a maximum jump. The envelopes show the threshold field (3). At an altitude of 16 km, the field after the lightning is equal to -17.4 kV/m. In the third variant (when the jump is minimal), the field is -7.49 kV/m, which satisfactory agrees with the observed data of about -5 kV/m [4]. We should take into account that the measuring balloon was usually sit-

uated dozens of kilometers from the strike point of a lightning identified with a given field jump.

Figure 3 exhibits the calculated altitude dependences for the field-jump values above a cloud for the third (curve 2) and fourth (curve 1) neutralization variants. A usual breakdown and the runaway-electron discharge are possible above the $E_{bd}(z)$ curve and the $E_{be}(z)$ curve, respectively. These dependences are obtained without allowance for the weakening of the field discontinuity due to the atmosphere polarization; however, we implied the electrosphere boundary at an altitude of 60 km while determining the positions of images. For various scenarios of layer neutralization, the threshold for the electron runaway is overcome at altitudes of 30–43 km and higher, whereas the usual breakdown can develop above 60–67 km, which is close to the results of [4]. The increase in the field jump (Fig. 3) at the heights greater than 60 km contradicts the physical standpoint and is completely a consequence of the roughness of the model accepted; namely, it allows for the electrosphere in the formation of images and ignores the field decrease caused by the polarization in the electrosphere. With the polarization taken into consideration, the field jump does not penetrate above 75 km and the maximum value of δ (which does not exceed 12.5) is attained in 20–25 ms after the lightning has begun at an altitude of 62 km. We can make a conclusion that the usual breakdown above the cloud is impossible since, in order for this to occur, it is necessary that $\delta \approx 15$.

Thus, our calculations have shown that the necessary conditions for the development of a relativistic runaway-electron avalanche and a specific form of a discharge can be attained within the altitude range of 30–73 km [10–12]. These conditions correspond to a relatively small size of both the stratus cloud and values of charges being transferred. It is this range that corresponds to observations of red sprites. However, in order to explain the observed glow intensity, overvoltages $\delta > 1.5$ –2 are necessary at small altitudes, which would provide an electron avalanche gain by a factor of 10^{17} [12]. Such an intense avalanche could be developed, e.g., beginning from 25 km in the field of a vertical electric dipole whose negative charge of -100 C is situated at an altitude of 18 km [12]. In the given calculations, the avalanche can be developed only above 30 km. In addition, in this case, the overvoltage at an altitude of 30 km is close to 1 and very slowly rises with the altitude. Therefore, the avalanche does not attain the required amplification at altitudes of 50–70 km. Thus, we can explain the blue jet observed at altitudes from cloud tops up to 35 km neither by the runaway-electron discharge nor, all the more, by a usual breakdown. In my opinion, the results obtained do not reject the concept that red sprite and blue jet are initiated in a certain way by jumps of the thunder field [2]. Indeed, here, a simplified model of a thundercloud is analyzed which does not take into account the variety of natural condi-

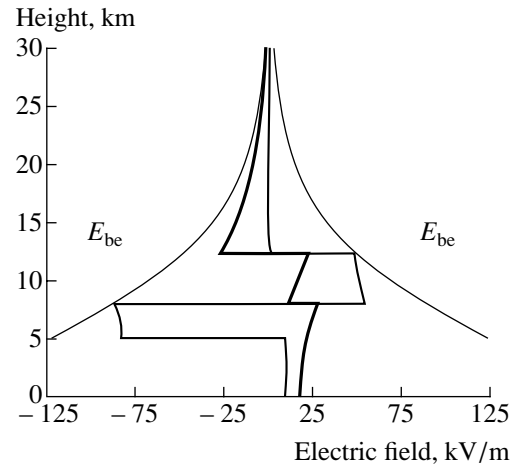


Fig. 2. Electric field on the cloud axis for $h_3 = 5$ km and $R = 10$ km prior to (thin line) and after (thick line) a lightning strike. (The case of the fourth variant of layer neutralization.)

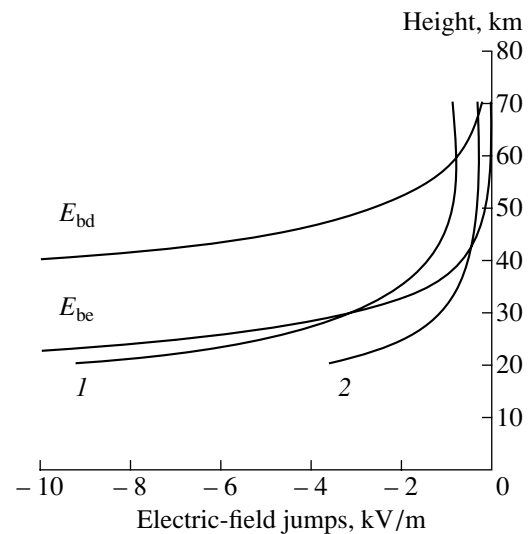


Fig. 3. Altitude dependence for the values of quasistatic electric-field jumps above a stratus cloud ($h_3 = 5$ km and $R = 10$ km) which accompany a positive lightning.

tions involved, e.g., nonuniformity and fluctuations of intracloud charge distribution and the specific features of charge transfer by lightning.

ACKNOWLEDGMENTS

This work was performed under the financial support of the International Scientific-Technological Center, project no. 490.

REFERENCES

1. D. D. Sentman and E. M. Wescott, *Phys. Plasmas* **2**, 2514 (1995).

2. D. J. Boccippio, E. R. Williams, S. J. Heckman, *et al.*, *Science* **269**, 1088 (1995).
3. W. A. Lyons, *Mon. Weather Rev.* **122**, 1940 (1994).
4. T. C. Marshall, M. Stolzenburg, and W. D. Rust, *J. Geophys. Res.* **101** (D3), 6979 (1996).
5. T. C. Marshall, M. P. McCarthy, and W. D. Rust, *J. Geophys. Res.* **100** (D4), 7097 (1995).
6. T. C. Marshall, W. Rison, W. D. Rust, *et al.*, *J. Geophys. Res.* **100** (D10), 20815 (1995).
7. T. C. Marshall and W. D. Rust, *Bull. Am. Meteorol. Soc.* **74**, 2159 (1993).
8. M. Stolzenburg, T. C. Marshall, W. D. Rust, *et al.*, *Mon. Weather Rev.* **122**, 1777 (1994).
9. M. A. Uman, *The Lightning Discharge* (Academic, San Diego, 1987).
10. A. V. Gurevich, G. M. Milikh, and R. A. Roussel-Dupre, *Phys. Lett. A* **165**, 463 (1992).
11. R. A. Roussel-Dupre, A. V. Gurevich, T. Tunnell, *et al.*, *Phys. Rev. E* **49**, 2257 (1994).
12. R. A. Roussel-Dupre and A. V. Gurevich, *J. Geophys. Res.* **101** (A2), 2297 (1996).

Translated by G. Merzon

Subnanosecond Switching of Gigawatt Peak Power Using a Silicon Avalanche Sharpener

S. K. Lyubutin, Academician G. A. Mesyats, S. N. Rukin,
B. G. Slovikovskii, and E. A. Alichkin

Received March 12, 2001

Electrical pulses with time durations from tenth fractions to several nanoseconds with a peak power of hundreds of megawatts to several gigawatts are required in various fields of electrophysics and its technological applications. Up to now, the sole method of producing such pulses was the use of ultrahigh-pressure gas spark gaps as switches. The well-known shortcomings of the spark gaps, e.g., their limited lifetime and pulse repetition rate, as well as the instability of the parameters of pulses formed, are the main obstacles that hamper the employment of powerful short pulses in technologies and high-precision physical experiments. In this connection, the development of new superintense and superfast semiconducting current switches is of great practical importance.

One of the most high-rate methods of current switching in semiconductors is based on the formation of a delayed shock-ionization wave in the base of p^+n-n^+ -diode. In this case, the rate of the base filling by the electron-hole plasma can exceed the carrier rate in the current saturation region by a factor of ten [1, 2]. At present, superfast semiconductor switches, the so-called silicon avalanche sharpeners (SAS) based on this principle, are being developed [3]. They are capable of forming subnanosecond pulses with a rise time on the order of 10^{-10} s. The most powerful SAS with several semiconducting structures connected in series form pulses with an amplitude on the order of 10^4 V and a peak power up to several megawatts [3, 4] at the 50- Ω load.

The development of an SAS with an operating voltage exceeding 100 kV and a switching power of hundreds of megawatts and higher is of practical interest. These SAS could be, in this case, an alternative to superhigh-pressure gas spark gaps. In this paper, the results of the first experiments on switching power by SAS on the basis of a delayed shock-ionization wave

were enhanced by more than two orders of magnitude and reached 1 GW at a pulse duration of 1.8 ns.

The sketch of the experiment is shown in Fig. 1. A solid-state SM-3NS short-pulse charging generator, whose characteristics are given in [5], was used to produce an overvoltage at the SAS under study. The output-pulse formation unit of the generator contains an inductive energy store L and a current semiconductor opening switch (SOS) on the basis of SOS-diodes with a subnanosecond current cutoff [6]. For exciting a delayed shock-ionization wave, a rise-time rate of the reverse voltage of $\sim 10^{12}$ V/s per one structure is required [2]. In our case, the generator provided a voltage rise time at the open output at a rate of $\sim 10^{14}$ V/s (450 kV for ~ 4 ns), which was sufficient for wave excitation when the number of in-series structures attained ~ 100 . A coaxial 50- Ω oil-filled pulse-forming line with an outer diameter of 90 mm was connected to the SM-3NS generator output. In the experiments, the line length varied from 5 to 20 cm. The SAS under study was mounted between the line output and the resistive load R_1 . A blocking diode I was installed between the output of the charging generator and the inner line conductor, which eliminates plasma injection into the SAS in the case of the appearance of a positive-voltage precursor pulse at the stage of SOS direct pumping.

The charging voltage of the pulse-forming line and the voltage in the load were monitored using capacitive broad-band voltage dividers, 2 and 3. The measurement of the current flowing through the SAS was carried out

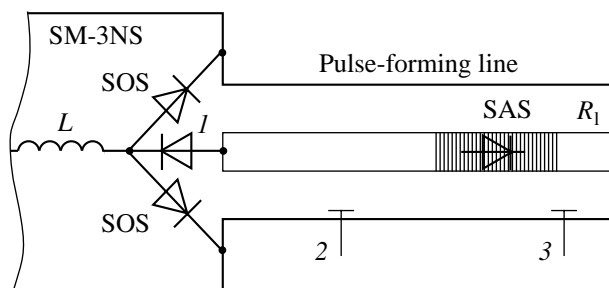


Fig. 1. Sketch of the experiment.

Institute of Electrophysics, Ural Division,
Russian Academy of Sciences,
ul. Amundsena 106, Yekaterinburg, 620016 Russia

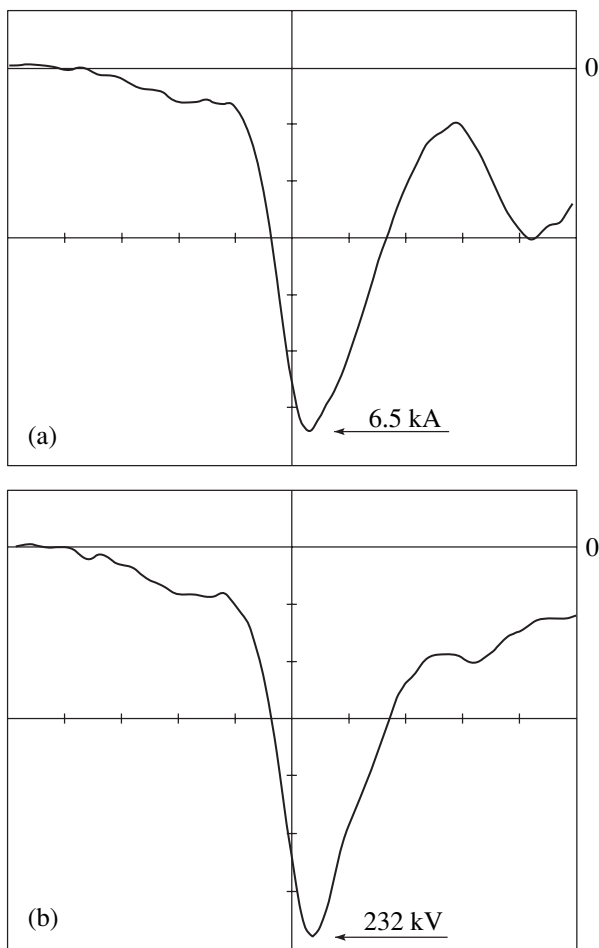


Fig. 2. Oscilloscope waveforms of (a) an SAS current pulse in the mode of the short-circuited load and (b) the voltage pulse for the load $R_1 = 53 \Omega$. The horizontal scale is 1 ns/division.

with the help of a low-inductive shunt mounted in the load circuit. A digital TDS684 oscilloscope with a 1-GHz transmission band was used for pulse recording. The intrinsic transient characteristic of the entire detection circuit was no longer than 500 ps. In the process of measurements, the signal attenuation in the measuring cables was taken into account. The overall measurement accuracy was no worse than 10%.

In preliminary experiments with an SAS terminated by a matched load $R_1 = 50 \Omega$, the length of the pulse-forming line was varied. This line determined the voltage at the SAS and the rate of the voltage rise. The number N of the series structures and their area S in the sharpener were adjusted to obtain a maximum pulsed power in the load. The optimized SAS contained $N = 144$ silicon semiconductor structures of p^+p-n-n^+ -type, which were connected in series. The structures were prepared according to diffusion technology with a deeply buried position of the $p-n$ -junction. The base length and the structure area were approximately 120 μm and 6.75 cm^2 , respectively. The length of the

entire device was 105 mm. The blocking diode I consisted of 60 identical structures each with an area of 2.25 cm^2 . The resistive load R_1 was assembled on the basis of TVO-2 low-inductive carbon resistors (12 in parallel).

In the case of current cutoff by the SOS switches, the pulse-forming line is charged from the inductive energy store L via the blocking diode I . In the experiments, the charging time and the line voltage lay within the ranges 3–5 ns and 240–350 kV, respectively. An oscillogram of the current through the SAS in the load short-circuited mode is shown in Fig. 2a. In this experiment, the length of the pulse-forming line was 7 cm. The line was charged up to ~ 300 kV for ~ 3 ns. When charging the line, the displacement current passes through the SAS, forming a precursor pulse, and then, the process of SAS switching-on follows. The amplitude of the current through the SAS was 6.5 kA. The precursor-pulse amplitude was 10% of that of the main pulse. Therefore, the switching time could be determined from the current and voltage oscillograms at the level of 0.2–0.9 of their amplitudes. Under these conditions, the current rise time in the load short-circuited mode was 0.68 ns. The current rise time in the steepest region of the switching characteristic was approximately 7 kA/ns.

In Fig. 2b, an oscillogram of the voltage pulse in a 53- Ω load is shown for a line length of 7 cm, a pulse amplitude of 232 kV, and a peak power of 1 GW. In this case, the rise time at the amplitude level of 0.2–0.9 was 0.85 ns and the pulse duration measured at the pulse half-height was 1.8 ns. The maximum rates for the rise of the current and the voltage were 3.6 kA/ns and 190 kV/ns, respectively.

The specific feature of the experimental operation is that the SAS does not represent a concentrated element but is a continuation of the inner conductor of the pulse-forming line, the SAS length in the majority of experiments exceeding the geometric length of the line. In the process of sharpener switching, the filling of the line section in which the SAS is installed occurs through the electric and magnetic field of the running electromagnetic wave. This fact explains the experimental data obtained. First, the duration of the pulses being formed coincides at their half-height with the time of double passage of the wave along the line, whose length is equal to the summary lengths of the pulse-forming line and of the SAS. Second, the pulse amplitude in the load is 70–80% of the charge voltage in the pulse-forming line instead of 50% when the charged line is switched in the matching load with a zero initial current.

We also tested the circuit in the frequency operation mode. The maximum pulse repetition rate was 3.5 kHz and was limited by the capabilities of the SM-3NS power-supply generator. Due to the limited power of the feeding circuit, the reduction of the generator input voltage occurred and, as a consequence, the amplitude of the output pulses decreased. At a pulse repetition rate

of 3.5 kHz, the mean power introduced into the load $R_1 = 53 \Omega$ attained 3.8 kW, while the pulse amplitude decreased to ~200 kV (~750 MW). In the mode with the maximum pulse repetition rate, the generator was switched for a time from 1 to 3.5 ns. The limitation was associated with the low shunted power (24 W) of the load resistors.

Thus, the work carried out has shown the feasibility of formation of super-powerful short pulses by a solid-state semiconductor device on the basis of a delayed shock-ionization wave. The levels attained in pulse power, voltage, and duration (1 GW, 230 kV, and 1.8 ns) correspond to the characteristics of frequency generators with high-pressure gas spark gaps: 0.3–3 GW, 140–210 kV, and 0.4–1.1 ns [7, 8]. The results obtained are explained, in the first turn, by the implementation of a powerful solid-state feeding generator with a high-rate output voltage rise in the experiment. This allowed us to realize the mode of the delayed shock-ionization wave in the sharpener with a large number of semiconductor structures. In this connection, further studies on the enhancement of the power being switched-on can be associated with the use of more powerful feeding generators and with increasing the number and area of structures involved in a sharpener.

REFERENCES

1. I. V. Grekhov and A. F. Kardo-Sysoev, *Pis'ma Zh. Tekh. Fiz.* **5**, 950 (1979) [*Sov. Tech. Phys. Lett.* **5**, 395 (1979)].
2. I. V. Grekhov, A. F. Kardo-Sysoev, L. S. Kostina, and S. V. Shenderei, *Zh. Tekh. Fiz.* **51**, 1709 (1981) [*Sov. Phys. Tech. Phys.* **26**, 984 (1981)].
3. V. M. Tuchkevich and I. V. Grekhov, *New Methods for High-Power Switching by Semiconductor Devices* (Nauka, Leningrad, 1988).
4. I. V. Grekhov, *Solid-State Electron.* **32**, 923 (1989).
5. S. K. Lyubutin, S. N. Rukin, B. G. Slovikovskii, and S. N. Tsyranov, *Prib. Tekh. Éksp.*, No. 3, 52 (2000).
6. S. K. Lyubutin, G. A. Mesyats, S. N. Rukin, and B. G. Slovikovskii, *Dokl. Akad. Nauk* **360**, 477 (1998) [*Dokl. Phys.* **43**, 349 (1998)].
7. M. I. Yalandin, S. K. Lyubutin, S. N. Rukin, *et al.*, *Pis'ma Zh. Tekh. Fiz.* **27**, 81 (2001) [*Tech. Phys. Lett.* **27**, 37 (2001)].
8. Yu. A. Andreev, Yu. I. Buyanov, V. A. Vizir', *et al.*, *Prib. Tekh. Éksp.*, No. 2, 82 (2000).

Translated by T. Galkina

Deformation Properties of High-Density Polyethylene-Filled with Rubber Particles

S. L. Bazhenov, G. P. Goncharuk, and O. A. Serenko

Presented by Academician N.F. Bakeev February 21, 2001

Received March 12, 2001

Recently, a new class of composite materials consisting of a polymer matrix and a filler in the form of small rubber particles with sizes on the order of 100 micron in diameter appeared [1–5]. In this study, we discovered that a gradual increase in filler concentration leads to two successive transitions of the deformation mechanism of a material made on the basis of a high-density polyethylene matrix. The first transition (from plastic to brittle failure) is observed after introducing into the material only several particles of an elastic filler per entire sample volume. For filler concentrations of 40–50 vol %, the second transition (from brittle to plastic failure) occurs. In this paper, we obtained the criterion for such a transition.

To prepare a composite material, we used high-density polyethylene with the trade mark 277-73. As a filler, we applied rubber particles prepared on the basis of ethylene-propylene-diene rubber obtained by grinding industrial rubber wastes. The size of the rubber particles varied between 100 and 600 μm .

The composite material was obtained by mixing in a melt with the help of a single-screw laboratory extruder. The filler concentrations were taken within the range between 2 and 95 wt % (1.8–94.5 vol %). We used the material obtained to make 2-mm-thick plates through hot pressing at 160°C and under 10-MPa pressure followed by cooling under pressure to room temperature. Next, for our investigations, we cut out samples in the form of a double-ended spade with dimensions of the useful part of 5 × 35 mm.

The mechanical properties of the composites were determined by a 2038 R-005 tension testing machine at room temperature. The deformation rate was 20 mm/min. After testing, the fracture surface was examined with the help of an MBS-9 optical microscope.

Figure 1 shows the stress–strain diagrams of unfilled high-density polyethylene (curve 1) and a series of

composites composed of high-density polyethylene with a different content of the filler (curves 2–5). The polyethylene deformation curve was characterized by forming a neck and a characteristic tooth-shaped yield curve. The neck propagation was unstable, and the samples failed in the process of the neck growth. In the course of deformation, polymer hardening did not occur and the rupture stress was equal to the lower limit of the yield stress.

Introducing rubber particles into polyethylene changed both the shape of the stress–strain diagram and the character of the material failure. For a relatively small rubber content, the deformation diagram acquired a shape typical of brittle materials (curves 2, 3 in Fig. 1). In order to determine the critical concentration of particles, which corresponds to the transition to brittle failure, we prepared samples containing only a

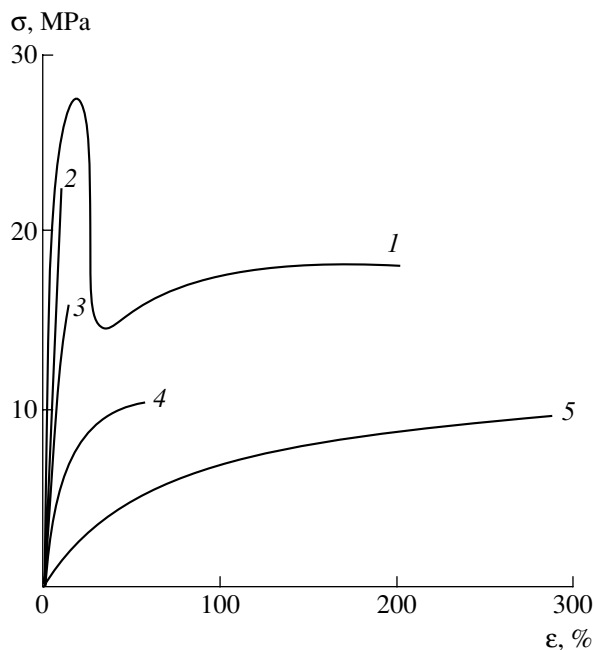


Fig. 1. Tensile stress σ as a function of strain ϵ for (1) unfilled high-density polyethylene and composites of high-density polyethylene with rubber. The filler content is (2) 4.3, (3) 26.7, (4) 46, and (5) 88.4 vol %.

few rubber particles. These samples exhibited brittle failure before neck formation. Their ultimate strength practically coincided with the upper yield point of the unfilled matrix. Thus, after introducing only one filler particle into the entire sample volume, the material becomes brittle. This fact is illustrated in Fig. 2 as a photograph of a sample containing a single rubber particle. Sample constriction in the fracture plane is absent, and the failure is actually brittle. The crack grew starting from the particle (that, apparently, served as its nucleus) rather than along the matrix–rubber interface. This fact indicates that the adhesion strength of the interfacial polyethylene–rubber boundary is higher than the particle’s strength.

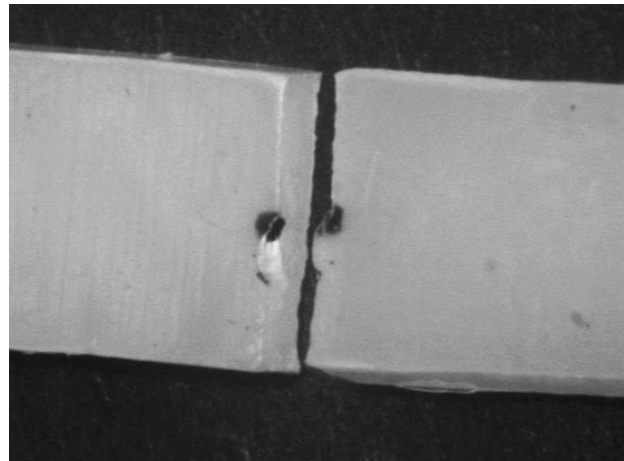


Fig. 2. Example of a sample containing one rubber particle.

At first glance, after introducing rubber particles, the brittle fracture of the polymer is unexpected. It is well known that introducing rubber particles makes it possible to obtain shock-proof thermoplastic polymers [6, 7]. In content, rubber plastics are analogs of shock-proof polymers but sharply differ in structure. First, the particle sizes are different. In shock-proof polymers, particle diameters are on the order of a few hundred nanometers compared to a few hundred microns in rubber plastics. Second, for a rubber concentration exceeding 40 vol %, shock-proof polymers undergo phase inversion and the material transforms into rubber filled with polymeric particles [8]. In contrast, in rubber plastics, the filling degree is as high as 95% but the polymer preserves the phase continuity and all matrix properties [9].

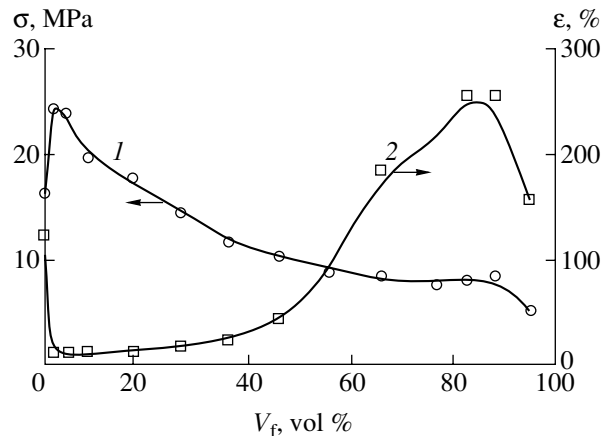


Fig. 3. Dependence of (1) strength σ_p and (2) fracturing strain ϵ_p of the composites as functions of the volume fraction of rubber particles V_f .

Figure 3 shows the strength (curve 1) and the fracturing deformation (curve 2) of the composites as functions of concentration of the rubber particles. After introducing an elastic filler, the ultimate strength increases and becomes higher than the polymer strength. This is explained by the transition to brittle failure. The strength of an unfilled polymer is equal to the neck propagation stress (lower yield stress). After introducing a filler, material failure occurs when the stress approaches the upper yield point, which causes an increase in the failure stress. The further increase in the filler concentration gives rise to monotonic reduction of the composite strength.

Introducing a filler causes a sharp decrease in the ultimate elongation (by a factor of approximately 20). For particle concentrations within the range between 2 and 30 vol %, the ultimate elongation is constant and equals 10–15%. A further increase in particle concentration up to $V_f = 40$ –50 vol % results in a gradual increase of the fracturing deformation of the composite (curve 1 in Fig. 3). For a filling degree higher than 50 vol %, the material is deformed macrouniformly. In the process of deformation, there appear a set of shear bands on the surfaces of the samples and microzones are formed in which the matrix plastic flow is localized. These facts indicate that, within this range of compositions, the material-deformation mechanism changes. It

is worth noting that the transition to the macrouniform deformation of a composite was previously observed in isotactic polypropylene filled with $\text{Al}(\text{OH})_3$ particles that were previously subjected to the action of an anti-adhesive substance in order to decrease adhesion to the matrix [10].

We now consider a model characterizing the transition from brittle to plastic deformation. In this model, the spherical particles are assumed to be situated in the sites of a regular cubic lattice (Fig. 4) [11–13]. It is natural to suppose that the material flow is initiated in the cross section AB in which the area of the polymer matrix is minimal. As was mentioned above, when the concentration of rubber particles exceeds 50 vol %, a large number of microzones is formed in the plastic flow. As a result, the sample consists of alternating areas of plastically deformed microzones and undistorted material. In the model under consideration, these zones correspond to planes crossing particle centers.

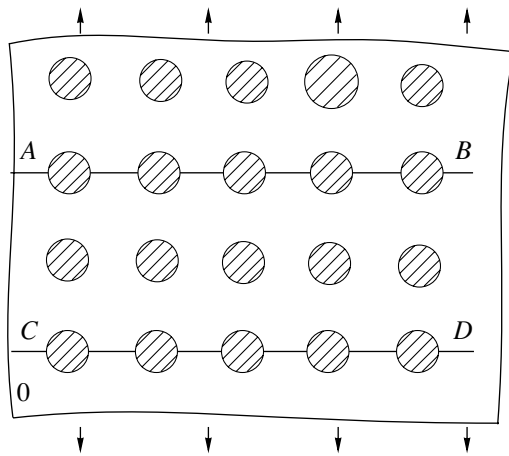


Fig. 4. Model of the composite. The arrows indicate the extension direction.

We assume that the first yield microzone was formed in the AB plane (Fig. 4). The next microzone in the CD plane can appear provided the strength of the formed zone is higher than that required for the appearance of the second microzone. Mathematically, this condition is written out in the form $\sigma_z > \sigma_y$, where σ_z is the strength of the microzone and σ_y is the upper yield stress of the composite. Thus, a criterion characterizing the transition from brittle to plastic deformation has the form [14]

$$\sigma_z = \sigma_y. \quad (1)$$

The deformation of the composite, while initiating plastic deformation, is not strong ($\sim 10\%$), and the stress in the rubber particles is negligible compared to that of the matrix. As a consequence, in the case of initiating plastic deformation, the particles behave like pores. The effect of pores on the upper yield stress σ_y of a composite was studied rather thoroughly, and σ_y is fairly well described by the relationship [15]

$$\sigma_y = \sigma_{ym} \left(1 - \sqrt[3]{\frac{9\pi}{16} V_f^{2/3}} \right), \quad (2)$$

where σ_{ym} is the upper yield point of the matrix and V_f is the volume fraction of the filler particles.

It is evident that the failure of the composite occurs through the crack growth along the weakest cross section of the material (the AB plane in Fig. 4). Unlike the initiation of plastic deformation, the stress in rubber particles in the course of failure can be compared to the matrix strength. The strength of the composite is equal to the sum of the strengths in both the matrix and the particles in the AB plane with allowance for their cross sections:

$$\sigma_z = \sigma_m S_m + \sigma_f S_f. \quad (3)$$

Here, σ_m is the matrix strength, equal to the lower yield point in our case; σ_f is the strength of the rubber parti-

cles; and S_m and S_f are the cross sections of the matrix and the rubber particles, respectively. It is easy to show that the area of particles in the AB plane is equal to

$\sqrt[3]{\frac{9\pi}{16} V_f^{2/3}}$. Thus, Eq. 3 takes the form

$$\sigma_z = \sigma_m \left(1 - \sqrt[3]{\frac{9\pi}{16} V_f^{2/3}} \right) + \sigma_f \sqrt[3]{\frac{9\pi}{16} V_f^{2/3}}. \quad (4)$$

The transition from material brittle behavior to plastic behavior is determined from Eqs. (1), (2), and (4):

$$V_f^* = \left(\sqrt[3]{\frac{16}{9\pi} \frac{\sigma_{ym} - \sigma_m}{\sigma_f + \sigma_{ym} - \sigma_m}} \right)^{3/2}, \quad (5)$$

where V_f^* is the critical degree of filling. According to Eq. (5), the critical concentration of the filler depends only on two parameters, namely, the strength of the particles and the height of the tooth shaped yield curve, which is equal to the difference $\sigma_{ym} - \sigma_m$.

The value $\sigma_f = 8$ MPa is determined by extrapolating the dependence of the composite strength to $V_f = 100\%$ (Fig. 3). The lower yield stress of the matrix σ_m is equal to 17 MPa. Substituting the characteristics of the matrix and the filler ($\sigma_{ym} = 28$ MPa, $\sigma_f = 8$ MPa, and $\sigma_m = 17$ MPa), we obtain $V_f^* \sim 35\%$. This estimate of the critical filler concentration is in satisfactory agreement with experimental data.

For the degree of filling $V_f < 35$ vol %, the strength of microzones is lower than the composite yield strength ($\sigma_z < \sigma_y$) and the composite failure occurs as brittle. At $V_f > 35$ vol %, the reversed inequality $\sigma_z > \sigma_y$ is valid and the composite is plastically deformed. The transition from brittle to plastic deformation is explained by the fact that the particles do not exfoliate from the matrix and undergo a load whose value is comparable to the height of the tooth-shaped yield curve. This fact leads to stabilization of the composite-material deformation.

Comparing Eqs. 2 and 4, we can see that the inequality $\sigma_z > \sigma_y$ is fulfilled for any degree of filling provided the matrix strength is higher than its upper yield point. This implies that there exists a principle possibility of avoiding composite brittle failure if the matrix capability of the strain hardening is so high that the ultimate strength exceeds the yield point.

REFERENCES

1. V. P. Skvortsov, V. N. Kuleznev, L. O. Bunina, *et al.*, *Plast. Massy*, No. 5, 39 (1989).
2. P. Rajalingam, J. Sharpe, and W. E. Baker, *Rubber Chem. Technol.* **66**, 664 (1993).
3. D. L. Titov, S. A. Pershin, M. I. Knunyants, and A. N. Kryuchkov, *Vysokomol. Soedin., Ser. A* **36**, 1353 (1994).

4. O. A. Serenko, G. P. Goncharuk, M. I. Knunyants, and A. N. Kryuchkov, *Vysokomol. Soedin.*, Ser. A **40**, 1186 (1998).
5. M. I. Knunyants, L. M. Chepel', A. N. Kryuchkov, *et al.*, *Mekh. Kompoz. Mater.*, No. 5, 927 (1988).
6. R. P. Burford and M. Pittolo, *J. Mater. Sci. Lett.* **6**, 969 (1987).
7. K. B. Baknell, *Shockproof Plastics* (Khimiya, Leningrad, 1981).
8. V. N. Kuleznev, *Mixtures of Polymers* (Khimiya, Moscow, 1980).
9. G. P. Goncharuk, A. N. Kryuchkov, M. I. Knunyants, *et al.*, in *Scientific and Informational Collection of Papers. Institute of Tyre Industry* (Moscow, 1999), No. 5.
10. I. L. Dubnikova, V. A. Topolkaev, T. V. Paramzina, and F. S. D'yachkovskii, *Vysokomol. Soedin.*, Ser. A **32**, 841 (1990).
11. T. L. Smith, *Trans. Soc. Rheol.* **3**, 113 (1959).
12. L. E. Nielsen, *J. Appl. Polym. Sci.* **10**, 97 (1966).
13. S. Bazhenov, J. X. Li, A. Hiltner, and E. Baer, *J. Appl. Polym. Sci.* **52**, 243 (1994).
14. S. Bazhenov, *Polym. Eng. Sci.* **35**, 813 (1995).
15. L. Nicolais and M. Narkis, *Polym. Eng. Sci.* **11**, 194 (1971).

Translated by Yu. Vishnyakov

On Stability in the Joukowski Sense for Trajectories of Classical Keplerian Motions

O. V. Druzhinina

Presented by Academician V.V. Rumyantsev March 3, 2001

Received March 19, 2001

In this paper, we prove that elliptic trajectories of classical unperturbed Keplerian motions, which are unstable in the sense of Lyapunov, are stable in the Joukowski sense.

The equations for unperturbed Keplerian motions have the form

$$\begin{aligned} \ddot{x}_i + K^2 r^{-3} x_i &= 0, \quad i = 1, 2, 3, \\ r^2 &= x_1^2 + x_2^2 + x_3^2, \end{aligned} \quad (1)$$

where $\ddot{x}_i = \frac{d^2 x_i}{dt^2}$ and K^2 is the gravitation constant.

Introducing a new independent variable s with the help of the relationship

$$\frac{dt}{ds} = r \quad (2)$$

and denoting

$$\begin{aligned} x_1 &= u_1^2 - u_2^2 - u_3^2 + u_4^2, \\ x_2 &= 2(u_1 u_2 - u_3 u_4), \quad x_3 = 2(u_1 u_3 - u_2 u_4), \end{aligned}$$

we arrive at the regularized differential equations in the variables u_j , which take the form

$$\begin{aligned} u_j'' + \frac{h}{2} u_j &= 0, \quad j = 1, 2, 3, 4, \\ r'' + 2hr &= K^2, \end{aligned} \quad (3)$$

where $-h$ is the total energy [1].

As was proved in [1], an arbitrary elliptic solution (with $h > 0$) to classical Newtonian equations (1) is unstable in the Lyapunov sense and any solution to regularized system (3) is stable in the Lyapunov sense for $h > 0$. We here prove that the trajectories of Keplerian motions (1) are stable in the Joukowski sense.

In what follows, we will use the general canonical theory [1] in the generalized phase space. Let q_i and p_i be the generalized coordinates and momenta, respectively, $H(p_i, q_i, t)$ be the Hamiltonian, and $P_i(p_k, q_k, t)$ be the nonconservative forces. The generalized Hamiltonian variational principle [1, 2] states that

$$\int_{t_1}^{t_2} \left\{ \delta \left[\sum_i p_i \dot{q}_i - H \right] + \sum_i P_i \delta q_i \right\} dt = 0, \quad (4)$$

where $H = H(p_i, q_i, t)$; $P_i = P_i(p_k, q_k, t)$; $i, k = 1, 2, \dots, n$; and the quantities δq_i are the displacements from the point (q_1, \dots, q_n) to the point $(q_1 + \delta q_1, \dots, q_n + \delta q_n)$, with these points being on the actual and varied trajectories in q -space, respectively, and corresponding to the same instant of time.

From (4), it is easy to obtain the following Euler equations of motion for the mechanical system:

$$\dot{q}_i = \frac{\partial H}{\partial p_i}, \quad \dot{p}_i = -\frac{\partial H}{\partial q_i} + P_i, \quad i = 1, 2, \dots, n. \quad (5)$$

We note that variational problem (4) is invariant with respect to arbitrary noncanonical transformations of the dependent variables q_i and p_i .

We now introduce a new independent variable by the following manner. Instead of (2), we consider the more general transformation

$$\frac{dt}{ds} = \mu > 0, \quad (6)$$

where μ is a continuously differentiable scalar function of q_1, q_2, \dots, q_n .

We now generalize the classical concept of the canonical transformation by introducing a differential transformation (6) of the independent variable. In this case, we treat the physical time t as a new coordinate q_0 and introduce the conjugate momentum p_0 in the variational principle. The meaning of the symbol P_0 will be

elucidated below. Then, variational principle (4) takes the following form:

$$\int_{s_1}^{s_2} \left\{ \delta \left[p_0 \frac{dq_i}{ds} + \sum_i P_i \frac{dq_i}{ds} - \mu(H + p_0) \right] + \mu P_0 \delta q_0 + \mu \sum_i P_i \delta q_i \right\} ds = 0, \quad (7)$$

$$H = H(p_i, q_i, t), \quad P_i = P_i(p_k, q_k, t),$$

$$\mu = \mu(p_i, q_i, p_0, q_0) > 0, \quad i, k = 1, 2, \dots, n.$$

Hence we obtain the following set of differential equations of motion:

$$\frac{dq_i}{ds} = \mu \frac{\partial H}{\partial p_i} + \{H + p_0\} \frac{\partial \mu}{\partial p_i}, \quad (8)$$

$$\frac{dq_0}{ds} = \mu + \{H + p_0\} \frac{\partial \mu}{\partial p_0}, \quad (9)$$

$$\frac{dp_i}{ds} = -\mu \frac{\partial H}{\partial q_i} - \{H + p_0\} \frac{\partial \mu}{\partial q_i} + \mu P_i, \quad (10)$$

$$\frac{dp_0}{ds} = -\mu \frac{\partial H}{\partial q_0} - \{H + p_0\} \frac{\partial \mu}{\partial q_0} + \mu P_0. \quad (11)$$

We specify the conditions required for the quantity

$$\mu(H + p_0) \quad (12)$$

(called a generalized homogeneous Hamiltonian) to be an integral of motion. For this purpose, we set

$$P_0 = -\sum_{j=1}^n P_j \frac{\partial H}{\partial p_j}, \quad (13)$$

where P_0 is a negative dissipative force.

We impose the initial conditions for p_0 at the instant of time $t = q_0 = s = 0$. If we set $p_0 = -H$, then the functions $\mu(H + p_0)$ and $H + p_0$ vanish on the trajectory. Under these conditions, the quantity p_0 is equal to the total negative energy and Eq. (9) reduces to

$$\frac{dq_0}{ds} = \mu;$$

thus, time transformation (6) becomes one of Eqs. (8)–(11). Finally, Eq. (11) acquires the form of the energy equation:

$$\frac{dp_0}{ds} = -\mu \frac{\partial H}{\partial q_0} + \mu P_0. \quad (14)$$

In the rectangular Cartesian coordinate system, with p_1 , p_2 , and p_3 being momenta, unperturbed Keplerian prob-

lem (1) is described by the Hamiltonian

$$H(t, x_1, x_2, x_3, p_1, p_2, p_3) = \frac{1}{2}(p_1^2 + p_2^2 + p_3^2) - K^2 r, \quad (15)$$

$$r^2 = x_1^2 + x_2^2 + x_3^2,$$

which generates a canonical system of six equations:

$$\frac{dx_k}{dt} = \frac{\partial H}{\partial p_k}, \quad \frac{dp_k}{dt} = -\frac{\partial H}{\partial x_k}, \quad k = 1, 2, 3. \quad (16)$$

The inclusion of the time transformation $\frac{dt}{ds} = \mu(x_1, x_2, x_3, p_1, p_2, p_3)$ necessitates introduction of the corresponding homogeneous Hamiltonian,

$$H_h = H + p_0 = \frac{1}{2}(p_1^2 + p_2^2 + p_3^2) - K^2 r^{-1} + p_0, \quad (17)$$

and an associated system of eight equations:

$$\frac{dx_j}{dt} = \frac{\partial H_h}{\partial p_j}, \quad \frac{dp_j}{dt} = -\frac{\partial H_h}{\partial x_j}, \quad j = 0, 1, 2, 3. \quad (18)$$

Here, $x_0(t) = t$, $p_0(t) = -H(t)$ is the total negative energy, and the initial conditions have the form

$$x_0(0) = 0, \quad p_0(0) = -H(0, x_1(0), x_2(0), x_3(0), p_1(0), p_2(0), p_3(0)).$$

Hence the new functions $x_k(s)$ and $p_k(s)$ of s can be found from the system of equations

$$\frac{dx_j}{dt} = \frac{\partial \tilde{H}_h}{\partial p_j}, \quad \frac{dp_j}{dt} = -\frac{\partial \tilde{H}_h}{\partial x_j}, \quad j = 0, 1, 2, 3, \quad (19)$$

where $\tilde{H}_h = \mu H_h$ and the initial conditions for problem (19) are the same as at $s = 0$. Therefore, the time transformation need not be taken into account since it coincides with one of Eqs. (19).

Next, we consider the cases when

$$\mu = r \quad (20)$$

or

$$\mu = \frac{r}{\sqrt{2p_0}}. \quad (21)$$

In the cases of (20) and (21), the fictitious time $\frac{1}{ds} =$

$x \frac{1}{dt}$ (i.e., $dt = x ds$) and the generalized eccentric anom-

aly $E = 2 \sqrt{\frac{h}{2}} s$, respectively, should be treated as independent variables.

Under the above conditions, variational problem (7) for the perturbed motion has the form

$$\int_{s_1}^{s_2} \left\{ \delta \left[p_0 \frac{dx_0}{ds} + \sum_i p_i \frac{dx_i}{ds} - \left(\frac{r}{2\sqrt{2}p_0} \sum_i p_i^2 - \frac{K^2}{\sqrt{2}p_0} + \frac{r}{\sqrt{2}p_0} \varepsilon V + \sqrt{\frac{p_0}{2}} r \right) \right] + \frac{r}{\sqrt{2}p_0} \varepsilon P_0 \delta x_0 \right. \tag{22}$$

$$\left. + \frac{r}{\sqrt{2}p_0} \varepsilon \sum_i P_i \delta x_i \right\} ds = 0,$$

$$P_0 = -\sum_j P_j p_j, \quad i, j = 1, 2, 3.$$

Here, $x_0 = q_0 = t$ is the physical time, p_0 is the total negative energy, V is the potential, εP_i are the forces that cannot be obtained from the potential, and ε is a small perturbation parameter.

For variational problem (22), the Euler equations lead to the following system of equations:

$$\frac{dx_i}{ds} = \frac{r}{\sqrt{2}p_0} p_i, \quad i = 1, 2, 3, \tag{23}$$

$$\begin{aligned} \frac{dx_0}{ds} &= \frac{r}{\sqrt{2}p_0} - \left\{ \frac{1}{2} \sum_i p_i^2 - \frac{K^2}{r} + \varepsilon V + p_0 \right\} \frac{r}{\sqrt{2}p_0^3} \\ &= \frac{r}{2\sqrt{2}p_0} - \left[\frac{r}{2} \sum_i p_i^2 - K^2 + \varepsilon r V \right] \frac{r}{\sqrt{2}p_0^3}, \end{aligned} \tag{24}$$

$$\begin{aligned} \frac{dp_i}{ds} &= \frac{r}{\sqrt{2}p_0} - \left(-\frac{K^2}{r^3} x_i - \varepsilon \frac{\partial V}{\partial x_i} \right) \\ &- \left\{ \frac{1}{2} \sum_i p_i^2 - \frac{K^2}{r} + \varepsilon V + p_0 \right\} \frac{x_i}{r\sqrt{2}p_0} \\ &+ \frac{r}{\sqrt{2}p_0} \varepsilon P_i = - \left(\frac{\sum_i p_i^2}{2\sqrt{2}p_0} + \sqrt{\frac{p_0}{2}} \right) \frac{x_i}{r} \end{aligned} \tag{25}$$

$$- \frac{\varepsilon}{\sqrt{2}p_0} \frac{\partial(rV)}{\partial x_i} + \frac{r}{\sqrt{2}p_0} \varepsilon P_i, \quad i = 1, 2, 3,$$

$$\frac{dp_0}{ds} = \frac{r}{\sqrt{2}p_0} \varepsilon \left[-\frac{\partial V}{\partial x_0} + P_0 \right]. \tag{26}$$

Let the solution $x_i(s), x_0(s), p_i(s), p_0(s)$ to Eqs. (23)–(26), which is specified by the initial conditions $\bar{x}_i(0),$

$\bar{p}_i(0),$ and $\bar{p}_0(0)$ at $s = 0,$ correspond to the solution $x_i(t)$ to Eqs. (1). The solution $x_i(t)$ to Eqs. (1) is referred to as stable in the Joukowski sense if, for each $\varepsilon > 0,$ there exist numbers $\delta_i > 0, i = 1, 2, 3,$ and 4, such that the inequalities

$$\begin{aligned} |x_i(0) - \bar{x}_i(0)| &< \delta_1, & |x_0(0) - \bar{x}_0(0)| &< \delta_2, \\ |p_i(0) - \bar{p}_i(0)| &< \delta_3, & |p_0(0) - \bar{p}_0(0)| &< \delta_4 \end{aligned}$$

follow from the inequalities

$$\begin{aligned} |x_i(s) - \bar{x}_i(s)| &< \varepsilon, & |x_0(s) - \bar{x}_0(s)| &< \varepsilon, \\ |p_i(s) - \bar{p}_i(s)| &< \varepsilon, & |p_0(s) - \bar{p}_0(s)| &< \varepsilon \quad \forall s > 0. \end{aligned}$$

This formulation of the stability in the Joukowski sense is a concrete definition of that introduced and studied in [3] for a general smooth dynamical system.

Theorem 1. Any solution $x_i(t)$ to Eqs. (1) is stable in the Joukowski sense if $h > 0.$

Proof. We substitute the variable defined by (6) into (1) and pass to Eqs. (23)–(26). We set $\varepsilon = 0$ and assume that the energy does not varied. It is sufficient to prove that any solution to system (23)–(26) is stable in the Lyapunov sense. For $\varepsilon = 0,$ system (23)–(26) has the following first integral:

$$x_0 = \frac{1}{2p_0} \left[\frac{K^2}{\sqrt{2}p_0} s - \sum_i x_i p_i \right] + C, \tag{27}$$

where C is an integration constant.

According to Kepler’s law, we have

$$\sum_i x_i p_i = \sqrt{2p_0} e \sin E, \tag{28}$$

where $E = s + \text{const}$ is the eccentric anomaly and e is the eccentricity.

The left-hand side of Eq. (28) is a periodic function. It follows from Eq. (28) that varying the initial conditions for the quantities x_i and p_i results in a periodic variation in the time $x_0.$ In this case, the coordinate x_0 (considered as a function of s) is stable in the Lyapunov sense. Multiplying Eqs. (23)–(26) by $\sqrt{2}p_0$ and eliminating the quantity p_i does not influence the stability in the Joukowski sense. Then, we obtain

$$\frac{d^2 x_i}{dt^2} - \frac{\sum_j x_j \frac{dx_j}{ds}}{r^2} \frac{dx_i}{ds} = - \left(\frac{\sum_j \left(\frac{dx_j}{ds} \right)^2}{2r^2} + p_0 \right) x_i \tag{29}$$

$$- r \varepsilon \frac{\partial(rV)}{\partial x_i} + r^2 \varepsilon P_i, \quad i = 1, 2, 3,$$

$$\frac{dp_0}{ds} = -\varepsilon \left[r \frac{\partial V}{\partial x_0} + \sum_j P_j \frac{dx_j}{ds} \right], \tag{30}$$

$$\frac{dx_0}{ds} = \frac{r}{2} - \left[\frac{\sum_j \left(\frac{dx_j}{ds} \right)^2}{2r} - K^2 + \varepsilon r V \right] \frac{1}{2p_0}. \quad (31)$$

In the system of equations (29)–(31), the quantity s is not a generalized eccentric anomaly, but it is proportional to this anomaly.

For $\varepsilon = 0$, the solutions to Eqs. (29) and (30) are stable in the Lyapunov sense. Equations (29) and (30) coincide with those for x_i and p_0 ($p_0 = h$) obtained in [4, 5], in which the stability in the Lyapunov sense was proved with the help of the Levi-Civita transformation.

Since the solutions to Eqs. (29) and (30) are stable in the Lyapunov sense for $\varepsilon = 0$, the solution to Eqs. (1) for $h > 0$ is stable in the Joukowski sense.

The proposed method of treating the stability for the trajectories of classical Keplerian motions does not employ the concept of a time variable introduced in [1] and can be used not only for ordinary coordinates but also for KS -coordinates. The corresponding vector KS -equations have the form

$$\frac{d^2 u}{ds^2} + \frac{h}{2} u = \frac{\varepsilon}{4} \frac{\partial}{\partial u} (|u|^2 V) + \frac{\varepsilon}{2} |u|^2 L^T P, \quad (32)$$

$$\frac{dh}{ds} = -\varepsilon |u|^2 \frac{\partial V}{\partial t} - 2\varepsilon \left(\frac{du}{ds}, L^T P \right), \quad (33)$$

$$\frac{dt}{ds} = \frac{1}{2} |u|^2 - \left[2 \left| \frac{du}{ds} \right|^2 - K^2 + \varepsilon |u|^2 V \right] \frac{1}{2h}, \quad (34)$$

where $p_0 = h$, $x_0 = t$.

ACKNOWLEDGMENTS

The author is grateful to Academician V.V. Rumyantsev and Prof. A.A. Shestakov for their attention to this work.

This work was supported by the Ministry of Education RF, project no. 020702-075.

REFERENCES

1. E. Stiefel and G. Scheifele, *Linear and Regular Celestial Mechanics* (Springer-Verlag, Berlin, 1971; Nauka, Moscow, 1975).
2. A. S. Galiullin and A. A. Shestakov, *Vestn. Ross. Univ. Druzhby Narodov, Ser. Prikl. Mat. Inf.*, No. 2, 20 (1996).
3. O. V. Dunaeva, *Dokl. Akad. Nauk* **355** (1), 51 (1997) [*Phys. Dokl.* **42**, 374 (1997)].
4. J. Baumgarte, *Celest. Mech.* **5**, 490 (1972).
5. J. Baumgarte, *Celest. Mech.* **13**, 247 (1976).

Translated by Yu. Vishnyakov

Nonintegrability of a Bounded Two-Body Problem on a Sphere

S. L. Ziglin

Presented by Academician V.V. Kozlov February 21, 2001

Received March 13, 2001

The bounded two-body problem on a sphere of unit radius is related to the Hamiltonian system with two degrees of freedom described by the Hamiltonian

$$H = \frac{1}{2} \left(p_\theta^2 + \frac{p_\varphi^2}{\sin^2 \theta} \right) + \omega (p_\theta \cos \varphi - p_\varphi \sin \varphi \cot \theta) - \alpha \cot \theta$$

(see [1–3]). Here, θ and φ are spherical coordinates in the moving reference system related to a body with nonzero mass, p_θ and p_φ are momentum components conjugated to these coordinates, ω is the angular velocity of a body with nonzero mass, and α is the gravitational constant.

We consider the system with Hamiltonian H in complexified phase space M^4 , which is the direct product of the complexified circle $S^1_{\mathbb{C}}$ with coordinate $\theta \pmod{2\pi}$

except for points 0 and π , the complexified circle $S^1_{\mathbb{C}}$ with coordinate φ , and the two complex straight lines \mathbb{C}^1 with coordinates p_θ and p_φ .

At $\alpha = 0$ or $\omega = 0$, the system under study has an additional analytical first integral (i. e., an integral functionally independent of the Hamiltonian).

According to the numerical calculations [3], this integral seems to be absent at $\alpha \neq 0$, $\omega \neq 0$. The main result of the present paper is the following theorem proving this conjecture.

Theorem. *At $\alpha \neq 0$, $\omega \neq 0$, the system with Hamiltonian H has no additional meromorphic first integral in the phase space M .*

Proof. Hamiltonian H is invariant with respect to the involutory symplectic diffeomorphism

$$J: M \rightarrow M, \quad J: (\theta, \varphi, p_\theta, p_\varphi) \mapsto (\theta + \pi, \varphi, p_\theta, p_\varphi).$$

The induced Hamiltonian system on the factor manifold $\bar{M} = M/J$ has a one-parameter family of phase curves $\Gamma(k)$, $k \in \mathbb{R}$. These curves do not correspond to

the equilibrium positions and are defined by the equations

$$\varphi = p_\varphi = 0, \quad \frac{1}{2} p^2 - \alpha \cot \theta = k,$$

where $p = p_\theta + \omega$, $k = h + \frac{\omega^2}{2}$, and h is the constant in the Hamiltonian.

In the phase curve $\Gamma(k)$, we have

$$\cot \theta = \frac{1}{\alpha} \left(\frac{1}{2} p^2 - k \right), \quad \dot{p} = -\frac{1}{4\alpha} \prod_{j=1}^4 (p - p_j),$$

$$p_1 = \sqrt{2(k + \alpha i)}, \quad p_2 = -p_1,$$

$$p_3 = \overline{p_1}, \quad p_4 = \overline{p_2}.$$

Taking p as a coordinate in the phase curve $\Gamma(k)$, we find that the latter is the complex plane \mathbb{C} except for the points p_j , $j = 1, 2, 3, 4$.

To simplify the notation, we denote $d\varphi$ as φ , dp_φ as p_φ , and the derivative with respect to p as prime. Then, we write the reduced set of variational equations along the phase curve $\Gamma(k)$, i. e., the constraints on the normal variational set of equations along this phase curve onto the zero equiscalar surface of its first integral dH (see [4]). These equations have the form

$$\varphi' = 2\omega\varphi \frac{p^2 - 2k}{4} - \frac{p_\varphi}{\alpha}, \quad \prod_{j=1}^4 (p - p_j) \tag{1}$$

$$p_\varphi' = -4\alpha\omega\varphi \frac{p - \omega}{4} - 2\omega p_\varphi \frac{p^2 - 2k}{4} \prod_{j=1}^4 (p - p_j).$$

Introducing the notation $x = p_\varphi p$, $y = \begin{pmatrix} \varphi \\ x \end{pmatrix}$, we rewrite Eqs. (1) in the form of a Fuchs set:

$$y' = \sum_{j=0}^4 \frac{A_j}{p - p_j} y, \tag{2}$$

where $p_0 = 0$,

$$A_0 = \begin{pmatrix} 0 & -\frac{1}{\alpha} \\ 0 & 1 \end{pmatrix}, \quad A_j = \begin{pmatrix} r_j & 0 \\ a_j & -r_j \end{pmatrix}, \quad j = 1, 2, 3, 4,$$

$$r_j = \frac{\omega}{2p_j}, \quad a_j \in \mathbb{C}, \quad \sum_{j=1}^4 A_j = 0.$$

It is obvious that all solutions to set (2) are holomorphic at the point p_0 .

Near the point $p_j, j = 1, 2, 3, 4$ set (2) has two linearly independent solutions in the form $y = (p - p_j)^{\pm r_j} f^{\pm}(p)$, where f^{\pm} are the holomorphic vector functions $f^{\pm}(p_j) \neq 0$ and $f^-(p_j) \parallel \begin{pmatrix} 0 \\ 1 \end{pmatrix}$.

Let us assume that the system with Hamiltonian H has an additional meromorphic first integral in the manifold M . Then, according to the lemma from Section 1.5 in [4], the induced Hamiltonian system in the factor manifold \bar{M} also has an additional meromorphic first integral. The eigenvalues of transformations generated by set (2) in the course of path-tracing around the points $p_j, j = 1, 2, 3, 4$ are not equal to the values of the square root from unity. Then, according to Theorem 2 from [4], the eigenvectors of these transformations coincide. Hence it follows that set (2) has two linearly independent solutions in the form

$$y = \prod_{j=1}^4 (p - p_j)^{q_j} f(p), \tag{3}$$

where $q_j = \pm r_j$ and f is the entire vector function. From this relationship and from set (2) it follows that, in the neighborhood of the infinite point, all solutions to this set can be represented in the form of a Laurent series

expansion:

$$y = \sum_{j=-\infty}^1 y_j p^j, \quad y_j \in \mathbb{C}^2. \tag{4}$$

Introducing the notation $s = \sum_{j=1}^4 q_j$, we obtain from relationships (3) and (4)

$$s \in \mathbb{Z}. \tag{5}$$

Let us choose the parameter k of the phase curve $\Gamma(k)$ in such a way that $4\text{Re}r_1$ is not an integer. Then, it follows from (5) that $s = 0$; hence

$$f = \begin{pmatrix} ap + b \\ ct + d \end{pmatrix}, \quad a, b, c, d \in \mathbb{C}.$$

Let us choose one of the two linearly independent solutions to set (2) in form (3) in such a way that equality $q_j = -r_j$ is valid for at least two j values ($j = 1, 2, 3, 4$). Then, for these j values, we have $ap_j + b = 0$; i.e., $a = b = 0$. Hence $\varphi \equiv 0, x \equiv 0$; i. e., $y \equiv 0$, which is incorrect. The theorem is proved.

ACKNOWLEDGMENTS

The author is grateful to A.V. Borisov for the posed problem and to V.V. Kozlov for valuable discussions.

REFERENCES

1. V. V. Kozlov, *Vestn. Mosk. Univ., Ser. 1: Mat. Mekh.*, No. 2, 28 (1994).
2. V. V. Kozlov and A. O. Harin, *Celest. Mech. Dyn. Astron.* **54**, 393 (1992).
3. A. V. Borisov and I. S. Mamaev, *Poisson Structures and Lie Algebras in Hamiltonian Mechanics* (Udmurtskiĭ Univ., Izhevsk, 1999).
4. S. L. Ziglin, *Funkts. Anal. Ego Prilozh.* **16** (3), 30 (1982).

Translated by K. Kugel

Steady Waves Generated by a Moving Body and Wave Drag

D. V. Maklakov

Presented by Academician G.G. Chernyi February 28, 2001

Received March 6, 2001

We consider a system of nonlinear periodic waves with wavelength λ . The waves move in a fluid from the right to the left with a constant phase velocity c above a flat horizontal bottom, the gravitational acceleration being g . The fluid is assumed to be perfect and incompressible. The motion is perceived to be two-dimensional and vortex-free. We introduce a coordinate system Oxy moving together with the waves in which the flow is steady. The x -axis is aligned with the bottom, and the y -axis is directed vertically upwards so that it intersects one of the wave crests. As may be inferred from dimensional analysis, a steady flow is determined by two dimensionless parameters. We denote these parameters as α and β (generally speaking, their specific choice is not of principle importance). We consider the wave shape and the velocity field to be known for the steady motion. The question arises as to whether it is possible to determine the phase velocity c of the wave motion from these data? Since the physical condition for determining c is absent, this cannot be done in general.

However, we assume that the wave system under consideration arises beyond a certain body as a result of its translatory motion parallel to the bottom with a constant velocity c and that the fluid motion becomes steady with time in the body frame of reference. Then, the velocity of the body's motion will coincide with the wave phase velocity c . We denote the height of the unperturbed fluid level above the bottom at the left infinity by h . For the steady motion at the left infinity, the following relations hold:

$$ch = Q, \quad (1)$$

$$c^2 + 2gh = B. \quad (2)$$

Here, B is the Bernoulli-integral constant. Since the velocity field is assumed to be known at the right infinity, the parameters Q , B , and g are also known. Conse-

quently, relations (1) and (2) can be considered a system of equations in terms of two unknowns c and h .

Let h_c and h_t be, respectively, the heights of crests and troughs of the waves at the right infinity and $\langle h \rangle$ be the mean wave depth:

$$\langle h \rangle = \frac{1}{\lambda} \int_{-\lambda/2}^{\lambda/2} y_s(x) dx.$$

Here, $y = y_s(x)$ is the λ -periodic function defining the shape of the free surface.

Based on the principle of the maximum modulus and the Cauchy theorem for analytic functions, we can prove the following theorems.

Theorem 1. *For an arbitrary steady system of periodic waves whose crests and troughs are in the symmetry axes, there are only two pairs of strictly positive numbers c_1, h_1 and c_2, h_2 that satisfy the system of equations (1), (2). For these pairs, the following inequalities are true:*

$$h_t < h_1 < h_c, \quad F_1 = \frac{c_1}{\sqrt{gh_1}} < 1, \quad (3)$$

$$h_2 < h_t, \quad F_2 = \frac{c_2}{\sqrt{gh_2}} > 1. \quad (4)$$

Theorem 2. *If periodic steady waves result from the translatory motion of a body with velocity c in a fluid layer with depth h and the fluid motion is steady in the body's frame of reference, then either $c = c_1, h = h_1$ or $c = c_2, h = h_2$. In the first case, the wave drag is*

$$D_1 = 3V + \rho g \Delta h \left[\frac{3}{2} \Delta h - (1 - F_1^2) h_1 \right], \quad (5)$$

$$\Delta h = h_1 - \langle h \rangle,$$

where ρ is the fluid density and V is the mean potential energy of the waves per unit area. In the second case,

the wave drag is

$$D_2 = D_1 - \frac{\rho g (h_1 - h_2)^3}{2 (h_1 + h_2)}.$$

The flow diagram for the cases $h = h_1$ and $h = h_2$ are shown in Fig. 1. According to theorem 1, the flow is subcritical (the Froude number $F_1 < 1$) in the first case and it is supercritical (the Froude number $F_2 > 1$) in the second case. We found numerically that the wave drag is $D_2 < 0$ for the second case. Therefore, flows of this type are physically unrealizable and are not considered hereafter. Thus, flow around a body with a downstream wave train is possible only for a subcritical flow regime.

It is worth noting that the statement of Theorem 1 remains valid for solitary waves too. In this case, the first inequality in (4) should be substituted by the equality $h_2 = h_1$, where h_1 is the height of the unperturbed level for the free surface at infinity. In the case of a fluid of infinite depth, it can also be shown that formula (5) of Theorem 2 is simplified and takes the form

$$D_1 = 3V - 2T,$$

where T is the wave mean kinetic energy per unit area.

Formulas (1), (2), and (5) allows us to find, for an arbitrary periodic wave system, the phase velocity $c = c_1$ that these waves would have if they were generated by a moving body. These formulas also make it possible to find the depth of the unperturbed level $h = h_1$, the Froude number $F = F_1$, and the wave drag $D = D_1$. Consequently, we can write out

$$\begin{aligned} F &= f(\alpha, \beta), \quad \frac{\lambda}{h} = f_1(\alpha, \beta), \\ C_x &= \frac{D}{\rho g h^2} = f_2(\alpha, \beta), \end{aligned} \tag{6}$$

where f, f_1 , and f_2 are known (in the sense that they can be calculated) functions of the constitutive parameters α and β and C_x is the wave-drag coefficient.

We take $\alpha = \ln \frac{v_t}{v_c}$, where v_c and v_t are the velocities at wave crests and troughs, respectively. The parameter α varies between 0 and $+\infty$ and characterizes the wave slope. As $\alpha \rightarrow 0$, the wave has an infinitesimal amplitude; as $\alpha \rightarrow +\infty$, the wave approaches the Stokes limiting wave with an angular point of 120° at the wave vertex.

The quantity $r_0 = \exp(-d)$ is often chosen as the second constitutive parameter characterizing the wavelength. Here, $d = \frac{2\pi Q}{\lambda \cdot \langle v \rangle}$, $\langle v \rangle$ is the mean velocity of fluid particles over a single wave period in a steady

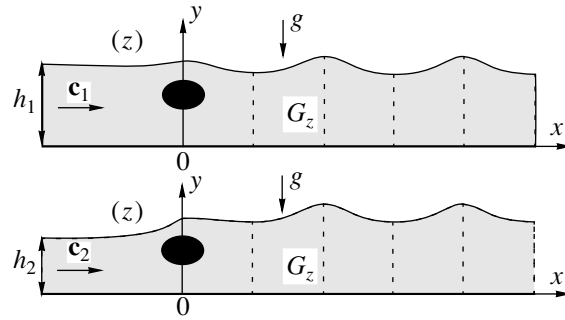


Fig. 1.

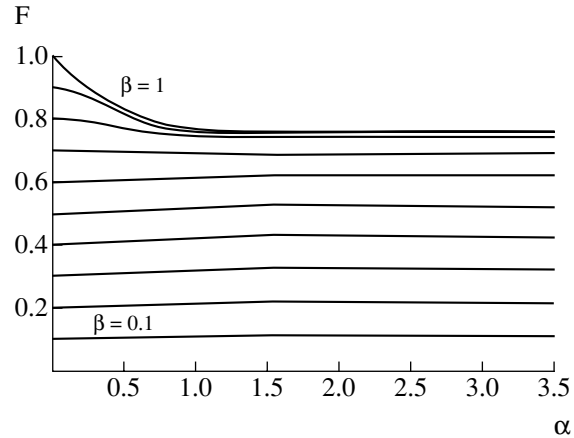


Fig. 2.

flow: $\langle v \rangle = \frac{\varphi(x + \lambda, y) - \varphi(x, y)}{\lambda}$; $\varphi(x, y)$ is the steady-flow potential (see, e.g., [1]). It is easy to see that r_0 is the inner radius of a ring onto which a single period of the wave region is conformally mapped, the external radius being equal to unity in this case. As the second parameter, we take

$$\beta = T(d), \quad T(d) = \sqrt{\frac{\tanh(d)}{d}}. \tag{7}$$

Similarly to r_0 , the parameter β varies from 0 to 1. The case $\beta = 0$ corresponds to infinitely deep waves; the case $\beta = 1$ corresponds to solitary waves. The main advantage of introducing the parameter β is that $\beta = F$ for waves with infinitesimal amplitudes. Indeed, let the wavelength obtained from the linear theory be denoted by λ_{lin} . This wavelength depends only on the Froude number $F = F_1$ and is determined from the equation (see [2, p. 34])

$$F = T \frac{2\pi h}{\lambda_{lin}}. \tag{8}$$

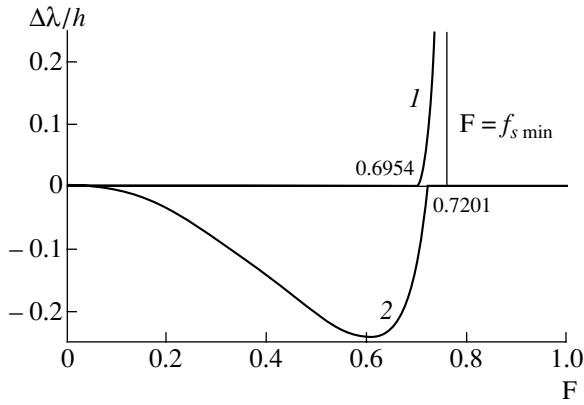


Fig. 3.

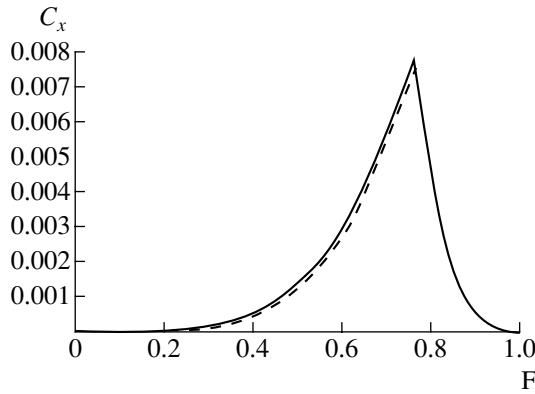


Fig. 4.

As $\alpha \rightarrow 0$, we have $\lambda \rightarrow \lambda_{lin}$, $\frac{Q}{\langle v \rangle} \rightarrow h$; therefore, $f(0, \beta) = \beta$.

Figure 2 shows the α -dependence of the Froude number F for various fixed values of β (the values of β vary from 0.1 to 1 with a step of 0.1). The method proposed in [3] was employed for calculating the waves. We consider the function $\beta = f^{-1}(\alpha, F)$, which is inverse to the function $f(\alpha, \beta)$ for each fixed α . Numerical calculations have shown that the lines $F = f(\alpha, \beta = \text{const})$ never intersect. Therefore, they are the level lines for the function $\beta = f^{-1}(\alpha, F)$ and the region shown in Fig. 2 is the domain of definition for the function $\beta = f^{-1}(\alpha, F)$. We denote this region by G . Then,

$$G = \{(\alpha, F) \in R \times R, \alpha \geq 0, 0 \leq F \leq f_s(\alpha), f_s(\alpha) = f(\alpha, 1)\}.$$

Like the function $f(\alpha, \beta)$, the function $f^{-1}(\alpha, F)$ can be calculated for arbitrary values of $(\alpha, F) \in G$. The function $F = f_s(\alpha)$ bounds the region G from above and determines the dependence between the parameter α

and the Froude number F for solitary waves. We emphasize that, even for solitary waves, the Froude number introduced by us is $F = F_1 < 1$. The function $f_s(\alpha)$ as, incidentally, any function $f(\alpha, \beta = \text{const})$ is nonmonotone. According to the Longuet-Higgins–Fox asymptotic theory of almost ultimate waves [4], this function has an infinite sequence of alternating maxima and minima. Our calculations have shown that the first minimum of the function $f_s(\alpha)$ is attained at the point $\alpha = 1.5022$ and its value is $f_{s \min} = 0.760706$. (Hereafter, in all approximated numbers, the author assures an error no higher than one unit of the last decimal digit.) The other extrema of the function $f_s(\alpha)$ can be found by employing the asymptotic formula [4]

$$f_s(\alpha) = f_s(\infty) + a \exp(-3\alpha) \cos(k\alpha - b), \quad (9)$$

which is true for large values of α . Here, $k = 2.14293$ and, according to our calculations, $f_s(\infty) = 0.7629045093$ is the value of the Froude number for the limiting solitary wave; $a = 0.3469$ and $b = 1.0427$.

Using relations (6), we find

$$\frac{\lambda}{h} = f_1[\alpha, f^{-1}(\alpha, F)], \quad (10)$$

$$C_x = f_2[\alpha, f^{-1}(\alpha, F)], \quad (\alpha, F) \in G.$$

Formulas (10) make it possible to find the maxima and minima for the relative wavelength $\frac{\lambda}{h}$ and the drag coefficient C_x for each fixed number F . On the other hand, formulas (10) represent the parametrically specified function C_x depending on $\frac{\lambda}{h}$ for fixed values of F . Thus, if the wavelength λ beyond the body is known, the wave drag can be calculated exactly.

Figure 3 shows $\frac{\lambda_{\max} - \lambda_{lin}}{h}$ (curve 1) and $\frac{\lambda_{\min} - \lambda_{lin}}{h}$ (curve 2) as functions of the Froude number F , where λ_{lin} is determined from Eq. (8). Curve 1 has the vertical asymptote $F = f_{s \min} = 0.760706$. This implies that the wavelength λ beyond the body is finite for $F < f_{s \min}$. For $f_{s \min} \leq F < 1$, it can become infinite and the flow regime can transform to the ultimate runoff regime [3, 5]. The plots in Fig. 3 clarify the extreme properties of wavelength λ_{lin} determined from the linear theory. The linear theory yields the maximum possible wavelength for $0 \leq F \leq 0.6954$ and the minimum possible wavelength for $0.7201 \leq F < 1$; the wavelength λ_{lin} is neither maximum nor minimum in the narrow range $0.6954 < F < 0.7201$.

The variation domain for F and C_x in the case of steady wave regimes is shown in Fig. 4. It is worth noting that the drag coefficients for limiting waves (dashed line) are not the highest possible. The global maximum of the wave drag can be attained for $F = f_{s \min}$, and its value is $C_{x \max} = 0.00780053$.

ACKNOWLEDGMENTS

The author is grateful to G.Yu. Stepanov for valuable discussions and useful remarks.

This work was supported by the Russian Foundation for Basic Research, projects nos. 99-01-00169 and 99-01-00173.

REFERENCES

1. E. D. Cokelet, *Philos. Trans. R. Soc. London, Ser. A* **286**, 183 (1977).
2. L. N. Sretenskiĭ, *Theory of Wave Motion in Liquids* (Nauka, Moscow, 1977).
3. D. V. Maklakov, *Izv. Akad. Nauk, Mekh. Zhidk. Gaza*, No. 2, 108 (1995).
4. M. S. Longuet-Higgins and M. J. H. Fox, *J. Fluid Mech.* **317**, 1 (1996).
5. D. V. Maklakov, *Nonlinear Problems of Hydrodynamics of Potential Flows with Free Boundaries* (Yanus-K, Moscow, 1997).

Translated by V. Tsarev

Madelung Transformation for Vortex Flows of a Perfect Liquid

A. L. Sorokin

Presented by Academician V.E. Nakoryakov September 15, 2000

Received October 11, 2000

The Madelung transformation in quantum mechanics [1,2] is referred to as the representation in the form

$\psi = \sqrt{\rho} \exp\left(\frac{i\phi}{\beta}\right)$ of the solution to the Schrödinger equation (with an arbitrary real-valued potential U)

$$i\frac{\partial\psi}{\partial t} = -\frac{\beta}{2}\Delta\psi + U\psi. \quad (1)$$

This transformation results in an equivalent system of equations,

$$\begin{aligned} \frac{\partial\rho}{\partial t} + \nabla \cdot (\rho\nabla\phi) &= 0, \\ \frac{\partial\phi}{\partial t} + \frac{(\nabla\phi)^2}{2} &= -\beta U + \frac{\beta^2\Delta\sqrt{\rho}}{2\sqrt{\rho}}, \end{aligned} \quad (2)$$

which is similar to the Euler equations for the potential motion of a perfect liquid, except the last term in the right-hand side of the second equation. The relation between (1) and (2) was used in [1] to calculate the potential flow of a perfect liquid with a localized vorticity approximated by a distribution of vortex filaments. In this approach to the flow description, the vortex filaments correspond to intersecting surfaces whose implicit equations are determined by the equation $\psi = 0$.

In the present paper, we discuss a generalization of this approach to a perfect liquid with a distributed vorticity.

For completeness of the consideration, the original version of the Madelung transformation (with the notation modified for brevity) is discussed in Section 1. In Section 2, generalization of the Madelung transformation is performed. In Section 3, the equivalence between the system of equations (8) for two complex-valued functions and the system of equations for a perfect liquid in barotropy approximation is substantiated.

1. Following Madelung [2], we replace the variables

$$\rho = \psi\bar{\psi}, \quad \phi = -\frac{i\beta}{2}\ln\frac{\psi}{\bar{\psi}}$$

in continuity equation (2). Here, ψ is a complex-valued function and $\bar{\psi}$ is its complex conjugate function. After the substitution of new variables and factorization, we obtain

$$\bar{\psi}\left(\frac{\partial\psi}{\partial t} - \frac{i\beta}{2}\Delta\psi\right) + \text{c.c.} = 0. \quad (3)$$

Here, c.c. corresponds to the complex conjugate terms. According to Madelung [2], Eq. (3) is satisfied identically if the function ψ obeys the equation

$$\frac{\partial\psi}{\partial t} - \frac{i\beta}{2}\Delta\psi = -iU\psi, \quad (4)$$

where U is a real-valued function of coordinates, time, and/or ψ . The equivalence of (4) and (1) is evident. As applied to the potential motion of a continuum, the quantity ρ may be interpreted not only as the density of the liquid. This fact stipulates the appearance of various nonlinear modifications of the Schrödinger equation in quite different physical problems.

2. Furthermore, we consider the continuity equation

$$\frac{\partial\rho}{\partial t} + \nabla \cdot (\rho\mathbf{V}) = 0 \quad (5)$$

written out in dimensionless form. In order to describe the barotropic flow of a perfect liquid with a distributed vorticity, the number of variables must be doubled compared to the case of potential motion. We consider the following choice of variables:

$$\rho_k = \psi_k\bar{\psi}_k, \quad \phi_k = -\frac{i}{2}\ln\frac{\psi_k}{\bar{\psi}_k}, \quad (6)$$

$$\rho = \sum_k \rho_k, \quad \mathbf{J} = \rho\mathbf{V} = \sum_k \rho_k\nabla\phi_k,$$

where $k = 1, 2$. In terms of these variables, the velocity

Kutateladze Institute of Thermal Physics, Siberian Division,
Russian Academy of Sciences,
pr. Akademika Lavrent'eva 1, Novosibirsk, 630090 Russia

and the vorticity are, respectively,

$$\mathbf{V} = \frac{\rho_1}{\rho} \nabla \varphi_1 + \frac{\rho_2}{\rho} \nabla \varphi_2,$$

$$\nabla \times \mathbf{V} = \frac{\rho_1 \rho_2}{\rho^2} \nabla \ln \left(\frac{\rho_1}{\rho_2} \right) \times \mathbf{w},$$

where $\mathbf{w} = \nabla(\varphi_1 - \varphi_2)$. It is worth noting that within this choice of variables, the permutation of indices $1 \longleftrightarrow 2$ does not change the physical quantities. Since the velocity potentials are many valued, it is possible to describe a vector field with nonzero integral helicity in the form [3]

$$H = \int_V \mathbf{V} \cdot (\nabla \times \mathbf{V}) dV = \int_S \ln \frac{\rho_1}{\rho_2} \left(\frac{\rho_1 \rho_2}{\rho^2} \nabla \varphi_1 \times \nabla \varphi_2 \right) d\mathbf{S}$$

(the integral is calculated over an arbitrary closed surface).

Substituting relations (6) into Eq. (5) and using the method described in Section 1, we arrive at

$$\sum_{k=1}^2 \bar{\psi}_k \left(\frac{\partial \psi_k}{\partial t} - \frac{i}{2} \Delta \psi_k \right) + \text{c.c.} = 0. \tag{7}$$

Then, assuming

$$\frac{\partial \psi_k}{\partial t} - \frac{i}{2} \Delta \psi_k = U_k \psi_k, \tag{8}$$

we derive from (7) that $\rho_1 \Re U_1 + \rho_2 \Re U_2 = 0$. This condition is satisfied by the following choice of potentials:

$$U_1 = \frac{\rho_2 Q}{2\rho} - iV_1, \quad U_2 = -\frac{\rho_1 Q}{2\rho} - iV_2,$$

where Q , V_1 , and V_2 are arbitrary real-valued functions of coordinates, time, and/or ψ_1 and ψ_2 . The substitution $\psi_k = \sqrt{\rho_k} \exp(i\varphi_k)$ in (8) yields an equivalent system of equations:

$$\frac{\partial \rho_k}{\partial t} + \nabla \cdot (\rho_k \nabla \varphi_k) = (-1)^{k-1} \frac{\rho_1 \rho_2}{\rho} Q,$$

$$\frac{\partial \varphi_k}{\partial t} + \frac{(\nabla \varphi_k)^2}{2} = -V_k + \frac{1}{2} \frac{\Delta \sqrt{\rho_k}}{\sqrt{\rho_k}}. \tag{9}$$

3. We now demonstrate that the system of equations (9) [and also (8)] is equivalent to Euler equations provided that the potentials

$$V_1 = \Pi(\rho) - \frac{\rho_2^2}{2\rho^2} \mathbf{w}^2 + \frac{\Delta \sqrt{\rho_1}}{2\sqrt{\rho_1}},$$

$$V_2 = \Pi(\rho) - \frac{\rho_1^2}{2\rho^2} \mathbf{w}^2 + \frac{\Delta \sqrt{\rho_2}}{2\sqrt{\rho_2}}, \tag{10}$$

$$Q = \nabla \cdot \mathbf{w} + \frac{1}{\rho} \mathbf{w} \cdot \left(\rho_2 \frac{\nabla \rho_1}{\rho_1} + \rho_1 \frac{\nabla \rho_2}{\rho_2} \right)$$

are chosen, where $\Pi(\rho) = \int_0^\rho \frac{dp}{\rho}$. Potentials (10) are

invariant with respect to the Galilean transformation. Substituting potentials (10) into Eqs. (9), we arrive at the system of equations

$$\frac{\partial \rho_k}{\partial t} + \nabla \cdot (\rho_k \nabla \varphi_k) = (-1)^{k-1} \frac{\rho_1 \rho_2}{\rho} Q,$$

$$\frac{\partial \varphi_1}{\partial t} + \frac{(\nabla \varphi_1)^2}{2} = -\Pi + \frac{\rho_2^2}{2\rho^2} \mathbf{w}^2, \tag{11}$$

$$\frac{\partial \varphi_2}{\partial t} + \frac{(\nabla \varphi_2)^2}{2} = -\Pi + \frac{\rho_1^2}{2\rho^2} \mathbf{w}^2.$$

We note that in the case $\psi_1 \equiv \psi_2$, i.e., $\nabla \varphi_1 = \nabla \varphi_2$, $\rho_1 = \rho_2$, and $\mathbf{w}^2 = 0$, the system of equations (11) is transformed into Euler equations for a potential barotropic flow.

We now turn to the derivation of the Euler equations. We multiply both sides of Eqs. (11) by ρ_k , calculate the gradient for the resulting equations, and then add the mass balance equation multiplied by $\nabla \varphi_k$. Introducing the flows $\mathbf{j}_k = \rho_k \nabla \varphi_k$, we have after certain algebraic transformations

$$\frac{\partial \mathbf{J}}{\partial t} + \nabla \cdot \left(\frac{\mathbf{j}_1^2}{2\rho_1} + \frac{\mathbf{j}_2^2}{2\rho_2} \right) + \left\{ \nabla \rho_1 \frac{\partial \varphi_1}{\partial t} + \nabla \rho_2 \frac{\partial \varphi_2}{\partial t} \right\}$$

$$+ \left(\frac{\mathbf{j}_1 \nabla \cdot \mathbf{j}_1}{\rho_1} + \frac{\mathbf{j}_2 \nabla \cdot \mathbf{j}_2}{\rho_2} - \frac{\rho_1 \rho_2}{\rho} Q \mathbf{w} \right) \tag{12}$$

$$= \nabla \cdot \left(-\rho \Pi + \frac{\rho_1 \rho_2 \mathbf{w}^2}{\rho} \right).$$

Using auxiliary identities

$$\frac{\mathbf{J}^2}{2\rho} = \frac{\mathbf{j}_1^2}{2\rho_1} + \frac{\mathbf{j}_2^2}{2\rho_2} - \frac{\rho_1 \rho_2}{2\rho} \mathbf{w}^2,$$

$$\frac{1}{\rho} \mathbf{J} \nabla \cdot \mathbf{J} = \frac{\mathbf{j}_1 \nabla \cdot \mathbf{j}_1}{\rho_1} + \frac{\mathbf{j}_2 \nabla \cdot \mathbf{j}_2}{\rho_2}$$

$$- \frac{\rho_1 \rho_2}{\rho} \left(\frac{\nabla \cdot \mathbf{j}_1}{\rho_1} - \frac{\nabla \cdot \mathbf{j}_2}{\rho_2} \right) \mathbf{w},$$

and transforming (12), we arrive at the equation

$$\begin{aligned} & \frac{\partial \mathbf{J}}{\partial t} + \nabla \left(\frac{\mathbf{J}^2}{2\rho} \right) - \frac{\mathbf{J}^2}{2\rho} \frac{\nabla \rho}{\rho} + \frac{1}{\rho} \mathbf{J} \nabla \cdot \mathbf{J} \\ & + \left\{ \nabla \rho_1 \frac{\partial \varphi_1}{\partial t} + \nabla \rho_2 \frac{\partial \varphi_2}{\partial t} + \frac{\mathbf{J}^2}{2\rho} \frac{\nabla \rho}{\rho} + \Pi \nabla \rho \right\} \\ & + \frac{\rho_1 \rho_2}{\rho} \left(\frac{\nabla \cdot \mathbf{j}_1}{\rho_1} - \frac{\nabla \cdot \mathbf{j}_2}{\rho_2} - Q \right) \mathbf{w} = -\rho \nabla \Pi. \end{aligned}$$

The transformation of the terms in braces with the equation for velocity potential (11) and the first identity taken into account yields

$$\begin{aligned} & \frac{\partial \mathbf{J}}{\partial t} + \nabla \left(\frac{\mathbf{J}^2}{2\rho} \right) - \frac{\mathbf{J}^2}{2\rho} \frac{\nabla \rho}{\rho} + \frac{1}{\rho} \mathbf{J} \nabla \cdot \mathbf{J} \\ & + \rho \left\{ \frac{\rho_1 \rho_2}{\rho^2} \left(\frac{\partial \varphi_1}{\partial t} - \frac{\partial \varphi_2}{\partial t} \right) \nabla \ln \frac{\rho_1}{\rho_2} \right. \\ & \left. + \frac{\rho_1 \rho_2}{\rho^2} \left(\frac{\nabla \cdot \mathbf{j}_1}{\rho_1} - \frac{\nabla \cdot \mathbf{j}_2}{\rho_2} - Q \right) \mathbf{w} \right\} = -\rho \nabla \Pi. \end{aligned}$$

Further transformations of the terms in braces with allowance for the velocity-potential equation (11), auxiliary identities, definitions of Q , velocity, and vorticity yield

$$\begin{aligned} & \frac{\rho_1 \rho_2}{\rho^2} \left((\mathbf{V} \cdot \mathbf{w}) \nabla \ln \frac{\rho_1}{\rho_2} - \mathbf{V} \cdot \nabla \ln \frac{\rho_1}{\rho_2} \mathbf{w} \right) \\ & = \mathbf{V} \times \nabla \times \mathbf{V}. \end{aligned}$$

From the equation transformed

$$\begin{aligned} & \frac{\partial \mathbf{J}}{\partial t} + \nabla \left(\frac{\mathbf{J}^2}{2\rho} \right) - \frac{\mathbf{J}^2}{2\rho} \frac{\nabla \rho}{\rho} \\ & - \rho \mathbf{V} \times \nabla \times \mathbf{V} + \frac{1}{\rho} \mathbf{J} \nabla \cdot \mathbf{J} = -\rho \nabla \Pi \end{aligned}$$

with due regard to Eqs. (5) and transformation (6), we arrive at the Euler equation in the Lamb form:

$$\frac{\partial \mathbf{V}}{\partial t} + \nabla \left(\frac{\mathbf{V} \cdot \mathbf{V}}{2} \right) - \mathbf{V} \times \nabla \times \mathbf{V} = -\nabla \Pi,$$

which is the final goal of the transformations.

4. In hydrodynamic problems, the nonlinear Schrödinger equation appears in the case of using simplified assumptions and special choices of variables (see, e.g., [4,5]).

The generalization of the Madelung transformation considered in the present paper links the equations for a perfect liquid and the equivalent system of equations (8) and (11) under the single assumption of the barotropic nature of the flow. The proposed set of variables have a uniform dimension. Thus, the real and imaginary parts of ψ_k can be considered coordinates of a surface in a four-dimensional Euclidean space.

It follows from (6) that for flows characterized by a small Mach number M , the surface is close to a sphere with curvature radius variations on the order of M^2 . This geometric interpretation of the solution could be useful in analytical studies.

In the general case, the problem of conserving the correlation between the zeroes of the function ψ_k and the vortex axis in the three-dimensional vector field is of particular interest. If this correlation also holds for the suggested choice of variables, then we are able to rigorously define the three-dimensional vortex as a certain structure (the definition of a vortex is, to a large extent, intuitive in hydrodynamics). This definition would be similar to that of a point vortex in the classical two-dimensional hydrodynamics of perfect incompressible liquids.

REFERENCES

1. C. Nore, M. Abid, and M. Brachet, in *Lecture Notes in Physics* (Springer-Verlag, Berlin, 1995), pp. 105–112.
2. E. Madelung, *Die mathematischen Hilfsmittel des Physikers* (Springer-Verlag, Berlin, 1957; Fizmatgiz, Moscow, 1960).
3. J. W. Yakota, *Phys. Fluids* **9**, 2264 (1997).
4. O. Phillips, in *Journal of Fluid Mechanics. A Special Issue Celebrating the 25th Anniversary of the Journal*, Ed. by G. Batchelor and H. Moffatt (Cambridge Univ. Press, Cambridge, 1981; Mir, Moscow, 1984), Vol. 106.
5. H. Hasimoto, *J. Fluid Mech.* **51**, 477 (1972).

Translated by S. Kulagin

On Right-Hand Solutions to a Class of Lagrangian Systems with a Discontinuous Right-Hand Side

I. A. Finogenko

Presented by Academician V.M. Matrosov December 29, 2000

Received March 15, 2001

In this paper, a theory of right-hand solutions to a class of Lagrangian systems of the second kind with discontinuous controls is developed. A method of unambiguously regularizing the controls on discontinuity surfaces is proposed. Conditions for the existence of the solutions and their general properties are considered.

1. STATEMENT OF THE PROBLEM

We consider a mechanical system with n degrees of freedom which obeys the equations of motion

$$A(t, q)\ddot{q} = g(t, q, \dot{q}) + Q^A(t, q, \dot{q}) + B(t, q, \dot{q})u. \quad (1)$$

We use here conventional notation: $q = (q^1, \dots, q^n)^T$, $\dot{q} = (\dot{q}^1, \dots, \dot{q}^n)^T$, and $\ddot{q} = (\ddot{q}^1, \dots, \ddot{q}^n)^T$ are the vectors of the generalized coordinates, velocities, and accelerations, respectively; $Q^A = (Q_1^A, \dots, Q_n^A)^T$ and $g = (g_1, \dots, g_n)^T$ are continuous vector functions describing the forces acting upon the system (i.e., potential, drag, and generalized gyroscopic forces, force of a moving space, and others); and $A(t, q) = \|a_{ij}(t, q)\|_{i,j=1}^n$ is the matrix of the inertia coefficients that defines the quadratic form of the generalized velocities entering into the expression for the kinetic energy. The function $u = (u_1, \dots, u_n)^T$ specifies generalized control forces, and the matrix $B = \|b_{ij}(t, q, \dot{q})\|_{i,j=1}^n$ is nonsingular. The functions $a_{ij}(t, q)$ and $b_{ij}(t, q, \dot{q})$ are assumed to be continuously differentiable with respect to the sets of their arguments. Constraints taking the form

$$|u_i| \leq H_i(t, q, \dot{q}), \quad i = 1, 2, \dots, n \quad (2)$$

are imposed on the controls u_i , where $H_i = H_i(t, q, \dot{q})$ are continuous nonnegative functions. All the above-mentioned conditions are assumed to be satisfied in a

certain variability domain $\Omega \subset R^{2n+1}$ of the variables t , q , and \dot{q} .

The structure of the controls u_i is determined by the following problem of synthesizing control systems for mechanical systems on the basis of the decomposition principle [1]. It is required to find such controls that cause the motions of system (1) to attain (under certain additional assumptions) a smooth manifold (i.e., the goal set), which takes the form

$$S = \{(t, q, \dot{q}) \in \Omega: \phi_i(t, q, \dot{q}) = 0, i = 1, 2, \dots, n\}. \quad (3)$$

A certain quadratic form

$$v_\phi = \frac{1}{2} \sum_{i,j=1}^n c_{ij}(t, q) \phi_i \phi_j \quad (4)$$

is chosen as the measure of deviation of motions from set (3). Here, $C_\phi(t, q) = \|c_{ij}(t, q)\|_{i,j=1}^n$ is a positive definite symmetric continuously differentiable matrix. The control u is naturally determined from the condition of the minimum for the derivative \dot{v}_ϕ , with due regard for system (1). This control has the form

$$u_i = -H_i \operatorname{sgn} \chi_i, \quad i = 1, 2, \dots, n \quad (5)$$

under the condition $\chi_i \neq 0$, where $\chi_i = \chi_i(t, q, \dot{q})$ are continuously differentiable functions. The values of u_i for $\chi_i = 0$ should be regularized. System (1) with controls (5) represents a set of differential equations of the second order with a discontinuous right-hand side.

In this paper, we will study right-hand solutions. With allowance for inequalities (2), the controls u_i are unambiguously determined in the entire domain Ω , in particular, at discontinuity points. The controls to be found must be consistent with the conditions for the initiation of the motions over the goal set S . In order for the controls u_i to be unambiguously regularized at discontinuity points, we propose an implicit procedure generalizing certain known methods, such as the method

of equivalent control [3] (see also [2]) and the method of determining the Coulomb dry-friction forces at relative-rest points, which was described in [4] for systems with friction. For the closed set of equations (1), we prove that they are reduced to the explicit form

$$\ddot{q} = G(t, q, \dot{q}). \tag{6}$$

2. AN IMPLICIT METHOD FOR DETERMINATION OF GENERALIZED CONTROLS AT DISCONTINUITY POINTS

We assume that the functions ϕ_i are continuously differentiable. Then, we introduce the following notation: $\phi = (\phi_1, \dots, \phi_n)^T$, $J_{t,\phi}$ is a column consisting of partial derivatives of the functions ϕ_i with respect to t , and $J_{q,\phi}$ and $J_{\dot{q},\phi}$ are $n \times n$ matrices whose rows are gradients of the functions ϕ_i with respect to the variables q^j and \dot{q}^j , respectively. According to set (1), the derivative \dot{v}_ϕ takes the form $\dot{v}_\phi = u^T D^T \phi + F$, where

$$F = \phi^T C_\phi [J_{t,\phi} + J_{q,\phi} \dot{q} + J_{\dot{q},\phi} A^{-1} (g + Q^A)] + \frac{1}{2} \phi^T \dot{C}_\phi \phi, \\ D^T = B^T A^{-1} J_{\dot{q},\phi}^T C_\phi.$$

Since F is independent of u , the minimum of the function \dot{v}_ϕ is ensured, with regard to constraints (2), by controls (5) with the functions

$$\chi = D^T \phi = (\chi_1, \dots, \chi_n)^T. \tag{7}$$

If $C_\phi = A$ and $\phi_i = \dot{q}^i - f_i(t, q)$, with $i = 1, 2, \dots, n$, then the control is given by

$$u_i = -H_i \operatorname{sgn} \sum_{j=1}^n b_{ji} (\dot{q}^j - f_i(t, q)), \quad i = 1, 2, \dots, n.$$

If, in addition, $B = E$, then $u_i = -H_i \operatorname{sgn} (\dot{q}^i - f_i(t, q))$, $i = 1, 2, \dots, n$ (see [1, 5]).

To regularize the controls at discontinuity points, we now transform Eqs. (1). To do this, we assume that the matrix $J_{\dot{q},\phi}$ is continuously differentiable, with its determinant being nonzero, and that the equality $J_{\dot{q},\chi} = D^T J_{\dot{q},\phi}$ is valid, where $J_{\dot{q},\chi}$ is the Jacobian of the functions χ_i with respect to the variables \dot{q}^j . (The last equality is valid if the matrix D^T is independent of \dot{q} .) Since the matrix D^T is nonsingular, the matrix $J_{\dot{q},\chi}$ is also nonsingular.

We define the vector functions $\dot{\chi} = \dot{\chi}(t, q, \dot{q}, \ddot{q})$ and $R = R(t, q, \dot{q})$ and the matrix $P = P(t, q, \dot{q})$ by the equalities

$$\dot{\chi} = J_{t,\chi} + J_{q,\chi} \dot{q} + J_{\dot{q},\chi} \ddot{q}, \\ P = [B^T A^{-1} J_{\dot{q},\phi}^T C_\phi J_{\dot{q},\phi} A^{-1} B]^{-1}, \\ R = P(J_{t,\chi} + J_{q,\chi} \dot{q}) + B^{-1} (g + Q^A).$$

Then, Eqs. (1) can be written out in the form

$$P \dot{\chi} = R + u. \tag{8}$$

With regard to (5) and (2), we define the controls $u_i = u_i(t, q, \dot{q}, \chi)$ in the general form as

$$u_i = \begin{cases} -H_i \operatorname{sgn} \chi_i, & \text{if } \chi_i \neq 0 \\ Q_i, & \text{if } \chi_i = 0, \quad |Q_i| \leq H_i \\ H_i \operatorname{sgn} Q_i, & \text{if } \chi_i = 0, \quad |Q_i| > H_i. \end{cases} \tag{9}$$

Here,

$$Q_i = \sum_{j=1, i \neq j}^n p_{ij} \dot{\chi}_j - R_i,$$

p_{ij} are the matrix elements of P , and R_i are the components of vector R with $i = 1, 2, \dots, n$.

Input equation (1) and Eq. (8) with the function u given by formulas (9) represent differential equations unsolved with respect to the higher derivatives \ddot{q} , which also enter into the right-hand side via the function u . Since the matrix $J_{\dot{q},\chi}$ is nonsingular, the unambiguous solvability of Eqs. (8) with respect to $\dot{\chi}$ (serving as an independent variable) leads to the unambiguous solvability of Eqs. (1) with respect to \ddot{q} ; i.e., Eq. (1) is reduced to form (6). In this case, the controls u_i can be completely and unambiguously determined at each point $(t, q, \dot{q}) \in \Omega$; hence they do not enter into the function G .

We now consider right-hand solutions to set (1) with controls (9) assuming that they exist. In so doing, we treat $\dot{\chi}_i$ ($i = 1, 2, \dots, n$) as the right-hand derivatives of the functions χ_i along these solutions and assume that $\chi_i = 0$ and $|Q_i| \leq H_i$ for all $i = 1, 2, \dots, n$ in a certain time interval. In this case, $Q_i = -R_i$ and $u_i = -R_i$; hence the system moves along the intersection of the manifolds,

$$\tilde{S}_i = \{(t, q, \dot{q}) \in \Omega: \chi_i = 0\}, \quad i = 1, 2, \dots, n. \tag{10}$$

With regard to equality (7), this motion represents full sliding over manifold (3) [i.e., the motion in the decomposition regime described by the differential equations $\phi_i(t, q, \dot{q}) = 0$, $i = 1, 2, \dots, n$]. In this case, the method of equivalent control [3] is realized in system (1).

In the course of the motion of systems under constrained controls (provided that transient processes originate), either the inequality $|Q_i| \leq H_i$ or $|Q_i| > H_i$ can be satisfied on the surfaces \tilde{S}_i , depending on the subscripts i . Then, motion over the intersection of the surfaces \tilde{S}_i does not exist. In this case, formulas (9) describe the control that causes the system to move on the intersection of the surfaces \tilde{S}_i for which the inequalities $|Q_i| \leq H_i$ are satisfied (because $\dot{\chi}_i = 0$) and to leave the surfaces for which $|Q_i| > H_i$ (because $\dot{\chi}_i \neq 0$ and $\text{sgn} \dot{\chi}_i = \text{sgn} \chi_i$ for $\chi_i \neq 0$).

3. UNAMBIGUOUS SOLVABILITY OF EQUATIONS (1) WITH RESPECT TO \ddot{q}

We introduce the variable $z = (z_1, \dots, z_n)^T$, define the function $u_i = u_i(z)$ by equalities (9) with $\dot{\chi} = z$, and form the function $u(z) = (u_1, \dots, u_n)^T$. Let a point $(t, q, \dot{q}) \in \Omega$ be fixed. Then, we consider a set of algebraic equations with respect to z :

$$Pz = R + u(z). \quad (11)$$

Theorem 1. *The solution to Eqs. (11) exists and is unique.*

Corollary 1. *Equations (1) with controls (9) are unambiguously resolvable with respect to the generalized accelerations and can be reduced to form (6).*

Corollary 2. *For Eqs. (1) of arbitrary goal set (3) and arbitrary positive definite matrix C_ϕ of quadratic form (4), there exist controls (9) that can be unambiguously determined at each point $(t, q, \dot{q}) \in \Omega$.*

4. RIGHT-HAND SOLUTIONS

The absolutely continuous right-hand differentiable function $\{q(t), \dot{q}(t)\}$, which satisfies the condition $D^+ \dot{q}(t) = G(t, q(t), \dot{q}(t))$ at each point $t \in [t_0, t_1]$, is referred to as a right-hand solution to Eqs. (1) in the interval $[t_0, t_1]$ with the initial conditions $\dot{q}(t_0) = \dot{q}_0$ and $q(t_0) = q_0$, the function $D^+ \dot{q}(t)$ being continuous on the right.

Theorem 2. *For an arbitrary initial state, there exists a local right-hand solution to Eqs. (1) with controls u_i determined by formulas (9).*

In defining the right-hand uniqueness of the solutions (at a point and in the domain Ω), we will follow [2] (see p. 81).

Theorem 3. *Let, in addition to the conditions of Sections 1 and 2, the functions g_i , Q_i^A , and H_i ($i = 1, 2, \dots, n$) be continuously differentiable. Then, the right-hand uniqueness of the solutions to Eqs. (1) with controls (9)*

takes place in the domain $\{(t, q, \dot{q}) \in \Omega: H_i(t, q, \dot{q}) \neq 0, i = 1, 2, \dots, n\}$.

If H_i in Theorem 3 are constant quantities, then right-hand uniqueness evidently takes place in the entire domain Ω .

One of the known methods of solving Eqs. (1) with constraints (5) imposed on the control u consists in convex multiple-valued regularization of the right-hand sides of these equations and the introduction of differential switching [2]:

$$A(t, q)\ddot{q} \in g(t, q, \dot{q}) + Q^A(t, q, \dot{q}) + B(t, q, \dot{q})U, \quad (12)$$

where the set $U = U(t, q, \dot{q})$ is defined by the equality

$$U = \{u \in R^n: u_i = -H_i \text{sgn} \chi_i, \chi_i \neq 0; |u_i| \leq H_i, \chi_i = 0; i \in 1, 2, \dots, n\}.$$

In this case, the absolutely continuous function $\{q(t), \dot{q}(t)\}$ with the measurable second derivative $\ddot{q}(t)$ that obeys Eqs. (12) almost everywhere is treated as a solution to problem (1) (the Caratheodory solution). This solution becomes nondifferentiable when attaining or intersecting discontinuity surfaces for the functions u_i .

Theorem 4. *Differential switching (12) and Eqs. (1) with controls (9) are equivalent in the sense of coincidence of their Caratheodory solutions. Any Caratheodory solution to Eqs. (1) with controls (9) is a right-hand solution.*

As follows from Theorem 4, differential switching (12) and Eqs. (1) with controls (9) are equivalent in the sense that the sets of their right-hand solutions coincide. However, it is the unambiguous regularization by formulas (9) for the functions u_i on the discontinuity surfaces alone that allows us to solve the problem of existence and uniqueness for the right-hand solutions. Moreover, formulas (9) for Eqs. (1) necessarily follow from the condition of existence for local right-hand solutions to differential switching (12) for an arbitrary initial state.

Theorems 2–4 allow properties of the right-hand solutions to Eqs. (1) to be analyzed on the basis of the theory of differential switchings, which has been well developed recently. Known results of the theory of differential switchings with an upper semicontinuous convex right-hand side can be applied to Eqs. (1) [2]. Under the conditions of Theorem 3, the dependence of solutions to differential switchings on the initial conditions and on the right-hand sides that is semicontinuous from above turns into a continuous dependence of the right-hand solutions to Eqs. (1) on the same quantities. If the sets of initial values are compact or connected, then the theorems on the continuability of solutions onto the right maximum domain of their existence and the theorems on the compactness and connectedness of both the set of right-hand solutions and the integral funnel in the corresponding spaces are valid. In this case, conventional properties of approximate solutions (the

δ -solutions for which small variations of the boundaries of the continuity domains, as well as small variations of the right-hand sides of the equations in these domains, are taken into account) and properties of trajectories and ω -limiting sets for autonomous systems (see [2, pp. 59–64 and pp. 94–101]) take place.

In addition, the right-hand solutions to Eqs. (1) have specific properties that follow from the structure of these equations and controls (9). To describe one of them, we introduce the notation $S^0 = \{t, q, \dot{q}\} : \phi_i = 0, |R_i| < H_i, i = 1, 2, \dots, n\}$ and assume that $S^0 \neq \emptyset$ and $S = S^0$.

Statement 1. *For an arbitrary compact subset $K \subset S$ and for an arbitrary $\tau > 0$, there exists a β -neighborhood K^β of the set K such that the condition*

$$(t_0, z(t_0)) \in K^\beta \Rightarrow (t, z(t)) \in S \quad (13)$$

is satisfied for each right-hand solution $z(t) = (q(t), \dot{q}(t))$ to Eqs. (1) and for all $t \geq \tau$ in the domain of definition of $z(t)$. In this case, the numbers τ and β can be chosen to be so small that the solutions stay in an arbitrary preassigned ϵ -neighborhood of the set K during the initial time interval $[t_0, t_0 + \tau]$.

Similar properties for mechanical systems with Coulomb sliding friction were studied in [6].

If $\phi_i = \dot{q}^i - f_i(t, q)$, $B = E$, and $C_\phi = A$, we have $\chi = \phi$, $P = A$, $J_{t,\chi} = -J_{t,f}$, $J_{q,\chi} = -J_{q,f}$, and $J_{\dot{q},\chi} = E$. Under the condition $\phi_i = 0$ ($i = 1, 2, \dots, n$), the inequalities $|R_i| <$

H_i defining the set S^0 take the form

$$\left| \sum_{k=1}^n a_{ik} \left(\frac{\partial f_k}{\partial t} + \sum_{j=1}^n \frac{\partial f_k}{\partial q^j} f_j \right) - [g_i + Q_i^A] \right|_{\dot{q}=f(t,q)} < H_i|_{\dot{q}=f(t,q)}, \quad i = 1, 2, \dots, n. \quad (14)$$

Under the right-hand continuation of the solution $z(t)$, the equality $|R_i| = H_i$ can be valid at a certain $t > \tau$ provided that $S \neq S^0$. In this case (and only in this case), the solution can leave the goal set S .

ACKNOWLEDGMENTS

This work was supported by the Russian Foundation for Basic Research, project no. 00-01-00293.

REFERENCES

1. E. S. Pyatnitskiĭ, *Avtom. Telemekh.*, No. 1, 87 (1989); No. 2, 57 (1989).
2. A. F. Filippov, *Differential Equations with a Discontinuous Right Part* (Nauka, Moscow, 1985).
3. V. I. Utkin, *Sliding Regimes in Problems of Optimization and Control* (Nauka, Moscow, 1981).
4. V. M. Matrosov and I. A. Finogenko, *Prikl. Mat. Mekh.* **58** (6), 3 (1994).
5. V. I. Matyukhin, *Avtom. Telemekh.*, No. 4, 47 (1998).
6. I. A. Finogenko, *Diff. Uravn.* **34**, 1609 (1998).

Translated by V. Chechin

Theoretical Analysis of a Model for a Boundary Layer with Separation and Reattachment

N. V. Khusnutdinova

Presented by Academician M.M. Lavrent'ev January 26, 2001

Received February 9, 2001

INTRODUCTION

A boundary-value problem modeling the separation of a boundary layer and its subsequent reattachment to a surface bounding a flow is considered under increasing pressure. It is proven that, outside a certain bounded region adjacent to a wall in a fluid, the generalized solution to this problem is a classical positive solution to the Prandtl–Mises system of boundary-layer equations. Inside this region, local stagnation zones, the solution to which is equal to zero, can form near the wall. It is established that the alternation of suction with injection represents a possible way of controlling the boundary layer.

1. PRANDTL–MISES PROBLEM

The problem of extension of the Prandtl boundary layer is considered in the region $D = \{0 < x < \infty, 0 < \psi < \infty\}$ using the Mises variables [1, pp. 27, 28]. It has the form

$$\omega_x = \nu \sqrt{\omega} \omega_{\psi\psi} + 2UU_x, \quad (x, \psi) \in D, \quad (1)$$

$$\begin{aligned} \omega|_{x=0} &= \omega_0(\psi), \quad \omega|_{\psi=0} = 0, \\ \lim_{\psi \rightarrow \infty} \omega(x, \psi) &= U^2(x), \end{aligned} \quad (2)$$

where $\nu = \text{const} > 0$ is the viscosity and $U(x)$ is the external-flow velocity related to the pressure $p(x)$ through the Bernoulli law,

$$2p(x) + U^2(x) = \text{const} > 0.$$

It is assumed that

$$(a) \quad \omega_0(\psi) \in C^1[0, \infty) \cap C^{2+\alpha}(0, \infty), \quad \alpha \in (0, 1); \\ U^2(x) \in C^2[0, \infty);$$

$$(b) \quad 0 < \omega_0(\psi) \leq U^2(0), \quad \omega'_0(\psi) > 0; \quad \omega''_0(\psi) \leq 0 \text{ at } \psi > 0, \quad \omega_0(0) = 0, \quad \omega'_0(0) > 0, \quad \lim_{\psi \rightarrow \infty} \omega_0(\psi) = U^2(0),$$

$$\lim_{\psi \rightarrow \infty} \left[\frac{U^2(0) - \omega_0(\psi) + |\omega''_0(\psi)|}{\omega'_0(\psi)} \right] = k;$$

$$(c) \quad U(x) \geq \delta > 0, \quad U'(x) < 0 \text{ at } x > 0, \quad 0 < -[U^2(x)]' \leq \delta^2[k_1x + k_2]^{-\lambda} \text{ at } x \geq x_1, \text{ where } k, \delta, x_1, k_i > 0, \text{ and } \lambda > 3 \text{ are certain constants;}$$

$$(d) \quad U'(0) = 0, \quad \sqrt{\omega_0(\psi)} \omega''_0(\psi) = 0(\psi) \text{ at } \psi \rightarrow 0.$$

Due to the assumptions in (a)–(d), a smooth positive solution $\omega(x, \psi)$ to problem (1), (2) exists in the region $\{0 < x < A, 0 < \psi < \infty\}$ at certain A [1].

Let A_0 be the supremum of such A . If $A_0 < \infty$, we shall assume that separation of the boundary layer occurs at the point $x = A_0$.

It is usually believed that separation of the boundary layer arises at such a point where, being negative, the gradient of external-flow velocity $U'(x)$ reaches its maximum in absolute value [2, p. 388; 3, p. 408].

This observation is consistent with the integral condition [4] imposed on a value of $|U'|$ and ensures boundary-layer separation, including the case of a strictly positive external-flow velocity $U(x)$.

Boundary-layer separation from the surface of a high-drag body is accompanied by the formation of an extensive wake. Measurements of the pressure distribution along the surface bounding the flow show that, in certain cases, the pressure is almost constant along the separation area and practically coincides with its values at the outer boundary of the detached boundary layer. Under these conditions, near the surface bounding the flow in the zone of boundary-layer separation, the pressure is assumed to be constant and the fluid immovable [3, pp. 424–426].

2. MODEL OF THE BOUNDARY LAYER WITH SEPARATION

The following modified statement of the problem described in [4] is proposed for modeling flows with

Lavrent'ev Institute of Hydrodynamics, Siberian Division, Russian Academy of Sciences, pr. Akademika Lavrent'eva 15, Novosibirsk, 630090 Russia

boundary-layer separation and reattachment to the wall:

$$\omega_x = \nu\sqrt{\omega}\omega_{\psi\psi} + \varphi(x; \omega), \tag{3}$$

$$\omega(x, \psi) \geq 0, \quad (x, \psi) \in D,$$

$$\omega|_{x=0} = \omega_0(\psi), \quad \omega|_{\psi=0} = 0, \tag{4}$$

$$\lim_{\psi \rightarrow \infty} \omega(x, \psi) = U^2(x),$$

where $\varphi(x; \omega) \equiv 2U(x)U'(x)$ at $\omega > 0$, $\varphi(x; 0) = 0$.

Paper [4] presents the proof of existence of a nonnegative generalized solution to the boundary value problem (3), (4). This solution is bounded in the region D , continuous in the sense of Hölder at $(x, \psi) \in \bar{D} = \{0 \leq x < \infty, 0 \leq \psi < \infty\}$, and satisfies both conditions (4) and the integral identity

$$\iint_D \left[\omega f_x - \frac{8}{9} \nu \left(\frac{\partial \omega^{3/4}}{\partial \psi} \right)^2 f - \nu \sqrt{\omega} \omega_{\psi\psi} f_{\psi} + \varphi(x; \omega) f \right] dx d\psi + \int_0^{\infty} \omega_0(\psi) f(0, \psi) d\psi = 0.$$

Here, $f(x, \psi) \in C^1(\bar{D})$ is an arbitrary function equal to zero both at $\psi = 0$ and outside a finite region. Being positive in the range $0 \leq x < A_0$, this solution is classical for problem (1), (2).

The generalized solution to problem (3), (4) is constructed as the limit of a steadily decreasing (at $\varepsilon \rightarrow 0$) sequence of positive solutions,

$$\omega_\varepsilon = \omega(x, \psi, \varepsilon) \in C^{3+\alpha}(\bar{D}_\varepsilon),$$

$$\bar{D}_\varepsilon = \left\{ 0 \leq x < \infty, 0 \leq \psi \leq \frac{1}{\varepsilon} \right\},$$

to the following regularized boundary value problems:

$$\omega_x = \nu\sqrt{\omega}\omega_{\psi\psi} + 2UU' \frac{\omega - \varepsilon}{\omega + \varepsilon}, \quad (x, \psi) \in \bar{D}_\varepsilon, \tag{5}$$

$$\omega|_{x=0} = \omega_{0\varepsilon}(\psi), \quad \omega|_{\psi=0} = \varepsilon, \tag{6}$$

$$\omega|_{\psi=1/\varepsilon} = \omega_0\left(\frac{1}{\varepsilon}\right).$$

Here, $\{\omega_{0\varepsilon}(\psi)\} \in C^4[0, \infty)$ is the set of functions that converge uniformly to $\omega_0(\psi)$ ($0 < \psi < \infty$) as $\varepsilon \rightarrow 0$ and have the properties (b), (d) of the initial profile $\omega_0(\psi)$.

3. DOMAIN OF POSITIVENESS OF THE SOLUTIONS

Theorem 1. *Under the assumptions in (a)–(d), a solution $\omega(x, \psi)$ to problem (3), (4) is positive in*

a certain region

$$G_F = \{0 < x < \infty, F(x) < \psi < \infty\},$$

$F(x) \in C[0, \infty)$, $F(0) = F(x_0) = 0$, $F(x) > 0$ at $x \in (0, x_0)$, $F(x) \equiv 0$ at $x \geq x_0$, where it represents the classical solution to the Prandtl–Mises equation (1).

Schematic proof. As a result of the change of variables

$$x = x, \quad \eta = \psi - F(x),$$

the regions G_F and $D_\varepsilon \cap G_F$ turn into the regions $P_0 =$

$$\{0 < x < \infty, 0 < \eta < \infty\} \text{ and } P_\varepsilon = \left\{ 0 < x < \infty, 0 < \eta < \frac{1}{\varepsilon} -$$

$F(x) \right\}$, respectively. In addition, solutions $\omega(x, \psi)$ and

$\omega(x, \psi, \varepsilon)$ to problems (3), (4) and (5), (6) turn into the solutions $w(x, \eta) \equiv \omega(x, \eta + F)$ and $w_\varepsilon = w(x, \eta, \varepsilon) \equiv \omega(x, \eta + F, \varepsilon)$ of the following boundary-value problems:

$$L(w) \equiv \nu\sqrt{w}w_{\eta\eta} + F'(x)w_\eta - w_x = -2UU', \tag{7}$$

$$(x, \eta) \in P;$$

$$w|_{x=0} = \omega_0(\eta), \quad w|_{\eta=0} = \omega(x, F(x)), \tag{8}$$

$$\lim_{\eta \rightarrow \infty} w(x, \eta) = U^2(x);$$

$$L_\varepsilon(w) \equiv \nu\sqrt{w}w_{\eta\eta} + F'(x)w_\eta - w_x + 2UU' \frac{w - \varepsilon}{w + \varepsilon} = 0, \tag{9}$$

$$(x, \eta) \in P_\varepsilon;$$

$$w|_{x=0} \equiv \omega_{0\varepsilon}(\eta), \quad w|_{\eta=0} = \omega(x, F(x), \varepsilon), \tag{10}$$

$$w|_{\eta=\frac{1}{\varepsilon}-F} = \omega_0\left(\frac{1}{\varepsilon}\right).$$

We assume that $F(x) = x(2M - x)$ at $x \in [0, M]$,

$$F(x) = F_1(x) = M^2 - \int_M^x (1 - e^{-2(t-M)})[\beta(t-M) + 1]^{-1} dt$$

at $x \in [M, x_0]$, and $F(x) \equiv 0$ at $x > x_0$, where the point x_0 is determined by solving the equality $F_1(x_0) = 0$.

The function $F(x)$ is continuous in $[0, \infty)$ and doubly continuously differentiable in both ranges $[0, x_0]$ and $[x_0, \infty)$.

Further, we construct the barriers from below $\sigma_\varepsilon(x, \eta)$ for solutions $w_\varepsilon(x, \eta)$ of the boundary value problems (9), (10) such that

$$w_\varepsilon(x, \eta) \geq \sigma_\varepsilon(x, \eta) > \lim_{\varepsilon \rightarrow \infty} \sigma_\varepsilon(x, \eta) = \sigma(x, \eta), \tag{11}$$

$$(x, \eta) \in \bar{P}_\varepsilon,$$

where $\sigma(x, \eta) > 0$ at $\eta > 0$ and $\sigma(x, 0) = 0$.

Properties (11) are inherent in the functions

$$\sigma_\varepsilon(x, \eta) = \Phi(x)f(\eta + \varepsilon),$$

$$\sigma(x, \eta) = \Phi(x)f(\eta);$$

$$\Phi(x) \equiv U^2(x), \quad x \in \left[0, \frac{M}{2}\right];$$

$$\Phi(x) \equiv U^2\left(\frac{M}{2}\right) \left[2\beta\left(x - \frac{M}{2}\right) + 1\right]^2,$$

$$x \in \left[\frac{M}{2}, \infty\right], f(\eta) = a_1\eta + a_2\eta^{4/3} \text{ at } \eta \leq 1, a_1 + a_2 < 1,$$

$$f(1) \leq f(\eta) < 1, |f'| + |f''| \leq a_3, \eta \geq 1, f'(\eta) > 0 \text{ at } \eta \geq 0,$$

$$f'(\eta) \rightarrow 0, f''(\eta) \rightarrow 0 \text{ at } \eta \rightarrow \infty,$$

$$f(\eta) \in C^2[0, \infty), \quad \lim_{\eta \rightarrow \infty} f(\eta) = 1,$$

$$\lim_{\eta \rightarrow \infty} \frac{1 - f(\eta) + |f''(\eta)|}{f'(\eta)} = a_4.$$

According to the construction, the function $\Phi(x) \in C[0, \infty)$ and is continuously differentiable in the ranges

$$\left[0, \frac{M}{2}\right] \text{ and } \left[\frac{M}{2}, \infty\right).$$

The constants a_i and ε_1 , as well as the function $f(\eta)$, are chosen so that the inequalities

$$z(x, \eta, \varepsilon) = (w_\varepsilon(x, \eta) - \sigma_\varepsilon(x, \eta)) \geq 0, \quad (12)$$

$$(x, \eta) \in \Gamma_\varepsilon$$

are satisfied at the parabolic boundary $\Gamma_\varepsilon = \left\{x = 0, \right.$

$$\left. 0 \leq \eta \leq \frac{1}{\varepsilon}, \eta = 0, x \geq 0, \eta = \frac{1}{\varepsilon} - F, x \geq 0 \right\} \text{ of the region}$$

P_ε for $\varepsilon \leq \varepsilon_1 \ll 1$. Such a choice of $f(\eta)$ is possible due to the constraints (b) on the function $\omega_{0\varepsilon}(\psi)$ and the estimate $w_\varepsilon(x, \eta) \geq \varepsilon$ [4, p. 1198].

$$\text{In the regions } H_1 = \left\{0 < x < \frac{M}{2}, 0 < \eta < \frac{1}{\varepsilon} - F(x)\right\},$$

$$H_2 = \left\{\frac{M}{2} < x < x_0, 0 < \eta < \frac{1}{\varepsilon} - F(x)\right\}, \text{ and } H_3 = \left(x_0 < \right.$$

$$\left. x < \infty, 0 < \eta < \frac{1}{\varepsilon} - F(x)\right\}, \text{ the function } z = w_\varepsilon(x, \eta) -$$

$\sigma_\varepsilon(x, \eta)$ satisfies the linear parabolic equation

$$L_0(z) \equiv v\sqrt{w_\varepsilon}z_{\eta\eta} + F'(x)z_\eta - z_x + dz = -L_\varepsilon(\sigma_\varepsilon), \quad (13)$$

$$d = v\frac{\sigma_{\varepsilon\eta\eta}}{\sqrt{w_\varepsilon} + \sqrt{\sigma_\varepsilon}} + \frac{4UU'\varepsilon}{(w_\varepsilon + \varepsilon)(\sigma_\varepsilon + \varepsilon)},$$

$$L_\varepsilon(\sigma_\varepsilon) \equiv v\Phi\sqrt{\Phi}f''$$

$$+ F'(x)\Phi f' - \Phi_x f + 2UU'\frac{\sigma_\varepsilon - \varepsilon}{\sigma_\varepsilon + \varepsilon} > 0.$$

For $(x, \eta) \in H_1 \cup H_2 \cup H_3$, the inequality $L_\varepsilon(\sigma_\varepsilon) > 0$ is made valid by the choice of the constants M, β , and ε_1 ($0 < \varepsilon \leq \varepsilon_1 \ll 1$).

As a result, with allowance for (12) and according to the maximum principle applied successively in the regions H_1, H_2 , and H_3 , solutions to Eq. (13) satisfy the inequality

$$w_\varepsilon(x, \eta) \geq \sigma_\varepsilon \text{ at } (x, \eta) \in \bigcup_k \overline{H_k} = \overline{P_\varepsilon}.$$

Since the functions $w_\varepsilon(x, \eta) \in C^\alpha[0 \leq x \leq A, 0 \leq \eta \leq N]$ are compact for each $N > 0$ ($0 < \alpha' < \alpha$), similar inequalities are satisfied for the limiting functions $w(x, \eta) \equiv \omega(x, \psi)$ and $\sigma(x, \eta) \equiv \sigma(x, \psi - F)$, so that $\omega(x, \psi) \geq \sigma(x, \psi - F)$ at $(x, \psi) \in G_F$. Consequently, it follows from Theorem 2.1 [4] that the function $\omega(x, \psi)$ satisfying Eq. (3) and positive in G_F likewise represents the classical solution to Eq. (1).

4. EXISTENCE OF LOCAL STAGNATION ZONES

Theorem 2. *The generalized solution $\omega(x, \psi)$ to problem (3), (4) cannot have isolated zeros in the region $\{0 < x < x_0, 0 < \psi < F(x)\}$.*

Schematic proof. First, the maximum principle is used to establish the inequalities

$$q = \frac{\partial \omega_\varepsilon}{\partial \psi} \geq 0, \quad (x, \psi) \in \overline{D}_\varepsilon \quad (14)$$

for solutions $\omega_\varepsilon(x, \psi)$ of the boundary-value problems (5), (6).

The assumption is that both $\omega(x_1, \psi_1) = 0$ at $(x_1, \psi_1) \in D$ and $\omega(x_1, \psi) \neq 0$ at $\psi \in [0, \psi_1]$ contradict estimate (14). Consequently,

$$\omega(x_1, \psi) \equiv 0 \text{ at } \psi \in [0, \psi_1]. \quad (15)$$

Therefore, according to the properties of the function $\omega(x, \psi)$ [2, item 3],

$$\omega(x, \psi) \equiv 0 \text{ at } x \in \left[x_1, x_1 + \frac{(\psi_1 - \psi)^2}{24vm}\right], \quad (16)$$

$$\psi \in \left[\frac{\psi_1}{2}, \psi_1\right].$$

In particular, $\omega\left(x, \frac{\Psi_1}{2}\right) \equiv 0$ at $x \in [x_1, x_3]$, $x_3 = x_1 + \frac{\Psi_1^2}{96\nu m}$. Then, similarly to (15),

$$\omega(x, \psi) \equiv 0 \text{ at } x \in [x_1, x_3], \quad \psi \in \left[0, \frac{\Psi_1}{2}\right]. \quad (17)$$

Relations (16) and (17) yield that

$$\omega(x, \psi) \equiv 0 \text{ at } (x, \psi) \in Q_0 = (x_1, x_3) \times (\Psi_0, \Psi_1),$$

where $\Psi_0 = \{\Psi_1 - \sqrt{24\nu m(x - x_1)}, x_1 < x < x_3\}$. Thus, the region Q_0 represents a local stagnation zone; i.e., the point (x_1, Ψ_1) is not isolated.

CONTROL OF THE PRANDTL–MISES BOUNDARY LAYER

In the Mises variables, the flow in the boundary layer that forms near a porous wall with suction [$v_0(x) < 0$] or injection [$v_0(x) > 0$] through it is described by the following boundary-value problem [1, p. 29]:

$$\omega_x = \nu \sqrt{\omega} \omega_{\psi\psi} - v_0(x) \omega_\psi + 2UU_x, \quad (x, \psi) \in D, \quad (18)$$

$$\begin{aligned} \omega|_{x=0} &= \omega_0(\psi), \quad \omega|_{\psi=0} = 0, \\ \lim_{\psi \rightarrow \infty} \omega(x, \psi) &= U^2(x). \end{aligned} \quad (19)$$

The distribution of the velocity of fluid suction into a porous wall [$v_0(x) < 0$] that prevents separation of the boundary layer was constructed in [5]. On the other hand, the boundary layer always separates from the wall [6] when fluid injection occurs at any constant velocity [$v_0(x) \equiv \varepsilon = \text{const} > 0$].

Theorem 3. *Let assumptions (a)–(d) be satisfied and, in addition, $\omega_0(\psi) \equiv 0$ at $\psi \in [0, \Psi_0] \cup \left[\frac{1}{\Psi_0}, \infty\right)$ ($\Psi_0 = \text{const} > 0$).*

Then, there is the function $v_0(x) \in C[0, \infty)$, which satisfies the conditions $v_0(x) < 0$ at $x \in (0, x^0)$, $v_0(x) > 0$ at

$$x \in (x^0, x^1), \quad v_0(x) \equiv 0 \text{ at } x \in (x^1, \infty), \text{ and } \int_0^{x^1} v_0(t) dt = 0,$$

such that boundary-value problem (18), (19) is solvable in the region D and its solution $\omega(x, \psi) > 0$ at $\psi > 0$.

Schematic proof. At $v_0(x) \equiv -F'(x)$, problem (18), (19) does not differ from the already considered problem (7), (8), where the conditions $-F'(x) < 0$ (at $x \in [0, M)$) and $F'(x) > 0$ [at $x \in (M, x_0)$] correspond to suction and injection, respectively. This fact proves the statement of Theorem 3 that problem (18), (19) is solvable in the classical sense and its solution $\omega(x, \psi)$ has a minorant $\sigma(x, \psi)$: $\omega(x, \psi) \geq \sigma(x, \psi) > 0$ at $\psi > 0$ and $\sigma(x, 0) = 0$.

Thus, the separation-free flow in the Prandtl–Mises boundary layer can be realized by alternating a region of fluid suction into the wall with that where the identical fluid mass is injected into the boundary layer.

Remark. According to lemmas 2.1.8–2.1.13 [1], the solution $\omega(x, \psi)$ to problem (18), (19), which corresponds to the function $v_0(x)$ smoothed in the vicinity of the points $x = 0$ and $x = x_0$ so that $v_0(x) \in C^1[0, \infty)$ and $v_0(0) = 0$, satisfies the inequalities

$$\begin{aligned} |\omega_\psi| &\leq M, \quad |\sqrt{\omega} \omega_{\psi\psi}| \leq M, \quad (x, \psi) \in D, \\ |\omega_x| &\leq M\psi^{1-\beta}, \quad \omega_\psi \geq m > 0, \\ 0 &\leq \psi \leq \Psi_1, \quad 0 < \beta < \frac{1}{2}. \end{aligned}$$

These inequalities justify the inverse substitution of the Mises variables x, ψ by the original Eulerian coordinates x, y [1, Theorem 2.1.5].

ACKNOWLEDGMENTS

This work was supported in part by the Russian Foundation for Basic Research, project no. 99-01-00622, and the Program “Russian Universities,” project no. 1788.

REFERENCES

1. O. A. Oleĭnik and V. N. Samokhin, *Mathematical Methods in Boundary-Layer Theory* (Nauka, Moscow, 1997).
2. H. Schlichting, *Boundary Layer Theory* (McGraw-Hill, New York, 1968; Nauka, Moscow, 1974).
3. G. K. Batchelor, *An Introduction to Fluid Dynamics* (Cambridge Univ. Press, Cambridge, 1967; Mir, Moscow, 1973).
4. N. V. Khusnutdinova, *Sib. Mat. Zh.* **40**, 1195 (1999).
5. N. V. Khusnutdinova, *Sib. Mat. Zh.* **13**, 485 (1972).
6. A. I. Suslov, *Prikl. Mat. Mekh.* **38** (1), 166 (1974).

Translated by Yu. Verevchkin

The Elastoplastic State of a Plate Subjected to Biaxial Tension in the Presence of Longitudinal Shears

L. I. Afanas'eva and M. V. Mikhailova

Presented by Academician A. Yu. Ishlinskii February 12, 2001

Received March 1, 2001

L.A. Galin [1] gave a solution to the problem on the elastoplastic state of a plate having a circular hole and subjected to biaxial tension. At a later time, a number of approximate analytic solutions to elastoplastic problems were obtained. In this paper we consider, using a small-parameter method, the problem on the elastoplastic state of a plate having a circular hole and subjected to biaxial tension in the presence of longitudinal shears. Three approximations for the stresses are used in this problem.

1. As an initial unperturbed state, we consider an axisymmetric state of a thick-walled tube with internal and external radii a and b ($a < b$), respectively. This tube is acted upon by the internal and external pressures p and q and, at the internal boundary, by the tangential force τ . The tube material is assumed to be incompressible.

Below, we relate all the quantities having dimensions of stress to the yield strength k and all the quantities having dimensions of length to the radius ρ_s of the plastic zone. We will use the following notation:

$$\sigma_{ij} = \frac{\sigma_{ij}}{k}, \quad p = \frac{p}{k}, \quad q = \frac{q}{k}, \quad \tau = \frac{\tau}{k}, \quad G = \frac{G}{k},$$

$$\varepsilon_{ij} = \frac{\varepsilon_{ij}}{\rho_s}, \quad u = \frac{u}{\rho_s}, \quad v = \frac{v}{\rho_s},$$

$$w = \frac{w}{\rho_s}, \quad \alpha = \frac{a}{\rho_s}, \quad \beta = \frac{b}{\rho_s},$$

where σ_{ij} are the components of the stress tensor; ε_{ij} are the components of strain rates; u , v , w are the components of displacement rates along the axes ρ , θ , and z , respectively; and k is the yield strength.

It is evident that everywhere

$$\tau_{\rho\theta}^0 = \tau_{\theta z}^0 = 0, \quad \varepsilon_{\rho\theta}^0 = \varepsilon_{\theta z}^0 = 0, \quad v^0 = 0, \quad \varepsilon_z^0 = 0; \quad (1)$$

all other components of tensors of stress, strain rate, and displacement velocities depend solely on ρ .

The equilibrium equations have the form

$$\frac{d\sigma_\rho^0}{d\rho} + \frac{\sigma_\rho^0 - \sigma_\theta^0}{\rho} = 0, \quad \frac{d\tau_{\rho z}^0}{d\rho} + \frac{\tau_{\rho z}^0}{\rho} = 0, \quad (2)$$

with the boundary conditions

$$\sigma_\rho^0 = -p, \quad \tau_{\theta z}^0 = \tau \text{ for } \rho = \alpha \quad (3)$$

and

$$\sigma_\rho^0 = q \text{ for } \rho = \beta. \quad (4)$$

In the plastic region adjacent to the internal surface of the tube, the plasticity condition

$$(\sigma_\rho^0 - \sigma_z^0)^2 + 4\tau_{\rho z}^{02} = 4, \quad \sigma_\theta^0 = \sigma^0 + \frac{2}{3} \quad (5)$$

is satisfied. The second equation of system (2), with initial conditions (3), yields

$$\tau_{\rho z}^0 = \frac{\alpha\tau}{\rho}. \quad (6)$$

It follows from (5) and (6) that

$$\sigma_\rho^{0p} - \sigma_z^{0p} = -2 \frac{\sqrt{\rho^2 - \alpha^2 \tau^2}}{\rho}, \quad (7)$$

$$\sigma_\rho^{0p} - \sigma_\theta^{0p} = \frac{\sigma_\rho^{0p} - \sigma_z^{0p}}{2} - 1.$$

Using the first equation of system (2) and relationships (7) and (3), we obtain

$$\sigma_\rho^{0p} = \ln \frac{\rho}{\alpha} + \ln \frac{\rho + \sqrt{\rho^2 - \alpha^2 \tau^2}}{\alpha(1 + \sqrt{1 - \tau^2})} - \frac{\sqrt{\rho^2 - \alpha^2 \tau^2}}{\rho} + \sqrt{1 - \tau^2} - p,$$

$$\sigma_\theta^{0p} = \ln \frac{\rho}{\alpha} + \ln \frac{\rho + \sqrt{\rho^2 - \alpha^2 \tau^2}}{\alpha(1 + \sqrt{1 - \tau^2})} + 1 + \sqrt{1 - \tau^2} - p, \quad (8)$$

$$\sigma_z^{0p} = \ln \frac{\rho}{\alpha} + \ln \frac{\rho + \sqrt{\rho^2 - \alpha^2 \tau^2}}{\alpha(1 + \sqrt{1 - \tau^2})} + \frac{\sqrt{\rho^2 - \alpha^2 \tau^2}}{\rho} + \sqrt{1 - \tau^2} - p.$$

In the elastic region ($1 \leq \rho \leq \beta$), according to Hooke's law

$$\sigma_\rho^{0e} - \sigma_\theta^{0e} = 2G(\varepsilon_\rho^{0e} - \varepsilon_\theta^{0e}), \quad (9)$$

the incompressibility condition

$$\varepsilon_\rho^{0e} + \varepsilon_\theta^{0e} = 0, \quad (10)$$

and the boundary condition (4), the following equations are valid:

$$\sigma_\rho^{0e} = 2GC_1 \left(\frac{1}{\beta^2} - \frac{1}{\rho^2} \right) + q, \quad (11)$$

$$\sigma_\theta^{0e} = 2GC_1 \left(\frac{1}{\beta^2} + \frac{1}{\rho^2} \right) + q, \text{ where } C_1 = \text{const.}$$

At the boundary of the elastoplastic zone of the material, conjugation conditions are satisfied:

$$\sigma_\rho^{0e} = \sigma_\rho^{0p}, \quad \sigma_\theta^{0e} = \sigma_\theta^{0p} \text{ for } \rho = 1. \quad (12)$$

On account of (8), (11), and (12), we have

$$C_1 = \frac{t+1}{4G}, \quad t = \sqrt{1 - \alpha^2 \tau^2}, \quad (13)$$

$$-2 \ln \alpha + \ln \frac{1+t}{1 + \sqrt{1 - \tau^2}} + \sqrt{1 - \tau^2} + 1 - p = \frac{t+1}{2} \left(\frac{1}{\beta^2} + 1 \right) + q. \quad (14)$$

From (13), (8), and (7), we also obtain

$$\sigma_\rho^{0e} = \frac{t+1}{2} \left(\frac{1}{\beta^2} - \frac{1}{\rho^2} \right) + q, \quad (15)$$

$$\sigma_\theta^{0e} = \frac{t+1}{2} \left(\frac{1}{\beta^2} + \frac{1}{\rho^2} \right) + q.$$

For the plane with a circular hole, in formulas (15), $\beta = \infty$.

2. We now turn to the consideration of the elastoplastic state of an infinite plate with a circular hole of radius a . The problem is solved in the cylindrical frame of coordinates (ρ, θ, z) with the z -axis perpendicular to the plate plane. It is assumed that, on the $(\rho\theta)$ plane, the plate is stretched at infinity by mutually orthogonal forces p_1 and p_2 ($p_1 > p_2$) and, in addition, the normal pressure p and the tangential pressure τ , perpendicular to this plane, act at the hole contour.

In the elastic and plastic regions, the solution to the problem is sought in the form

$$\sigma_{ij} = \sigma_{ij}^0 + \delta \sigma_{ij}' + \delta^2 \sigma_{ij}'' + \delta^3 \sigma_{ij}''', \quad \delta = \frac{p_1 - p_2}{2}. \quad (16)$$

The boundary conditions at infinity are written as

$$\sigma_\rho^e = q - \delta \cos 2\theta, \quad \sigma_\theta^e = q + \delta \cos 2\theta, \quad (17)$$

$$\text{and } \tau_{\rho\theta}^e = \delta \sin 2\theta \text{ for } \rho = \infty,$$

where $q = \frac{p_1 + p_2}{2}$.

At the hole contour, we define the following conditions:

$$\sigma_\rho^p = -p, \quad \tau_{\rho\theta}^p = 0 \text{ for } \rho = \alpha. \quad (18)$$

Since the internal contour and external loads on it are fixed in the problem at hand, we have

$$\sigma_{ij}^p = 0, \quad \sigma_{ij}^{\prime p} = 0, \quad \sigma_{ij}^{\prime\prime p} = 0. \quad (19)$$

Let us define the components of the stressed state in the elastic region. The boundary conditions (17) at infinity take the form

$$\sigma_\rho^e = -\cos 2\theta, \quad \tau_{\rho\theta}^e = \sin 2\theta \text{ for } \rho = \infty, \quad (20)$$

$$\sigma_\rho^{\prime e} = 0, \quad \tau_{\rho\theta}^{\prime e} = 0 \text{ for } \rho = \infty, \quad (21)$$

$$\sigma_\rho^{\prime\prime e} = 0, \quad \tau_{\rho\theta}^{\prime\prime e} = 0 \text{ for } \rho = \infty. \quad (22)$$

Using the conditions of conjugation [2],

$$\left[\sigma_{ij}' + \frac{\partial \sigma_{ij}^0}{\partial \rho} \rho_{1s} \right] = 0 \text{ for } \rho = 1, \quad (23)$$

and taking (1), (8), (15), and (19) into account, we obtain

$$\sigma_\rho^{\prime e} = \tau_{\rho\theta}^{\prime e} = 0 \text{ for } \rho = 1 \quad (24)$$

and

$$\sigma_\theta^{\prime e} = \frac{(t+1)^2}{t} \rho_{1s} \text{ for } \rho = 1. \quad (25)$$

The boundary conditions (20) and (24) define, according to [2], the solution in the elastic region:

$$\sigma_\rho^{\prime e} = \left(-1 + \frac{4}{\rho^2} - \frac{3}{\rho^4} \right) \cos 2\theta,$$

$$\sigma_\theta^{\prime e} = \left(1 + \frac{3}{\rho^4} \right) \cos 2\theta, \quad (26)$$

$$\tau_{\rho\theta}^{\prime e} = \left(1 + \frac{2}{\rho^2} - \frac{3}{\rho^4} \right) \sin 2\theta.$$

From (26) and (25) we have

$$\rho_{1s} = \frac{4t}{(t+1)^2} \cos 2\theta. \tag{27}$$

In the second approximation, using the conjugation conditions [2]

$$\sigma''_{ij} + \frac{\partial \sigma'_{ij}}{\partial \rho} \rho_{1s} + \frac{\partial^2 \sigma^0_{ij}}{\partial \rho^2} \frac{\rho_{1s}^2}{2} + \frac{\partial \sigma^0_{ij}}{\partial \rho} \rho_{2s} = 0 \text{ for } \rho = 1$$

and formulas (1), (8), (15), (19), (26), and (27), we obtain

$$\sigma_p''' = -\frac{4t}{(t+1)^2} (1 + \cos 4\theta), \tag{28}$$

$$\tau_{p\theta}'' = -\frac{16t}{(t+1)^2} \sin 4\theta \text{ for } \rho = 1,$$

$$\begin{aligned} \sigma_\theta''' - 8 \cos^2 2\theta \frac{(5-3t)t}{t+1} \\ = \frac{(t+1)^2}{t} \rho_{2s} \text{ for } \rho = 1. \end{aligned} \tag{29}$$

The boundary conditions (21) and (28) define, according to [2], the solution in the elastic region:

$$\sigma_p''' = \frac{4t}{(t+1)^2} \left(-\frac{1}{\rho^2} + \left(\frac{9}{\rho^4} - \frac{10}{\rho^6} \right) \cos 4\theta \right),$$

$$\sigma_\theta''' = \frac{4t}{(t+1)^2} \left(\frac{1}{\rho^2} + \left(-\frac{3}{\rho^4} + \frac{10}{\rho^6} \right) \cos 4\theta \right), \tag{30}$$

$$\tau_{p\theta}'' = \frac{8t}{(t+1)^2} \left(\frac{3}{\rho^4} - \frac{5}{\rho^6} \right) \sin 4\theta.$$

Then, from (30) and (29), we have

$$\rho_{2s} = \frac{4t^2}{(t+1)^4} \tag{31}$$

$$\times ((3t^2 - 2t - 4) + (3t^2 - 2t + 2) \cos 4\theta).$$

In the third approximation, the conjugation conditions [2]

$$\begin{aligned} \sigma'''_{ij} + \frac{\partial \sigma''_{ij}}{\partial \rho} \rho_{1s} + \frac{\partial^2 \sigma'_{ij}}{\partial \rho^2} \frac{\rho_{1s}^2}{2} + \frac{\partial^3 \sigma^0_{ij}}{\partial \rho^3} \frac{\rho_{1s}^3}{3!} \\ + \frac{\partial \sigma^0_{ij}}{\partial \rho} \rho_{3s} + \frac{\partial \sigma'_{ij}}{\partial \rho} \rho_{2s} + \frac{\partial^2 \sigma^0_{ij}}{\partial \rho^2} \rho_{1s} \rho_{2s} = 0 \text{ (for } \rho = 1) \end{aligned}$$

yield, on account of (1), (8), (15), (19), (26), (27), (30),

and (31), the following expressions:

$$\begin{aligned} \sigma_p''' = -\frac{8}{(t+1)^4} \left[(7t^2 - 2t + 1) \cos 2\theta \right. \\ \left. + \frac{51t^2 - 2t + 1}{3} \cos 6\theta \right], \end{aligned} \tag{32}$$

$$\begin{aligned} \tau_{p\theta}''' = -\frac{16t^2}{(t+1)^4} \left[(3t^2 - 2t + 2) \sin 2\theta \right. \\ \left. + (3t^2 - 2t + 14) \sin 6\theta \right] \text{ for } \rho = 1, \end{aligned}$$

and

$$\begin{aligned} \sigma_\theta''' - \frac{16}{t^2(t+1)^4} \left[\frac{18t^5 - 2t^4 - 16t^3 + 14t^2 - 6t + 3}{2} \right. \\ \left. \times \cos 2\theta \right. \\ \left. + \frac{18t^5 + 90t^4 + 8t^3 + 2t^2 - 6t + 3}{6} \cos 6\theta \right] = \frac{(t+1)^2}{t} \rho_{3s}. \end{aligned} \tag{33}$$

The boundary conditions (22) and (32) define, according to [2], the solution in the elastic region:

$$\begin{aligned} \sigma_p''' = \frac{16}{(t+1)^4} \left[\left(\frac{-12t^4 + 8t^3 - t^2 - 2t + 1}{2\rho^4} \right. \right. \\ \left. \left. + \frac{(t-1)(6t^3 + 2t^2 - t + 1)}{\rho^2} \right) \cos 2\theta \right. \\ \left. + \left(\frac{-24t^4 + 16t^3 - 61t^2 - 2t + 1}{2\rho^8} \right. \right. \\ \left. \left. + \frac{2(18t^4 - 12t^3 + 33t^2 + 2t - 1)}{3\rho^6} \right) \cos 6\theta \right], \end{aligned}$$

$$\begin{aligned} \sigma_\theta''' = \frac{16}{(t+1)^4} \left[-\left(\frac{-12t^4 + 8t^3 - t^2 - 2t + 1}{2\rho^4} \right) \cos 2\theta \right. \\ \left. + \left(\frac{-24t^4 + 16t^3 - 61t^2 - 2t + 1}{2\rho^8} \right. \right. \\ \left. \left. + \frac{(18t^4 - 12t^3 + 33t^2 + 2t - 1)}{3\rho^6} \right) \cos 6\theta \right], \end{aligned} \tag{34}$$

$$\begin{aligned} \tau_{p\theta}''' = \frac{16}{(t+1)^4} \left[\left(\frac{-12t^4 + 8t^3 - t^2 - 2t + 1}{2\rho^4} \right. \right. \\ \left. \left. + \frac{(t-1)(6t^3 + 2t^2 - t + 1)}{\rho^2} \right) \sin 2\theta \right. \\ \left. + \left(\frac{-24t^4 + 16t^3 - 61t^2 - 2t + 1}{2\rho^8} \right. \right. \end{aligned}$$

$$+ \frac{(18t^4 - 12t^3 + 33t^2 + 2t - 1)}{2\rho^6} \sin 6\theta \Big].$$

From (33) and (34) we have

$$\rho_{3s} = \frac{8}{t(t+1)^6} \quad (35)$$

$$\times [(12t^6 - 26t^5 + 3t^4 + 18t^3 - 15t^2 + 6t - 3)\cos 2\theta$$

$$+ (12t^6 - 14t^5 + 9t^4 - 2t^3 - t^2 + 2t - 1)\cos 6\theta].$$

In the special case when longitudinal shears are

absent, $t = 1$ ($\tau = 0$) and expressions (26)–(35) take a form similar to that of the relationships obtained in [2].

REFERENCES

1. L. A. Galin, *Prikl. Mat. Mekh.* **10** (3) (1946).
2. D. D. Ivlev and L. V. Ershov, *Perturbation Method in the Theory of an Elasticoplastic Body* (Nauka, Moscow, 1978).
3. A. Yu. Ishlinskiĭ, *Applied Problems in Mechanics. Vol. 1: Mechanics of Elastoplastic and Incompletely Elastic Bodies* (Nauka, Moscow, 1986).

Translated by A. Kozlenkov

On the Trajectory Stability in the Joukowski Sense in Relativistic Celestial Mechanics

O. V. Druzhinina

Presented by Academician V.V. Rumyantsev March 7, 2001

Received March 19, 2001

The fundamental studies of A.M. Lyapunov [1] and N.E. Joukowski [2] initiated numerous, fundamental investigations in the field of stability of motion and trajectory stability, as well as in the application of these theories to various problems of natural science and technology. In the context of classical mechanics and Newtonian celestial mechanics (NCM), fundamental papers [3–5] and some others (see also review [6]) were dedicated to problems of the stability theory in the Lyapunov sense. At the same time, problems of the trajectory-stability theory in the Joukowski sense were studied in [7–11]. In the framework of relativistic celestial mechanics (RCM), the problem of the stability of motion in the Lyapunov sense was studied in [12, 13], whereas the problem of the trajectory stability in the Joukowski sense was not posed at all. Meanwhile, RCM has its specific features (the absence of absolute time and the Riemannian nature of the manifold). In this context, the concept of trajectory stability in the Joukowski sense more adequately characterizes the inertia (or noncompliance) of a motion and its trajectories than the concept of motion stability in the Lyapunov sense proposed in [12, 13]. The former concept does not use synchronous correspondence in time for points in its definition and is based on the correspondence of a points in the normal. At the same time, the latter concept is based on replacing the correspondence in time by the correspondence in arc length for unperturbed and perturbed trajectories.

In the present paper, the problem of the trajectory stability in the Joukowski sense is posed in the framework of RCM. A criterion for the stability of a geodetic trajectory (geodetic) is also proved in the M^4 Riemann space-time with a metric whose tensor $g_{\alpha\beta}(x_1, x_2, x_3, x_4)$ has the signature $(+---)$.

We now cite certain necessary information from the general theory of relativity [14, 15]. The system of non-

linear Einstein equations of the form

$$G^{\alpha\beta} \equiv R^{\alpha\beta} - \frac{1}{2}g^{\alpha\beta}R - g^{\alpha\beta}\Lambda = -8c^{-4}\pi\gamma T^{\alpha\beta} \quad (1)$$

is the kernel of this theory. A material system characterized by an energy-momentum tensor $T^{\alpha\beta}$ moves in an M^4 four-dimensional space-time with a metric $ds^2 = g_{\alpha\beta}dx^\alpha dx^\beta$. The invariant ds is referred to as the space-time interval; $g_{\alpha\beta}$ and $g^{\alpha\beta}$ are covariant and contravariant metric tensors, respectively; x^α are the coordinates of points in M^4 ; γ is the Newtonian gravitational constant; c is the speed of light in free space; and Λ is the cosmological constant. The summation over repeated indices α, β, \dots is assumed in the case when one of them is upper and the other is lower. The indices $\alpha, \beta, \mu, \nu, \dots$ take the values 0, 1, 2, 3. The tensors $g^{\alpha\beta}$ and $g_{\alpha\beta}$ satisfy the condition $g^{\alpha\mu}g_{\beta\mu} = \delta_\beta^\alpha$, where δ_β^α is the Kronecker delta. The Ricci tensor $R_{\alpha\beta}$ is provided by the convolution of the Riemann–Christoffel curvature tensor

$$R^{\mu}_{\alpha\beta\nu} \equiv \frac{\partial\Gamma^{\mu}_{\alpha\nu}}{\partial x^\beta} - \frac{\partial\Gamma^{\mu}_{\alpha\beta}}{\partial x^\nu} + \Gamma^{\sigma}_{\alpha\nu}\Gamma^{\mu}_{\beta\sigma} - \Gamma^{\sigma}_{\alpha\beta}\Gamma^{\mu}_{\nu\sigma} \quad (2)$$

over the indices μ and ν ; i.e., $R_{\alpha\beta} \equiv R^{\mu}_{\alpha\beta\mu}$. The quantities $\Gamma^{\mu}_{\alpha\beta}$ are referred to as second-kind Christoffel symbols. They are equal to

$$\Gamma^{\mu}_{\alpha\beta} \equiv \frac{1}{2}g^{\mu\sigma} \left(\frac{\partial g_{\alpha\sigma}}{\partial x^\beta} + \frac{\partial g_{\beta\sigma}}{\partial x^\alpha} - \frac{\partial g_{\alpha\beta}}{\partial x^\sigma} \right) = \Gamma^{\mu}_{\beta\alpha}. \quad (3)$$

The invariant R (scalar curvature of M^4) is determined by the formulas

$$R^{\beta}_{\alpha} \equiv g^{\beta\sigma} R_{\alpha\sigma}, \quad R \equiv R^{\alpha}_{\alpha}. \quad (4)$$

System (1) is a system of ten nonlinear partial differential equations of the second order in ten desired functions $g_{\alpha\beta}(x^\nu)$. A variation of the right-hand side of (1) causes a change of the solution to the system. The quantity $T^{\alpha\beta}$ (the energy-momentum tensor of matter) contains $g_{\alpha\beta}$ apart from physical quantities (masses,

charges, velocities, angular momenta and magnetic moments of bodies, etc.). It is well known that Eq. (1) is satisfied by four identities that express the fact that the covariant divergence $G^{\alpha\beta}$ of the Einstein tensor is zero. This results in the validity of the equality $T^{\alpha\beta}_{;\beta} = 0$, where the semicolon implies the covariant partial derivative. The last equality leads to the energy-momentum conservation laws for a material system and to equations of motion in any approximation. In particular, from this equality, we can easily derive the exact equations of motion for a tentative particle in the external gravitational field,

$$\frac{Du^\alpha}{ds} \equiv \frac{du^\alpha}{ds} + \Gamma_{\beta\mu}^\alpha u^\beta u^\mu = 0; \tag{5}$$

the equations of motion for a tentative charged particle,

$$\frac{Du^\alpha}{ds} = \frac{e_0}{mc^2} u^\beta f_\beta^\alpha; \tag{6}$$

and the equations of translational and rotational motions for the rotating part,

$$\frac{D}{ds} \left(m c u^\alpha + u^\beta \frac{DS^{\alpha\beta}}{ds} \right) + \frac{1}{2} R^\alpha_{\beta\mu\nu} u^\beta S^{\mu\nu} = 0, \tag{7}$$

$$\frac{DS^{\alpha\beta}}{ds} + u_\mu \left(u^\alpha \frac{DS^{\beta\mu}}{ds} - u^\beta \frac{DS^{\alpha\mu}}{ds} \right) = 0. \tag{8}$$

In Eqs. (5)–(8), operator D is the absolute-differentiation operator; $u^\alpha \equiv \frac{dx^\alpha}{ds}$ are the components of the particle’s 4-velocity; m and e_0 are the particle’s mass and charge; $S^{\alpha\beta} = -S^{\beta\alpha}$ is a tensor characterizing the particle’s momentum; $\Gamma_{\beta\mu}^\alpha$ are the Christoffel symbols; $R^\alpha_{\beta\mu\nu}$ is the Riemann–Christoffel curvature tensor; and f_β^α is the tensor of an electromagnetic field linked to the four-vector A_α through the relation $f_{\alpha\beta} = A_{\alpha;\beta} - A_{\beta;\alpha}$.

The absence of the usual parallelism for tensor fields makes their comparison ambiguous. The reason for this is that the comparison in M^4 takes a meaning only once the translation of a tensor from a point in which it is determined by presetting the field to a point in which we wish to compare it with a given tensor has been specified. In the M^4 manifold, this depends on both the path and method of the translation (a parallel translation in the Levi-Civita sense, etc.) [7, 12].

Since the concept of stability is related to the notion of point closeness in unperturbed and perturbed trajectories, the correspondence between points in C and \bar{C} has to be established. It is well known that in the framework of NCM, such a correspondence is established owing to the presence of an external absolute param-

eter, i.e., time. Namely, points in the perturbed and unperturbed trajectories are considered as corresponding to each other if the same time (measured by a certain hypothetical absolute clock) corresponds to them. Evidently, this definition of the correspondence is meaningless in the framework of RCM, where time has no sense of the absolute parameter. Therefore, we establish the correspondence between points in C and \bar{C} based on the “correspondence in the normal”.

Definition 1. We say that points in unperturbed and perturbed trajectories C and \bar{C} are in orthogonal correspondence (correspondence in the normal) if these points are intersections of the indicated geodetics with a surface Π orthogonal to the geodetic C .

It follows from Definition 1 that if P and \bar{P} are arbitrary corresponding points in C and \bar{C} , respectively, then point P is the closest in C to $\bar{P} \in \bar{C}$.

In M^4 , the tentative-particle trajectory (in the particular case of equilibrium) defines a world line whose equation is determined by solving the differential equations

$$\frac{\delta}{\delta s} p^\alpha = E^\alpha, \tag{9}$$

which satisfy certain initial conditions. Here, $p^\alpha = m \frac{dx^\alpha}{ds}$ is the particle momentum, F^α is the force four-

vector, m is the tentative-particle mass, and $\frac{\delta}{\delta s}$ is the operator of covariant differentiation along the line.

Definition 2. Let $\bar{x}^\alpha(s)$ and $x^\alpha(s)$ be coordinates of points \bar{P} and P corresponding in the normal for the perturbed \bar{C} and unperturbed C trajectories and $\bar{u}^\alpha(s)$ and $u^\alpha(s)$ be the four-velocity coordinates at the points \bar{P} and P , respectively. Let $\bar{\bar{u}}^\alpha(s)$ also be a vector $\bar{u}^\alpha(s)$ translated in parallel to its own direction from the point \bar{P} to point P . The unperturbed trajectory C is referred to as

(i) stable in the Joukowski sense if, for every number $\varepsilon > 0$, a number $\delta(\varepsilon) > 0$ can be found such that the following inequalities are fulfilled:

$$|\bar{x}^\alpha(s) - x^\alpha(s)| < \varepsilon, \quad |\bar{\bar{u}}^\alpha(s) - \bar{u}^\alpha(s)| < \varepsilon \quad \forall s > s_0,$$

if

$$|\bar{x}^\alpha(s_0) - x^\alpha(s_0)| < \delta, \quad |\bar{\bar{u}}^\alpha(s_0) - \bar{u}^\alpha(s_0)| < \delta;$$

(ii) unstable in the Joukowski sense if it is not stable in the Joukowski sense;

(iii) asymptotically stable in the Joukowski sense if it is stable in the Joukowski sense and, in addition,

$$|\bar{x}^\alpha(s) - x^\alpha(s)| \longrightarrow 0, \quad |\bar{u}^\alpha(s) - u^\alpha(s)| \longrightarrow 0 \text{ for } s \longrightarrow +\infty.$$

Definition 3. An unperturbed trajectory C is referred to as stable in the Joukowski sense with respect to the trajectory coordinates $x^\alpha(s)$, four-velocity $u^\alpha(s)$, and spin $S^\alpha(s)$ if, for every number $\epsilon > 0$, a number $\delta(\epsilon) > 0$ can be found such that $|\bar{x}^\alpha(s) - x^\alpha(s)| < \epsilon$, $|\bar{u}^\alpha(s) - u^\alpha(s)| < \epsilon$, and $|\bar{S}^\alpha(s) - S^\alpha(s)| < \epsilon \forall s > s_0$ as soon as $|\bar{x}^\alpha(s_0) - x^\alpha(s_0)| < \delta$, $|\bar{u}^\alpha(s_0) - u^\alpha(s_0)| < \delta$, and $|\bar{S}^\alpha(s_0) - S^\alpha(s_0)| < \delta$. If, according to a given ϵ , it is not always possible to find $\delta(\epsilon) > 0$ such that all indicated conditions are satisfied, then the unperturbed motion is referred to as unstable with respect to $x^\alpha(s)$, $u^\alpha(s)$, and $S^\alpha(s)$.

Remark 1. For steady-state differential equations of NCM, the normal correspondence of the trajectory points and inequalities analogous to those of Definition 2 were used as a definition of the trajectory stability in the Joukowski sense [11]. Therefore, Definition 2 is a generalization of the definition of the stability in the Joukowski sense given in [11].

Remark 2. Definitions 2 and 3 relate to different types of exact equations of motion for tentative bodies. In particular, Definition 3 is concerned with the case when there are also equations for the particle spin [12].

In the free-motion case, Eq. (9) determines a geodesic:

$$\frac{\delta}{\delta s} u^\alpha = 0. \tag{10}$$

Here, s is the canonical parameter. Furthermore, we study only geodesics. Let a direction u_0^α be given at a point $x_0^\alpha \in M^4$. Then, Eqs. (10) determine the unperturbed geodesic C . We assume that geodesic C is uniquely determined by the solution to Eqs. (10), which correspond to the initial conditions

$$x^\alpha(s_0) = x_0^\alpha, \quad u^\alpha(s_0) = u_0^\alpha. \tag{11}$$

We also assume that there exists a neighborhood K of the geodesic C in which the theorem of uniqueness and existence for the solutions to Eqs. (10) holds. Under the conditions indicated, a change (as small as is wished) of initial conditions (11) determines a new geodesic \bar{C} in M^4 , which below is referred to as the perturbed geodesic.

The concept of stability in the Joukowski sense is associated with the notion of point closeness in unperturbed and perturbed geodesics, and, hence, it rests on the notion of correspondence between points of the geodesics C and \bar{C} . Let P be an arbitrary point in C and \bar{P} be a point corresponding to P in \bar{C} for the case of

orthogonal correspondence. We now connect P and \bar{P} by a geodesic. This geodesic is unique. Drawing a tangent vector y^α at a point $P \in C$, we can write out with an accuracy to terms higher than the first order of smallness that

$$\bar{x}^\alpha(s) = x^\alpha(s) + y^\alpha(s), \tag{12}$$

where $x^\alpha(s)$ and $\bar{x}^\alpha(s)$ are coordinates of the corresponding points in C and \bar{C} , respectively.

We elucidate the condition under which the geodesics are determined by the functions $x^\alpha(s)$ and $\bar{x}^\alpha(s)$. To do this, we assume that the function y^α is twice differentiable along C . Then, we differentiate (12) twice with respect to \bar{s} and add to both sides of the result obtained the expression

$$\Gamma_{\sigma\tau}^\alpha u^\sigma u^\tau - u^\alpha \frac{d}{ds} \ln \frac{ds}{d\bar{s}}.$$

Here, $\Gamma_{\alpha\tau}^\alpha$ is the Riemannian connectedness in \bar{C} and s is the canonical parameter in \bar{C} . Since \bar{C} is geodesic, we have

$$\ddot{y}^\alpha + \Gamma_{\sigma\tau}^\alpha u^\sigma u^\tau - u^\alpha \dot{\rho} + \dot{u}^\alpha = 0, \tag{13}$$

where $\rho = \ln \frac{ds}{d\bar{s}}$. We now expand $\Gamma_{\sigma\tau}^\alpha$ in the neighborhood of C into a series:

$$\Gamma_{\sigma\tau}^\alpha = \Gamma_{\sigma\tau}^\alpha + \partial_\nu \Gamma_{\sigma\tau}^\alpha y^\nu + \dots \tag{14}$$

Substituting (14) into (13) and taking into account that C is geodesic and s is its canonical parameter, we obtain after simple transformations

$$\frac{\delta^2}{\delta s^2} y^\alpha + R_{\sigma\tau}^\alpha u^\sigma y^\tau u^\mu + \dot{\rho}(u^\alpha + y^\alpha) + F^\alpha(y^\alpha, \dot{y}^\alpha) = 0, \tag{15}$$

where F^α are terms of a higher degree compared to the first one in the quantities involved and $R_{\sigma\tau\mu}^\alpha$ is the curvature tensor for M^4 calculated on the unperturbed geodesic C .

It is easy to see that the unperturbed geodesic C is determined by the zero solution to Eq. (15).

Let \bar{u}^α be a tensor obtained by translating u^α to the corresponding point $P \in C$ along the geodesic connecting these points. The difference

$$z^\alpha = \bar{u}^\alpha - u^\alpha \tag{16}$$

is referred to as the four-velocity perturbation. We also assume that the orders of smallness for y^α and z^α are the same.

For a special case of geodesics, Definition 2 of the stability in the Joukowski sense is formulated as follows.

Definition 4. An unperturbed geodetic C is referred to as ε in the Joukowski sense if, for every number $\varepsilon > 0$, a number $\delta > 0$ exists such that

$$|y^\alpha| < \varepsilon, \quad |z^\alpha| < \varepsilon \quad \forall s > s_0, \quad (17a)$$

if, for $s = s_0$,

$$|y_0^\alpha| < \delta, \quad |z_0^\alpha| < \delta. \quad (17b)$$

Otherwise, the unperturbed geodetic C is referred to as unstable in the Joukowski sense.

Definition 4 is an analog of the stability definition (in the Lyapunov sense) for the zero solution to Eqs. (15) if the translation is such that a system of first-order differential equations in y^α and z^α arises. By virtue of the uniqueness, independent of the translation, the zero initial conditions correspond to the zero solution $y^\alpha = 0$ to system (15) and, consequently, $z^\alpha = 0$. It is worth noting that the definition of stability is the same in the case when unperturbed and perturbed geodetics determine world lines.

We assume that \bar{u}^α is obtained by the Levi-Civita translation [14] of the vector u^α from $\bar{P} \in \bar{C}$ to the corresponding point $P \in C$ along the geodetic connecting P with \bar{P} . Then, from $\delta u^\alpha = 0$, with an accuracy to terms of the first-order of smallness, it follows that

$$u^\alpha(s) = \bar{u}^\alpha(s) - \Gamma_{\sigma\tau}^\alpha y^\sigma u^\tau. \quad (18)$$

From (10) and (18), we have

$$z^\alpha = \frac{\delta}{\delta s} y^\alpha. \quad (19)$$

Relations (10) and (19) are found with an accuracy to the first-order terms of smallness with respect to a perturbation provided that y^α is a vector field along geodetic C . However, these relations can be considered as a substitution of variables, which helps to reduce the order for a system of equations from the second to the first one.

The following theorem holds.

Theorem 1. *Let the quantity z^α be a vector; i.e., it is determined by an invariant translation. Then, the notion of the stability in the Joukowski sense (Definition 2) is invariant with respect to coordinate transformations that satisfy the inequality*

$$\left| \frac{\partial x^{\alpha'}}{\partial x^\alpha} \right| < L. \quad (20)$$

Proof. We show that the orbit C is stable in the Joukowski sense in the new coordinate system if inequality (20) is satisfied. Since z^α is a vector, we find that in the new coordinate system,

$$y^{\alpha'} = \left| \frac{\partial x^{\alpha'}}{\partial x^\alpha} \right| y^\alpha, \quad z^{\alpha'} = \left| \frac{\partial x^{\alpha'}}{\partial x^\alpha} \right| z^\alpha. \quad (21)$$

Passing to absolute values in (21), we arrive at the following estimates:

$$|y^{\alpha'}| \leq \left| \frac{\partial x^{\alpha'}}{\partial x^\alpha} \right| |y^\alpha|, \quad |z^{\alpha'}| \leq \left| \frac{\partial x^{\alpha'}}{\partial x^\alpha} \right| |z^\alpha|.$$

From the property of stability for the unperturbed trajectory C and from inequality (20), it follows that $|y^\alpha| < 4L\varepsilon$ and $|z^\alpha| < 4L\varepsilon \quad \forall s > s_0$ if, for $s = s_0$, the inequalities $|y_0^\alpha| < 4L\delta$ and $|z_0^\alpha| < 4L\delta$ are true.

In the initial coordinate system, by virtue of the C -geodetic stability for a given $\varepsilon > 0$, there exists $\delta_1 > 0$ such that $|y^\alpha| < \frac{1}{4}\varepsilon L^{-1}$, $|z^\alpha| < \frac{1}{4}\varepsilon L^{-1} \quad \forall s > s_0$ if, for $s = s_0$,

the following inequalities are valid: $|y_0^\alpha| < \delta_1$ and $|z_0^\alpha| < \delta_1$.

We now denote $\delta_2 = 4L\delta_1$. Then, for a given number $\varepsilon > 0$, a number $\delta_2 > 0$ can always be found such that $|y^\alpha| < \varepsilon$ and $|z^\alpha| < \varepsilon \quad \forall s > s_0$ if, for $s = s_0$, the following inequalities are fulfilled: $|y_0^\alpha| < \delta_2$ and $|z_0^\alpha| < \delta_2$.

Therefore, the unperturbed geodetic C is stable in the Joukowski sense in the new coordinate system. Thus, the theorem is proved.

Let us call the indicator the norm of the vector $g_{\alpha\beta} u^\alpha u^\beta$. In this case, the following theorem holds.

Theorem 2. *For geodetic C to be stable in the Joukowski sense with respect to the quantities z^α and y^α in the M^4 Riemann manifold, it is necessary and sufficient that geodetic C be stable in the Joukowski sense with respect to perturbations that conserve the indicator sign of the normal vector.*

The proof of the theorem is based on the fact that, for an unperturbed geodetic, the normal-vector indicator is determined by the formula $\bar{\pi} = \pi + \Delta(y^\alpha, y^\alpha)$, where π is the unperturbed-geodetic indicator.

ACKNOWLEDGMENTS

The author is grateful to Academician V.V. Rumyantsev and Professor A.A. Shestakov for their attention to this work.

This study was supported by the Ministry of Education, project no. 020702-2-075.

REFERENCES

1. A. M. Lyapunov, *General Problem on Stability of Motion* (Izd. Kharkov. Mat. O–va, Kharkov, 1892).
2. N. E. Joukovski, Uch. Zap. Mosk. Gos. Univ., Otd. Fiz.-Mat. **4**, 1 (1882).
3. N. G. Chetaev, *Stability of Motion. Papers on Analytical Mechanics* (Akad. Nauk SSSR, Moscow, 1962).

4. V. V. Rumyantsev and A. S. Oziraner, *Stability and Stabilization of Motion with Respect to a Part of Variables* (Nauka, Moscow, 1987).
5. G. N. Duboshin, *Celestial Mechanics. Analytical and Qualitative Methods* (Nauka, Moscow, 1964).
6. V. V. Rumyantsev, *Diff. Uravn.* **19**, 739 (1983).
7. J. L. Synge, *Tensorial Methods in Dynamics* (Univ. of Toronto Press, Toronto, 1936; Inostrannaya Literatura, Moscow, 1947).
8. M. Sh. Aminov, *Tr. Kazan. Aviats. Inst.* **24**, 3 (1949).
9. V. I. Zubov, *Dynamics of Controllable Systems* (Vysshaya Shkola, Moscow, 1982).
10. G. A. Leonov and D. V. Ponomarenko, *Izv. Vyssh. Uchebn. Zaved., Ser. Mat.*, No. 4, 88 (1993).
11. O. V. Dunaeva, *Dokl. Akad. Nauk* **355**, 51 (1997) [*Phys. Dokl.* **42**, 374 (1997)].
12. K. A. Piragas, Doctoral Dissertation in Mathematical Physics (Kiev, 1973).
13. A. P. Ryabushko, *Problem of Stability for Body's Motion in General Relativity Theory* (Vysshaya Shkola, Minsk, 1987).
14. V. A. Brumberg, *Relativistic Celestial Mechanics* (Nauka, Moscow, 1972).
15. A. Z. Petrov, *New Methods in General Relativity Theory* (Nauka, Moscow, 1966).

Translated by V. Tsarev

On the Determination of a Velocity Field for a Perfectly Plastic Flow: The Case of the General Plane Problem

D. D. Ivlev*, L. A. Maksimova*, and R. I. Nepershin**

Presented by Academician A. Yu. Ishlinskiĭ February 28, 2001

Received March 13, 2001

Relations determining the field of displacement velocities in a perfectly plastic body in the state of full plasticity under the Tresca–Saint-Venant condition were considered in papers [1, 2].

This paper presents formulas for displacement velocities in the case of a general plane problem of perfect plasticity [3], when a vector of displacement velocity depends on the coordinates x and y . If the longitudinal displacement velocity w directed along the z -axis is equal to zero, there are known relations for the plane strain [4].

The problem under consideration concerns die indentation into a perfectly plastic half-space with non-zero longitudinal velocity.

1. Taking the tensile–compressive yield stress of the perfectly plastic body as a unit of stress, we write the condition of full plasticity in the space of the principal stresses as

$$\sigma_1 = \sigma_2, \quad \sigma_3 = \sigma_1 + 1. \quad (1.1)$$

Components of the stress tensor that satisfy condition (1.1) can be expressed in terms of both the average stress σ and the functions θ and φ in the form

$$\begin{aligned} \sigma_x &= \sigma - \frac{1}{3} + \frac{1}{2}(1 + \cos\theta)\cos^2\varphi, \\ \sigma_y &= \sigma - \frac{1}{3} + \frac{1}{2}(1 + \cos\theta)\sin^2\varphi, \\ \sigma_z &= \sigma - \frac{1}{3} + \frac{1}{2}(1 - \cos\theta), \\ \sigma &= \frac{1}{3}(\sigma_x + \sigma_y + \sigma_z), \end{aligned} \quad (1.2)$$

$$\tau_{xy} = \frac{1}{2}(1 + \cos\theta)\sin\varphi\cos\varphi,$$

$$\tau_{xz} = \frac{1}{2}\sin\theta\cos\varphi, \quad \tau_{yz} = \frac{1}{2}\sin\theta\sin\varphi.$$

Direction cosines of the principal stress σ_3 with respect to the x -, y -, and z -axes of coordinates are determined by the angles θ and φ as

$$n_1 = \cos\frac{\theta}{2}\cos\varphi, \quad n_2 = \cos\frac{\theta}{2}\sin\varphi, \quad n_3 = \sin\frac{\theta}{2}. \quad (1.3)$$

In the case of a general plane problem, the quantities σ , θ , and φ , as well as the components u , v , and w of the displacement-velocity vector, do not depend on the coordinate z . Substituting the expressions for stresses (1.2) into the equilibrium equations leads to quasilinear differential hyperbolic-type equations for the functions σ , θ , and φ with the three characteristic curves α , β , and γ , as well as to the differential relations

$$\left(\frac{dy}{dx}\right)_{\beta, \alpha} = \tan\left[\varphi \pm \left(\frac{\pi}{4} + \mu\right)\right], \quad \tan 2\mu = \frac{1 - \cos\theta}{2\sqrt{\cos\theta}}, \quad (1.4)$$

$$d\sigma \pm \left(\frac{1 + \cos\theta}{2\sqrt{\cos\theta}}\right)d\varphi = 0 \text{ along } \beta \text{ and } \alpha, \quad (1.5)$$

$$\left(\frac{dy}{dx}\right)_{\gamma} = \tan\varphi, \quad (1.6)$$

$$\left(\frac{2\sin\theta}{1 + \cos\theta}\right)d\sigma + \sin\theta\sin 2\varphi d\varphi + d\theta = 0 \quad (1.7)$$

along γ .

The field of displacement velocities must satisfy the conditions of incompressibility,

$$\frac{\partial u}{\partial x} + \frac{\partial v}{\partial y} = 0, \quad (1.8)$$

and isotropy [1, 2], where, with the use of relations (1.3) for the direction cosines, the latter condition can be

* Yakovlev Chuvash State Pedagogical University,
ul. Dzerzhinskogo 20, Cheboksary, 428000 Russia

** Moscow State Academy
of Instrumentation Engineering and Informatics,
ul. Stromynka 20, Moscow, 107846 Russia

written in the form of the equations

$$2 \frac{\partial u}{\partial x} + \left(\frac{\partial u}{\partial y} + \frac{\partial v}{\partial x} \right) \left(\frac{n_2}{n_1} - \frac{n_1}{n_2} \right) - 2 \frac{\partial v}{\partial y} + \frac{\partial w n_3}{\partial x n_1} - \frac{\partial w n_3}{\partial y n_2} = 0, \tag{1.9}$$

$$2 \frac{\partial u}{\partial x} + \left(\frac{\partial u}{\partial y} + \frac{\partial v}{\partial x} \right) \frac{n_2}{n_1} + \frac{\partial w}{\partial x} \left(\frac{n_3}{n_1} - \frac{n_1}{n_3} \right) - \frac{\partial w n_2}{\partial y n_3} = 0. \tag{1.10}$$

The system of equations (1.8)–(1.10) in the unknown displacement velocities u , v , and w is of the hyperbolic type and has the three characteristic curves from (1.4) and (1.6). Differential relations for du , $d\mathbf{v}$,

and dw , which are valid along the characteristic curves, are derived by using the characteristic determinant of the system. These relations are

$$du + \left(\frac{dy}{dx} \right)_{\alpha, \beta, \gamma} d\mathbf{v} - f_{\alpha, \beta, \gamma} dw = 0, \tag{1.11}$$

$$f_{\alpha, \beta, \gamma} = \frac{n_3(1 - 2n_2^2)}{n_1(1 - 2n_1^2) + n_2(1 - 2n_2^2)} \left(\frac{dx}{dy} \right)_{\alpha, \beta, \gamma}. \tag{1.12}$$

For the characteristic curves α and β , which are determined by the differential equations (1.4), formulas (1.3) for the direction cosines n_1 , n_2 , and n_3 allow function (1.12) to be expressed in terms of the angles θ and φ as

$$f_{\alpha, \beta} = \frac{\tan \frac{\theta}{2} \cos \theta}{\cos \varphi (1 - (1 + \cos \theta) \cos^2 \varphi) + \sin \varphi (1 - (1 + \cos \theta) \sin^2 \varphi)} \left(\frac{dx}{dy} \right)_{\alpha, \beta}. \tag{1.13}$$

For the characteristic curve γ , using Eqs. (1.3), (1.6), and (1.12) turns the differential relation (1.11) into

$$\tan \theta (du \cos \varphi + d\mathbf{v} \sin \varphi) - dw = 0 \text{ along } \gamma. \tag{1.14}$$

At $\theta = 0$, Eqs. (1.4) and (1.5) determine the orthogonal characteristic curves of plane strain and Hencky's relations for the stress field. In the case of plane strain, the longitudinal flow velocity $w = 0$ and the differential relations (1.11) for the displacement velocities u and \mathbf{v} express the condition of characteristic-curve orthogonality in the physical (x, y) and hodograph (u, \mathbf{v}) planes according to Geiringer's equations.

The condition $0 < \theta < \frac{\pi}{2}$ corresponds to the general plane strain when the characteristic curves α and β (1.4) are not orthogonal and have the characteristic curve γ (1.6) as a bisector of the angle between them.

For the general plane strain, the problem of constructing fields of stresses and displacement velocities is statically determinate. First, Eqs. (1.4)–(1.7) should be used to determine the fields of characteristic curves and stresses at specified boundary conditions for the functions σ , θ , and φ . Then, once the functions θ and φ used in the differential relations (1.11)–(1.14) are already known, the field of displacement velocities can be constructed at specified kinematic boundary conditions.

In the plastic region, the rate of energy dissipation must be positive so that

$$D = \sigma_1 \varepsilon_1 + \sigma_2 \varepsilon_2 + \sigma_3 \varepsilon_3 \geq 0, \tag{1.15}$$

where ε_1 , ε_2 , and ε_3 are the principal strain rates. Under the condition of full plasticity (1.1), inequality (1.15) takes the form $\varepsilon_3 > 0$. In the case of calculating displacement velocities, this inequality is convenient for check along the characteristic curve γ . Under the assumption that $\varphi = 0$ in (1.3), the relation for ε_3 takes the form

$$\varepsilon_3 = \cos \frac{\theta}{2} \left(\frac{d\mathbf{v}_\gamma}{ds} \cos \frac{\theta}{2} + \frac{dw}{ds} \sin \frac{\theta}{2} \right), \tag{1.16}$$

where \mathbf{v}_γ is the projection of the velocities u and \mathbf{v} onto the direction of the characteristic curve γ . The associated plastic-flow rule for edge (1.1) of the Tresca prism leads to the following inequalities for the other two principal strain rates [4]:

$$\varepsilon_1 \leq 0, \quad \varepsilon_2 \leq 0. \tag{1.17}$$

2. We now consider the problem of flat-die indentation into the rigid-plastic half-space (Fig. 1). If the die length in the longitudinal direction (along the z -axis) exceeds considerably its width in the transverse direction (along the x -axis), indentation and longitudinal slip of the rough die are accompanied by the onset of plastic general plane-strain flow in the cross sections $z = \text{const}$. The die width and the magnitude of velocity of its translational oblique (to the normal to the half-space boundary) motion are taken as scales of length and velocity, respectively.

The direction of the die velocity is defined by the angles λ and ψ , which determine the velocities of die

plastic-region velocities at the rigid-plastic boundary *ODBC*:

$$u = [v]_{\alpha} \cos \xi, \quad v = [v]_{\alpha} \sin \xi, \quad w = 0. \quad (2.9)$$

Thus, having calculated the characteristic-curve and stress fields, we determine the boundary conditions for velocities (2.9) at the rigid-plastic boundary. Together with condition (2.7) specified at the die boundary, they allow calculation of the velocity field in the plastic region through integration of the differential relations (1.11)–(1.14) for displacement velocities.

In the case of plane strain [$\theta \equiv 0$ and $\psi = 0$ in kinematic condition (2.1)], it is possible to obtain a simple exact analytic solution to the problem by using Hencky's and Geiringer's equations. Below, we discuss a numerical solution to the equations of the general plane strain, which, as $\theta \rightarrow 0$ and $\psi \rightarrow 0$, turns into the exact solution to the plane-strain problem.

3. The characteristic-curve and stress fields are calculated by integrating the differential relations (1.7)–(1.14) for the functions σ , φ , and θ with the boundary conditions (2.2)–(2.5). At regular nodes of the mesh of the characteristic curves, which do not belong to the singular point *A* and the die boundary *OA*, we solve the elementary Cauchy problem for the functions σ , φ , and θ known at points *1* and *2* of the Cauchy contour (Fig. 2). To find the solution, the functions φ and θ are approximated by their average values calculated along the characteristic curves and the differentials entering Eqs. (1.3)–(1.6) are substituted by the finite differences. The coordinates x , y of point *P* satisfy three differential equations of the characteristic curves, which, in the case of the finite-difference approximation, have the form

$$\frac{y - y_1}{x - x_1} = \tan \left[\varphi - \left(\frac{\pi}{4} + \mu \right) \right] \text{ in } \alpha, \quad (3.1)$$

$$\frac{y - y_2}{x - x_2} = \tan \left[\varphi + \left(\frac{\pi}{4} + \mu \right) \right] \text{ in } \beta, \quad (3.2)$$

$$\frac{y - y_3}{x - x_3} = \tan \varphi \text{ in } \gamma. \quad (3.3)$$

Unknown coordinates of point *3* are found as the coordinates of intersection of the characteristic curve γ with the Cauchy contour, which is approximated by the chord connecting points *1* and *2*, and, therefore, satisfy the equation

$$\frac{y_3 - y_1}{x_3 - x_1} = \frac{y_2 - y_1}{x_2 - x_1}. \quad (3.4)$$

When the coordinates of point *3* are known, the values of the functions σ , φ , and θ at this point are calculated by linearly interpolating these functions between points *1* and *2*.

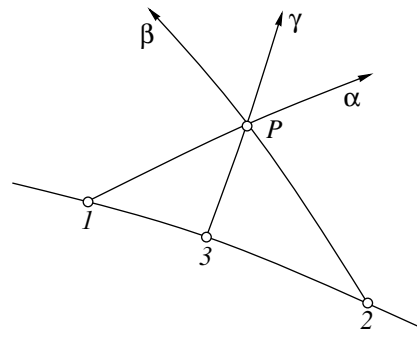


Fig. 2.

The differential relations along the characteristic curves are written in the form

$$\sigma - \sigma_1 = \left(\frac{1 + \cos \theta}{2\sqrt{\cos \theta}} \right) (\varphi - \varphi_1) \text{ in } \alpha, \quad (3.5)$$

$$\sigma - \sigma_2 = - \left(\frac{1 + \cos \theta}{2\sqrt{\cos \theta}} \right) (\varphi - \varphi_1) \text{ in } \beta, \quad (3.6)$$

$$\theta_3 - \theta = \left(\frac{2 \sin \theta}{1 + \cos \theta} \right) (\sigma - \sigma_3) \quad (3.7)$$

$$+ \sin \theta \sin 2\varphi (\varphi - \varphi_3) \text{ in } \gamma,$$

where σ_1 , σ_2 , and σ_3 represent the values of σ at points *1*, *2*, and *3*.

Equations (3.1)–(3.7) in the unknowns presented through the coordinates of point *P*, the functions σ , φ , and θ there, and the coordinates of point *3* are solved by simple iterations. Known values of the angles φ and θ at points *1* and *2* are used to calculate x and y from Eqs. (3.1) and (3.2). The values of σ and φ at point *P* are then determined from Eqs. (3.5) and (3.6). Coordinates of point *3* are calculated from Eqs. (3.3) and (3.4), while values of σ , φ , and θ occurring there are found through linear interpolation between points *1* and *2*. Equation (3.7) is used to calculate θ at point *P*. The calculations are repeated with the use of average values of the angles φ and θ along the characteristic curves connecting points *1*–*P*, *2*–*P*, and *3*–*P*. Absolute differences of successive values of φ and θ calculated at point *P* reach the order of magnitude of 10^{-5} after two–three iterations performed almost instantly on a Pentium-133.

In the region *ABD* (Fig. 1), the field of the characteristic curves is determined by solving the Goursat problem, where the functions σ , φ , and θ are known in the β -type characteristic curve *AB* and at the singular point *A*, while the regular nodes of the mesh formed by the characteristic curves are calculated using Eqs. (3.1)–(3.7). Then, in the region *OAD*, we solve the mixed problem with the functions σ , φ , and θ known in the β -type characteristic curve *AD* and with boundary conditions specified at *OA*. Since φ and θ at *OA* are specified by boundary conditions (2.2), the coordinates x and values of σ

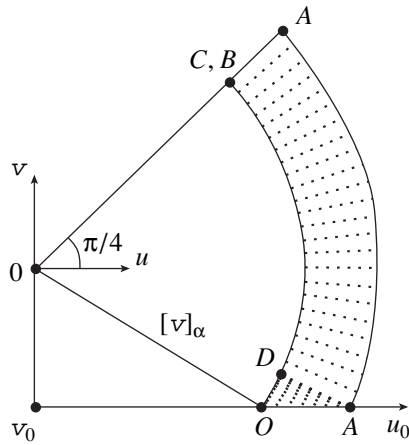


Fig. 3.

at the nodes situated there are calculated using the linear equations (3.1) and (3.5).

In the region $OABD$, the field of the characteristic curves is determined accurate to an unknown length L of the characteristic curve AB . This length is calculated from the condition that the coordinate x_0 of point O is equal to zero. An algorithm for constructing the field of the characteristic curves determines x_0 as a continuous function of the parameters L , which satisfies the condition

$$x_0(L) = 0. \tag{3.8}$$

Equation (3.8) is solved using the iterative Newton method, where the derivative is approximated by a finite-difference ratio and the plane-strain length L of the boundary AC is taken as the initial approximation. In two–three steps, the iterative Newton process makes solutions to Eq. (3.8) to be accurate to the order of 10^{-6} . For a pair of values φ^* and θ^* specified at boundary OA , the calculation of characteristic-curve and stress fields takes about 1 s on a Pentium-133. This fact reveals the high efficiency of the numerical algorithms for solving the hyperbolic problems of perfect-plasticity theory [5].

For the shearing forces $P_x = 0.269$ and $P_z = 0.159$, Fig. 1 shows the field of the characteristic curves and the normal stress distribution along the die boundary calculated at $\theta^* = 1$ and $\varphi^* = 0.388$. Being almost constant, the pressure applied to the die increases slightly near the singular point A . The indentation force $P_y = 2.075$. When the magnitude of the contact shearing force $P_{xz} = \sqrt{P_x^2 + P_y^2}$ approaches its limiting value $\frac{1}{2}$, the characteristic-curve field degenerates into a line that coincides with the die boundary. The case $\varphi = \frac{\pi}{2}$ and $\theta \rightarrow \frac{\pi}{2}$ corresponds to longitudinal die shear along

the z -axis at $P_x = 0$ and $P_z = \frac{1}{2}$. Then, according to Eqs. (2.5) and (1.2), $\sigma = -\frac{2}{3}$, $\sigma_y = -\frac{1}{2}$, and $\sigma_z = -\frac{1}{2}$. This is the case of pure shear at the minimum pressure applied to the die, for which

$$P_y = \frac{1}{2}, \quad P_x = 0, \quad P_z = \frac{1}{2} \quad \text{at } \varphi = \theta = \frac{\pi}{2}. \tag{3.9}$$

Thus, variation in the shearing forces changes the limiting pressure applied to the die from its maximum value $1 + \frac{\pi}{2}$, which corresponds to a smooth Prandtl die, to the minimum value $\frac{1}{2}$, which corresponds to the pure longitudinal shear of an absolutely rough die.

The calculated field of the characteristic curves determines the kinematic boundary conditions (2.9) at the rigid-plastic boundary $ODBC$ (Fig. 1). Together with the boundary condition (2.7) specified at the die boundary, these conditions allow construction of the field of displacement velocities through solving both the mixed problem for Eqs. (1.11)–(1.14) in the region OAD and the Goursat problem in the region ADB . According to the calculations, $\theta = 0$ both at boundary AB and in the region ABC , $f_{\alpha, \beta} = 0$ in (1.13) and equations (1.11) turn into Geiringer’s equations. The velocities u and v occurring in the region ABC are constant along the characteristic curves α , while the velocities w do not vary along the characteristic curves γ according to Eq. (1.14) at $\theta = 0$.

The elementary Cauchy problem for Eqs. (1.11) and (1.14) approximated using finite differences leads to the following system of linear equations in the velocities u , v , and w :

$$(u - u_1) + (v - v_1) \left(\frac{dy}{dx} \right)_\alpha - (w - w_1) f_\alpha = 0, \tag{3.10}$$

$$(u - u_2) + (v - v_2) \left(\frac{dy}{dx} \right)_\beta - (w - w_2) f_\beta = 0, \tag{3.11}$$

$$\begin{aligned} & \tan \theta ((u - u_3) \cos \varphi \\ & + (v - v_3) \sin \varphi) - (w - w_3) = 0. \end{aligned} \tag{3.12}$$

where the unknowns are calculated at the regular nodes P of the mesh formed by the characteristic curves (Fig. 2) and the velocities used in the calculations are specified on the Cauchy contour $1-3-2$.

Coefficients of the system of equations (3.10)–(3.12) are calculated with the use of the angles θ and φ averaged along the characteristic curves $1-P$, $2-P$, and $3-P$, which are known as a result of solving the system of equations (3.1)–(3.7). At the mesh nodes formed by the characteristic curves at the die boundary, the velocity v is specified by boundary condition (2.7), while the

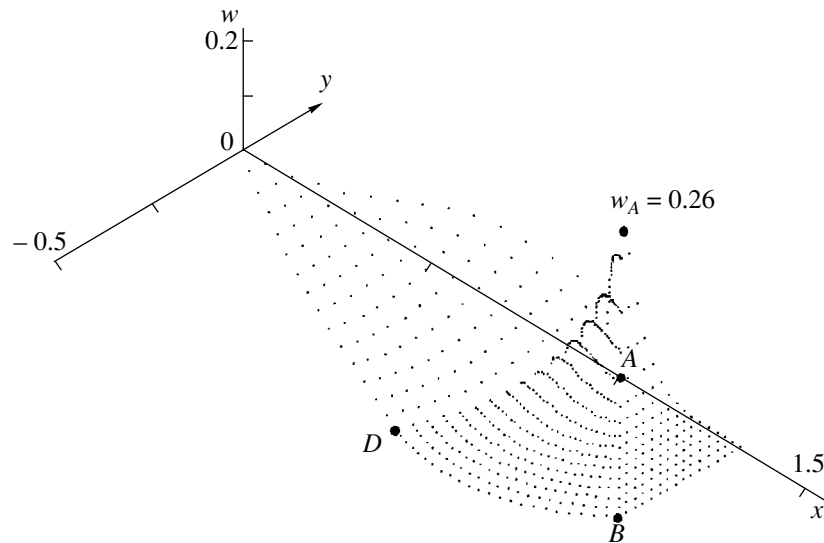


Fig. 4.

velocities u and w there are found by using Eqs. (3.11) and (3.12) to solve the mixed problem for the velocities.

Figure 3 presents the field of the displacement velocities u , v in the hodograph plane. It corresponds to the characteristic-curve field shown in Fig. 1 and to the oblique die indentation with velocities $u_0 = 0.833$, $v_0 = -0.315$, and $w_0 = 0.455$. In contrast to the plane strain, the longitudinal shear is accompanied by a nonuniform velocity distribution in the region OAD situated under the die and along the characteristic curves β , which converge to the singular point A in the region of the centered fan ABD . In the region of the uniform stressed state ABC , the velocity field turns out to be nonuniform with the velocities u and v decreasing along boundary AC .

For the characteristic-curve field plotted in Fig. 1, Fig. 4 shows the distribution of the longitudinal velocity w as an isometric projection of the surface $w(x, y)$. The velocity w is positive and increases in the directions from the rigid-plastic boundary ODB to the die boundary OA and to the singular point A , at which it has a polar singularity and takes a maximum value equal to $w_A = 0.26$. The plastic material is pulled by the longitudinal stress of the contact friction in the direction of die slip. However, the velocity w of the plastic material is

lower than the longitudinal velocity of die motion $w_0 = 0.455$, and, therefore, the energy dissipation caused by the longitudinal friction forces is positive. In the region of the uniform plane stressed state occurring from the right of boundary AB , $\theta = 0$ and the differential relation (1.14) yields that $w = \text{const}$ along the straight characteristic curves γ parallel to the y -axis.

For the presented field of displacement velocities, the dissipation of energy of the plastic flow is positive.

REFERENCES

1. A. Yu. Ishlinskiĭ, *Applied Problems of Mechanics* (Nauka, Moscow, 1986), Vol. 1, pp. 62–83.
2. D. D. Ivlev, Dokl. Akad. Nauk SSSR **124**, 546 (1959) [Sov. Phys. Dokl. **4**, 217 (1959)].
3. D. D. Ivlev and L. A. Maksimova, Dokl. Akad. Nauk **373**, 39 (2000) [Dokl. Phys. **45**, 330 (2000)].
4. D. D. Ivlev, *Theory of Perfect Plasticity* (Nauka, Moscow, 1966).
5. D. D. Ivlev and A. Yu. Ishlinskiĭ, Dokl. Akad. Nauk **368**, 333 (1999) [Dokl. Phys. **44**, 642 (1999)].

Translated by Yu. Verevchkin

Features of the Thermocapillary Drift for a Heated Droplet in a Viscous Fluid Placed into an Electromagnetic Field

Yu. I. Yalamov*, N. V. Malaĭ**, and E. R. Shchukin***

Presented by Academician R.F. Ganiev December 20, 2000

Received February 9, 2001

Study of the motion of a droplet in an electromagnetic field is an important and urgent problem [1, 2]. This motion is caused by a nonuniform distribution of temperature along the droplet surface. In this case, additional tangential stresses appear owing to the temperature dependence of the droplet surface-tension coefficient; these stresses are responsible for the ordered motion of the droplet. The nonuniform distribution of temperature can be induced by various factors, for example, by an external constant gradient of temperature [3, 4], a chemical reaction on the droplet surface [5], the presence of surface-active substances in a fluid [6], etc. If the droplet moves due to the nonuniform distribution of inner heat sources, this motion is called photophoretic [7].

In the past few years, interest in the droplet motion for considerable temperature drops in their neighborhood has grown [8–10]. In this paper, in contrast to previous studies, we took into account the exponential temperature dependence of the coefficient of dynamic viscosity in the thermocapillary drift of a droplet and the influence of fluid motion on the temperature distribution.

The analysis carried out in this work showed that, along with the temperature dependence of the coefficient of dynamic viscosity, the convective transport can also substantially influence the thermocapillary drift of droplets heated by inner heat sources. In particular, it was shown that, if the droplets absorb radiation as a blackbody, two qualitatively different motions of the particle are possible: in the direction of propagation of radiation and in the opposite direction. This circumstance is caused by a marked influence of the convective motion of fluid (large Prandtl numbers) on the angular nonuniformity of the temperature distribution

in the neighborhood of a droplet for significant radial temperature drops.

PROBLEM FORMULATION

We consider the steady motion of a nonuniformly heated spherical droplet of radius R , density ρ_i , and heat conductivity λ_i in an immiscible viscous incompressible fluid with a density ρ_e and a heat conductivity λ_e filling the whole space. The fluid is at rest at infinity. As a heated particle, we understand that the particle's mean surface temperature considerably exceeds the environment temperature.

The heated surface of the droplet can have a substantial effect on the thermal characteristics of the environment and, thus, on the distribution of velocity fields and pressure in its neighborhood.

Among the parameters of fluid transport, only the viscosity coefficient depends strongly on temperature. Taking the temperature dependence of viscosity into account, we used formula (1) proposed in [3] (for $F_n = 0$, this formula can be reduced to the Reynolds formula [11]):

$$\mu_e = \mu_\infty \left[1 + \sum_{n=1}^{\infty} F_n \left(\frac{T_e}{T_\infty} - 1 \right)^n \right] \exp \left\{ -A \left(\frac{T_e}{T_\infty} - 1 \right) \right\}. \quad (1)$$

Here, A and F_n are constants, T_∞ is the temperature of the fluid far from the heated droplet, $\mu_\infty = \mu_e(T_\infty)$; hereafter, the subscripts e and i refer to the external fluid and the droplet, respectively.

The fluid viscosity is known to decrease with temperature according to the exponential law [11]. Analysis of the available semiempirical formulas showed that expression (1) makes it possible to best describe the change in viscosity in a wide range of temperatures with an arbitrary desired accuracy. For illustration, we list in Table 1 the values of F_n for water ($A = 5.779$, $F_1 = -2.318$, $F_2 = 9.118$, and $T_\infty = 273$ K); μ_{calcd} is the dynamic viscosity calculated from formula (1) and μ_{expt} is the experimental value of the dynamic viscosity. The relative error is less than 2%.

* Moscow Pedagogical University,
ul. Radio 10a, Moscow, 105007 Russia

** Belgorod State University, Belgorod, Russia

*** Institute of High Temperatures Scientific Association
(IVTAN), Russian Academy of Sciences,
Izhorskaya ul. 13/19, Moscow, 127412 Russia

The heat-conductivity coefficient of a droplet is assumed to considerably exceed the heat-conductivity coefficient of the medium; the density (ρ), heat capacity (c_p), and heat conductivity (λ) are considered to be constant values; droplet motion is reasonably slow (small Peclet and Reynolds numbers); the surface-tension coefficient σ is an arbitrary function of temperature [$\sigma = \sigma(T)$]; and the droplet is assumed to retain its spherical shape (this assumption is valid under the condition $\frac{\mu_e U}{R} \ll \frac{\sigma}{R}$, where U is the droplet drift velocity [12]).

It is convenient to introduce a reference system related to the center of the moving droplet. In this case, the problem is reduced to analysis of the steady flow around the droplet by a homogeneous fluid whose velocity at infinity (\mathbf{U}_∞) is to be defined ($\mathbf{U}_\infty = -\mathbf{U}$).

In terms of the above assumptions describing this flow, the dimensionless conservation equations and boundary conditions can be reduced to the form [12]

$$\eta_i \Delta \mathbf{V}_i = \nabla p_i, \quad \text{div} \mathbf{V}_i = 0, \quad \eta = \frac{\mu}{\mu_\infty}; \quad (2)$$

$$\nabla p_e = \eta_e \Delta \mathbf{V}_e + 2(\nabla \eta_e \nabla) \mathbf{V}_e + [\nabla \eta_e \times \text{rot} \mathbf{V}_e], \quad \text{div} \mathbf{V}_e = 0; \quad (3)$$

$$\text{Re}_\infty \text{Pr}_\infty (\mathbf{V}_e \nabla) t_e = \Delta t_e, \quad \Delta t_i = -\frac{q_i R^2}{\lambda_i T_\infty}; \quad (4)$$

$$y = 1, \quad \lambda_i \frac{\partial t_i}{\partial y} = \lambda_e \frac{\partial t_e}{\partial y}, \quad V_r^e = V_r^i = 0, \quad V_\theta^e = V_\theta^i,$$

$$\begin{aligned} \mu_e \left[\frac{\partial V_\theta^e}{\partial y} + \frac{1}{y} \frac{\partial V_r^e}{\partial \theta} - \frac{V_\theta^e}{y} \right] + \frac{1}{y U_\infty} \frac{\partial \sigma}{\partial t_i} \frac{\partial t_i}{\partial \theta} \\ = \mu_i \left[\frac{\partial V_\theta^i}{\partial y} + \frac{1}{y} \frac{\partial V_r^i}{\partial \theta} - \frac{V_\theta^i}{y} \right]; \end{aligned} \quad (5)$$

$$y \rightarrow \infty, \quad \mathbf{V}_e \rightarrow \cos \theta \mathbf{e}_r - \sin \theta \mathbf{e}_\theta, \quad t_e \rightarrow 1, \quad p_e \rightarrow 1; \quad (6)$$

$$y \rightarrow 0, \quad |\mathbf{V}_i| \neq \infty, \quad t_i \neq \infty, \quad p_i \neq \infty. \quad (7)$$

Here, V_r and V_θ are the radial and tangential components of the mass velocity, while \mathbf{e}_r and \mathbf{e}_θ are the unit vectors in the spherical system of coordinates, respectively; $y = \frac{r}{R}$ is the dimensionless radial coordinate;

$\text{Re}_\infty = \frac{\rho_e U_\infty R}{\mu_\infty}$ and $\text{Pr}_\infty = \frac{\mu_\infty c_p}{\lambda_e}$ are the Reynolds and Prandtl numbers, respectively; and $U_\infty = |\mathbf{U}_\infty|$.

Table 1

| T, K | $\mu_{\text{calcd}}, \text{Pa s}$ | $\mu_{\text{expt}}, \text{Pa s}$ | $\frac{ \mu_{\text{calcd}} - \mu_{\text{expt}} }{\mu_{\text{calcd}}} \times 100, \%$ |
|---------------|-----------------------------------|----------------------------------|--|
| 279 | 0.0017525 | 0.0017525 | 0.00 |
| 293 | 0.0010089 | 0.0010015 | 0.74 |
| 313 | 0.0006433 | 0.0006513 | 1.22 |
| 333 | 0.0004581 | 0.0004630 | 1.06 |
| 353 | 0.0003556 | 0.0003509 | 1.35 |
| 363 | 0.0003199 | 0.0003113 | 2.76 |

The variables are made dimensionless by using the following characteristic values: R (the droplet radius), $T_\infty, P_\infty, \mu_\infty$, and U_∞ ($t = \frac{T}{T_\infty}, p = \frac{P}{P_\infty}$, and $\mathbf{V} = \frac{\mathbf{U}}{U_\infty}$).

For $\text{Re}_\infty \ll 1$, the incoming flow exerts only a perturbing action. Therefore, the solution to the equations of hydrodynamics and heat transfer can be sought in the form

$$\begin{aligned} \mathbf{V} &= \mathbf{V}^{(0)} + \text{Re}_\infty \mathbf{V}^{(1)} + \dots, \\ p &= p^{(0)} + \text{Re}_\infty p^{(1)} + \dots, \\ t &= t^{(0)} + \text{Re}_\infty t^{(1)} + \dots \end{aligned} \quad (8)$$

When finding the force acting on a nonuniformly heated droplet and its thermocapillary-drift velocity, we restrict our consideration to first-order corrections with respect to Re_∞ .

The form of boundary conditions (5)–(7) makes it possible to seek the solution as follows:

$$\begin{aligned} V_r^{(0)} &= G(y) \cos \theta, \quad V_\theta^{(0)} = -g(y) \sin \theta, \\ p^{(0)} &= 1 + h(y) \cos \theta. \end{aligned} \quad (9)$$

Taking into account the inequality $\lambda_e \ll \lambda_i$, we can ignore the dependence of the coefficient of dynamic viscosity on the angle θ in the droplet–fluid system and assume that $\mu_e(t_e(y, \theta)) = \mu_e(t_e^{(0)})$. Using this fact and substituting (8), (9) into Eqs. (2)–(4), we make sure that the variables are separated and obtain, as a result, linear partial differential equations for perturbed values. In finding the distribution of temperature in the vicinity of a heated droplet, we used the method of joining asymptotic expansions [8]. As a result, the following expressions were obtained for the velocity fields and the temperatures outside and inside a particle:

$$V_r^e(y, \theta) = \cos \theta (1 + A_1 G_1 + A_2 G_2),$$

$$V_6^e(y, \theta) = -\sin\theta(1 + A_1G_3 + A_2G_4),$$

$$V_i^j(y, \theta) = \cos\theta(A_3 + A_4y^2),$$

$$V_6^i(y, \theta) = -\sin\theta(A_3 + 2A_4y^2),$$

$$t_e(y, \theta) = t_e^{(0)} + \text{Re}_\infty t_e^{(1)}, \quad t_i(y, \theta) = t_i^{(0)} + \text{Re}_\infty t_i^{(0)},$$

where

$$G_1 = -\frac{1}{y^3} \sum_{n=0}^{\infty} \frac{\Delta_n^{(1)}}{(n+3)y^n}, \quad G_3 = G_1 + \frac{y}{2}G_1^I,$$

$$G_4 = G_2 + \frac{y}{2}G_2^I,$$

$$G_2 = -\frac{1}{y} \sum_{n=0}^{\infty} \frac{\Delta_n^{(2)}}{(n+1)y^n}$$

$$-\frac{\alpha}{y^3} \sum_{n=0}^{\infty} \left[(n+3) \ln \frac{1}{y} - 1 \right] \frac{\Delta_n^{(1)}}{(n+3)^2 y^n},$$

$$t_e^{(1)}(y, \theta) = \frac{\omega}{2y}(1-y) + \left\{ \frac{\Gamma}{y^2} + \omega \sum_{k=1}^3 A_k \tau_k \right\} \cos\theta,$$

$$t_e^{(0)}(y) = 1 + \frac{\gamma}{y},$$

$$t_i^{(0)}(y) = B_0 + \frac{1}{4\pi R T_\infty \lambda_i y} \int_V q_i dV + \int_1^y \frac{\Psi_0}{y} dy - \frac{1}{y} \int_1^y \Psi_0 dy,$$

$$\omega = \gamma \text{Pr}_\infty, \tag{10}$$

$$t_i^{(1)}(y) = By + \frac{1}{4\pi R^2 T_\infty \lambda_i y^2} \int_V q_i z dV$$

$$+ \frac{1}{3} \left[y \int_1^y \frac{\Psi_1}{y^2} dy - \frac{1}{y^2} \int_1^y \Psi_1 y dy \right],$$

$$\tau_1(y) = -\frac{1}{y^3} \sum_{n=0}^{\infty} \frac{\Delta_n^{(1)}}{(n+1)(n+3)(n+4)y^n},$$

$$\tau_3 = \frac{1}{2}, \quad A_3 = 1,$$

$$\tau_2(y) = -\frac{1}{y} \left\{ -\frac{1}{2} + \frac{\Delta_1^{(2)}}{6y} \ln y - \sum_{n=2}^{\infty} \frac{\Delta_n^{(2)}}{(n^2-1)(n+2)y^n} \right.$$

$$\left. -\frac{\alpha}{y^2} \sum_{n=0}^{\infty} \left[(n+1)(n+3)(n+4) \ln \frac{1}{y} - 3n^2 - 16n - 19 \right] \times \frac{\Delta_n^{(1)}}{(n+1)^2(n+3)^2(n+4)^2 y^n} \right\},$$

$$\Psi_n(y) = -\frac{R^2}{\lambda_i T_\infty} y^2 \frac{2n+1}{2} \int_{-1}^{+1} q_i P_n(\cos\theta) d(\cos\theta),$$

$P_n(\cos\theta)$ are the Legendre polynomials, $\gamma = t_s - 1$, $t_s = \frac{T_s}{T_\infty}$, and T_s is the mean temperature of the heated droplet surface determined by the formula

$$\frac{T_s}{T_\infty} = 1 + \frac{1}{4\pi R \lambda_i T_\infty} \int_V q_i dV. \tag{11}$$

In (10), G_k^I , G_k^{II} , and G_k^{III} are the first, second, and third derivatives of the corresponding functions with respect to y ($k = 1, 2$). The values of the coefficients $\Delta_n^{(1)}$ and $\Delta_n^{(2)}$ can be obtained using the following recurrence relations:

$$\Delta_n^{(1)} = -\frac{1}{n(n+5)} \sum_{k=1}^n [(n+4-k)$$

$$\times \{ \alpha_k^{(1)}(n+5-k) - \alpha_k^2 \} + \alpha_k^{(3)}] \gamma^k \Delta_{n-k}^{(1)} \quad (n \geq 1),$$

$$\Delta_n^{(2)} = -\frac{1}{(n+3)(n-2)} \left[-6\alpha_n^{(4)} \gamma^n \tag{12}$$

$$+ \sum_{k=1}^n \{ (n+2-k)[(n+3-k)\alpha_k^{(1)} - \alpha_k^{(2)}] + \alpha_k^{(3)} \} \gamma^k \Delta_{n-k}^{(2)}$$

$$+ \alpha \sum_{k=0}^n \{ (2n+5-2k)\alpha_k^{(1)} - \alpha_k^{(2)} \} \gamma^k \Delta_{n-k-2}^{(1)} \quad (n \geq 3).$$

When calculating the coefficients $\Delta_n^{(1)}$ and $\Delta_n^{(2)}$ from formulas (12), it is necessary to take into account the following equalities:

$$\Delta_0^{(1)} = -3, \quad \Delta_0^{(2)} = -1, \quad \Delta_2^{(2)} = 1, \quad \alpha_0^{(3)} = -4,$$

$$\alpha_n^{(1)} = F_n, \quad \alpha_0^{(2)} = 4, \quad \alpha_0^{(1)} = \alpha_0^{(4)} = 1,$$

$$\alpha_n^{(2)} = (4-n)F_n + AF_{n-1}, \quad \alpha_n^{(4)} = \frac{A^n}{n!},$$

$$\alpha = -\frac{\gamma}{15}\{[3(4\alpha_1^{(1)} - \alpha_1^{(2)}) + \alpha_1^{(3)}]\Delta_1^{(2)} - [2(3\alpha_2^{(1)} - \alpha_2^{(2)}) + \alpha_2^{(3)}]\gamma - 6\alpha_2^{(4)}\gamma\},$$

$$\alpha_n^{(3)} = 2AF_{n-1} - 2(2+n)F_n,$$

$$\Delta_1^{(2)} = -\frac{\gamma}{4}[6\alpha_1^{(4)} + 2(3\alpha_1^{(1)} - \alpha_1^{(2)}) + \alpha_1^{(3)}].$$

The integration constants $A_1, A_2, A_3, A_4, B_0, B$, and Γ are determined from the corresponding boundary conditions on the droplet surface.

Our prime interest is the solution for the asymmetric part of perturbed values, which will enable us to determine the force and velocity of the thermocapillary-drift. For this purpose, we specify the nature of the thermal sources. The heating of a particle is assumed to take place through the absorption of electromagnetic radiation, and the droplet absorbs the radiation as a blackbody. In this case, the radiation is absorbed in a thin layer of thickness $\delta R \ll R$ adjoining the heated area of the particle surface. The thermal-source density within the layer of thickness δR is determined from the following formula:

$$q_i(r, \theta) = \begin{cases} -\frac{I}{\delta R} \cos \theta, & \frac{\pi}{2} \leq \theta \leq \pi, \quad R - \delta R \leq r \leq R \\ 0, & 0 \leq \theta \leq \frac{\pi}{2}, \end{cases}$$

where I is the incident radiation intensity.

The expression for the total force acting on the particle is obtained by integrating the stress tensor over the droplet surface. This expression is made up of the viscous force \mathbf{F}_μ and the force \mathbf{F}_{ph} , whose appearance is caused by the nonuniformity of the distribution of thermal-source density in the body of the particle with allowance for the convective terms in the heat-conductivity equation. In the general case, these expressions can be represented in the form

$$\mathbf{F} = \mathbf{F}_\mu + \text{Re}_\infty \mathbf{F}_{\text{ph}}, \quad (13)$$

where

$$\mathbf{F}_\mu = 6\pi R \mu_\infty U_\infty f_\mu \mathbf{e}_z, \quad \mathbf{F}_{\text{ph}} = -6\pi R \mu_\infty f_{\text{ph}} \mathbf{e}_z,$$

$$f_\mu = \frac{2}{3\Delta} \left(N_3 + \frac{\mu_e^s}{3\mu_i^s} N_4 \right) \exp\{-A\gamma\},$$

$$\delta = 1 + 2 \frac{\lambda_e^s}{\lambda_i^s}, \quad V = \frac{4}{3} \pi R^3,$$

$$\Delta = N_1 + \frac{\mu_e^s}{3\mu_i^s} - \frac{2\rho_e \omega \lambda_e^s}{3\mu_i^s \delta \mu_\infty \lambda_i^s} (G_1 \Phi_2 - G_2 \Phi_1) \frac{\partial \sigma}{\partial t_i},$$

$$\Phi_k = 2\tau_k + \tau_k^1, \quad k = 1, 2,$$

$$f_{\text{ph}} = \frac{4}{9\mu_i^s \Delta} \exp\{-A\gamma\} \frac{G_1 \xi_{\text{ph}}}{\lambda_i^s \delta} \frac{\partial \sigma}{\partial t_i},$$

$$\xi_{\text{ph}} = \omega \lambda_e^s \left(1 - \frac{\Phi_1}{G_1} \right) - \frac{RI}{2T_\infty},$$

and \mathbf{e}_z is the unit vector along the z -axis.

In estimating the coefficients f_μ and f_{ph} , it is necessary to take into account that the subscript s designates values of physical quantities taken at a mean droplet-surface temperature T_s , which is determined from formula (11); the functions $\Phi_1, \Phi_2, G_1, G_2, N_1, N_2, N_3$, and N_4 are taken for $y = 1$ [$N_1 = G_1 G_2^I - G_2 G_1^I$, $N_2 = G_2(2G_1^I + G_1^{II}) - G_1(2G_2^I + G_2^{II})$, $N_3 = -G_1^I$, and $N_4 = 2G_1^I + G_1^{II}$].

In the case when droplet-surface heating is reasonably weak, i.e., when the mean droplet-surface temperature differs insignificantly from the environment temperature at infinity ($\gamma \rightarrow 0$), the temperature dependence of the viscosity coefficient can be ignored. In this case, $G_1 = 1$, $G_1^I = -3$, $G_1^{II} = 12$, $G_2 = 1$, $G_2^I = -1$, $G_2^{II} = 1$, $G_2^{III} = 2$, $N_1 = 2$, $N_2 = 6$, $N_3 = 3$, $N_4 = 6$, $\tau_1 = -\frac{1}{4}$, $\tau_1^I = \frac{3}{4}$, $\tau_2 = \frac{1}{2}$, and $\tau_2^I = -\frac{1}{2}$.

Setting the total force equal to zero, we obtain the expression for the thermocapillary-drift velocity:

$$\mathbf{U} = -\text{Re}_\infty h_{\text{ph}} \mathbf{e}_z, \quad h_{\text{ph}} = \frac{f_{\text{ph}}}{f_\mu}. \quad (14)$$

Formulas (13) and (14) enable us to estimate the force acting on a spherical droplet heated by an electromagnetic field in a viscous fluid and its thermocapillary-drift velocity. These estimates are made for arbitrary temperature drops between the droplet surface and the region far from this surface with allowance for the temperature dependence of the viscosity coefficient represented in the form of an exponential series and for the influence of fluid motion on the droplet drift.

We consider the expression

$$\xi_{\text{ph}} = \gamma \text{Pr}_\infty \lambda_e^s \left(1 - \frac{\Phi_1}{G_1} \right) - \frac{RI}{2T_\infty}, \quad (15)$$

Table 2

| ξ_{ph} | ξ_{ph}^* | $I, 10^2 \text{ W/cm}^2$ |
|-------------------|---------------------|--------------------------|
| 0 | 0 | 0 |
| 0.167 | -0.0429 | 1.2 |
| 0.346 | -0.0882 | 2.4 |
| 0.534 | -0.1356 | 3.7 |
| 0.730 | -0.1846 | 5.1 |
| 0.934 | -0.2355 | 6.4 |
| 1.142 | -0.2871 | 7.8 |
| 1.354 | -0.3395 | 9.3 |
| 1.566 | -0.3921 | 10.7 |
| 1.780 | -0.4451 | 12.2 |

which contains two terms entering it with opposite signs. Consequently, there are qualitatively different droplet motions along the direction of propagation of radiation and in the opposite direction. This is due to the contribution of convective terms to the total force and velocity entering the heat-conductivity equation [the term proportional to Pr_∞ in formula (4)]. Moreover, the contribution from the former term can be so important that it can be comparable to the major effect (the latter term). From (15) it follows that this term is proportional to the product of the Prandtl number and the relative temperature drop γ . Taking into account that the Prandtl number in a fluid can be large and the motion for considerable temperature drops in the droplet neighborhood is investigated, this effect can be significant in the proper choice of the fluid.

To illustrate the contribution of the fluid motion to the force and velocity of the thermocapillary-drift, we

list in Table 2 data relating the values ξ_{ph} and ξ_{ph}^* to the intensity I for large-size mercury droplets with radius $R = 2 \times 10^{-5} \text{ m}$ moving in water at $T_\infty = 273 \text{ K}$. The values of ξ_{ph} were estimated from formula (15), while ξ_{ph}^* were estimated from formula (15) for $\gamma = 0$; i.e., no fluid motion was taken into account. The molecular transport coefficients were taken at the mean surface temperature ($T_e = T_s$). In Table 3, we give numerical estimates for the influence of droplet-surface heating and the convective terms in the heat-conductivity equation on the thermocapillary-drift velocity of the droplet. The value of h_{ph} was estimated from formula (14); the value of h_{ph}^{B} , from formula (14) without convective terms (i.e., for $\omega = 0$). The value of h_{ph}^* was determined for low relative temperature drops ($\gamma \rightarrow 0$), the molecular-transport coefficients being taken at $T_e = T_s$. The coefficient of dynamic viscosity for water is described by the values $A = 5.779$, $F_1 = -2.318$, and $F_2 = 9.118$ in the temperature range from 273 to 363 K with a relative accuracy to within 2%; $\text{Pr}_\infty = 12.99$. If we consider the motion of a mercury droplet in glycerin, this effect is especially significant because, for example, the Prandtl number $\text{Pr}_\infty = 4753$ at $T_\infty = 303 \text{ K}$.

From the above numerical estimates it follows that the convective terms should be taken into account in the heat-conductivity equation when the mean temperature of the surface of heated droplets differs significantly from the environment temperature. For low relative temperature drops, this effect must be taken into account for fluids with high Prandtl numbers. In this case, the contribution can be as high as 20%. In a gas, this effect should not be taken into account because the Prandtl number for most gases is on the order of unity.

Table 3

| $T_s, \text{ K}$ | h_{ph} | h_{ph}^{B} | h_{ph}^* | $h_{\text{ph}}^{\text{B}*}$ |
|------------------|-------------------------|----------------------------|-------------------------|-----------------------------|
| 273 | 0 | 0 | 0 | 0 |
| 283 | -3.032×10^{-4} | 7.785×10^{-5} | -2.017×10^{-4} | 8.108×10^{-5} |
| 293 | -6.658×10^{-4} | 1.700×10^{-4} | -2.944×10^{-4} | 1.828×10^{-4} |
| 303 | -1.080×10^{-3} | 2.743×10^{-4} | -3.101×10^{-4} | 3.025×10^{-4} |
| 313 | -1.538×10^{-3} | 3.891×10^{-4} | -2.707×10^{-4} | 4.367×10^{-4} |
| 323 | -2.039×10^{-3} | 5.141×10^{-4} | -1.913×10^{-4} | 5.841×10^{-4} |
| 333 | -2.575×10^{-3} | 6.473×10^{-4} | -8.426×10^{-5} | 7.408×10^{-4} |
| 343 | -3.143×10^{-3} | 7.883×10^{-4} | 4.303×10^{-5} | 9.060×10^{-4} |
| 353 | -3.734×10^{-3} | 9.350×10^{-4} | 1.885×10^{-4} | 1.077×10^{-3} |
| 363 | -4.342×10^{-3} | 1.086×10^{-3} | 3.414×10^{-4} | 1.252×10^{-3} |

REFERENCES

1. G. M. Hidy and J. R. Brock, *J. Geophys. Res.* **72**, 455 (1967).
2. Yu. I. Yalamov, V. B. Kutukov, and E. R. Shchukin, *Dokl. Akad. Nauk SSSR* **234**, 1047 (1977) [*Sov. Phys. Dokl.* **22**, 314 (1977)].
3. E. R. Shchukin, *Inzh.-Fiz. Zh.* **50**, 681 (1986).
4. E. R. Shchukin and N. V. Malař, *Teplofiz. Vys. Temp.* **28**, 829 (1990).
5. Yu. S. Ryazantsev, *Izv. Akad. Nauk SSSR, Mekh. Zhidk. Gaza*, No. 3, 180 (1985).
6. A. I. Fedoseev, *Zh. Fiz. Khim.* **30**, 223 (1956).
7. V. B. Kutukov, E. R. Shchukin, and Yu. I. Yalamov, *Zh. Tekh. Fiz.* **46**, 626 (1976) [*Sov. Phys. Tech. Phys.* **21**, 361 (1976)].
8. V. I. Nařdenov, *Prikl. Mat. Mekh.* **38**, 162 (1974).
9. Yu. I. Yalamov, E. R. Shchukin, and O. A. Popov, *Dokl. Akad. Nauk SSSR* **297**, 91 (1987) [*Sov. Phys. Dokl.* **32**, 898 (1987)].
10. E. R. Shchukin, N. V. Malař, and Yu. I. Yalamov, *Teplofiz. Vys. Temp.* **25**, 1020 (1988).
11. St. Bretsznajder, *Properties of Gases and Liquids. Engineering Methods of Calculation* (Wydawnictwo Naukowo-Techniczne, Warsaw, 1962; Moscow, 1966), translated from Polish.
12. Yu. I. Yalamov and V. S. Galoyan, *Dynamics of Droplets in Inhomogeneous Viscous Media* (Yerevan, 1985).
13. M. van Dyke, *Perturbation Methods in Fluid Mechanics* (Academic, New York, 1964; Mir, Moscow, 1967).

Translated by V. Bukhanov

**Erratum: “Reflection and Absorption Characteristics
of Various Physical Objects
in a Millimeter Radio-Wave Range”
[*Doklady Physics* 45 (10), 510 (2001)]**

**V. I. Zagatin, V. V. Meriakri, G. S. Mizezhnikov,
E. E. Chigryaĭ, and V. B. Shteĭnshleĭger**

In our paper “Reflection and Absorption Characteristics of Various Physical Objects in a Millimeter Radio-Wave Range,” which was published in *Doklady Physics*, vol. 45, no. 10, pp. 510–511, the beginning of the last item should be read as “The results of the measurements of the reflection coefficient... .”

V.I. Zagatin, V.V. Meriakri,
G.S. Mizezhnikov, E.E. Chigryaĭ,
V.B. Shteĭnshleĭger